Appendix J
Engineering and Operational Risk and Reliability Analysis

Table of Contents

Executive Summary

The mission of the IPET risk and reliability analysis is to examine the risks to life and property posed by the New Orleans hurricane protection system that was in place prior to Katrina and by the system as it is expected to exist at the start of the next hurricane season (1 June 2006). The risk analysis will consider the expected performance of the various elements of the system and the consequences associated with that performance. All engineered systems impose risks that result from humans using technology to create conditions or activities that are not produced by nature. For instance, the hurricane protection system in New Orleans has been designed to control interior flooding within New Orleans and protection to the city from storm induced surges and waves. The hurricane protection system (HPS) project is designed to perform this function without imposing unacceptable risks to public safety, property and welfare.

The risk analysis covers four states that represent the condition of the New Orleans hurricane protection system.

- The system as it existed before the arrival of Hurricane Katrina.

Knowledge gained from IPET studies will be considered in the analysis.

- After Hurricane Katrina with repairs that have been completed prior to the 2006 hurricane season. Some projects may be ongoing after 1 June 2006.

- After Hurricane Katrina with all repair and improvement projects complete, but prior to longer-term increases in the authorized level of protection.

- The system as authorized before the arrival of Hurricane Katrina. All authorized components of the HPS are constructed and knowledge gained from IPET studies will be considered in the analysis.

The difference in relative risks among the three states will be a unified measure for fully evaluating the performance of the integrated system before Hurricane Katrina, after Hurricane Katrina, and during the interim recovery period.

Two groups of questions concerning the performance of the hurricane protection system (HPS) are addressed by the risk and reliability analyses:

Pre-Katrina: The system as it existed before the arrival of Hurricane Katrina. This state is the baseline for estimating risk, and includes the following:

1. What was the reliability of the hurricane protection system to prevent flooding of protected areas of the HPS that was in existence before the arrival of Katrina, for the standard project hurricane? Note that some components of the authorized projects had not been constructed prior to Katrina.

2. What was the reliability of the hurricane protection system to prevent flooding of protected areas with all of the authorization projects completed, for the standard project hurricane?

3. What is the estimated annual rate of occurrence of system failure due to hurricane events?

4. What are the probability distributions and annual rates of consequences that would result from failure of the hurricane protection system as defined in terms of life loss and economic impact?

5. What is the uncertainty in these estimates?

The pre-Katrina analysis does not attempt to recreate the design intent or knowledge that the designers used to determine the configuration of the HPS. Engineering parameters, foundation conditions and operational information gained by IPET through exploration and testing since the hurricane are used. This allows for an assessment of the actual risks that existed pre-Katrina. An additional analysis was conducted on the authorized HPS that includes all features in the original design that were not completed prior to Katrina.

Post-Katrina: After Hurricane Katrina with repairs made prior to the 2006 hurricane season, and during the interim recovery period after the hurricane protection system has been strengthened and improved, but prior

to longer-term increases in the authorized level of protection. This group includes:

1. What is the reliability of the HPS to prevent flooding of protected areas for the authorized standard project hurricane with the system repairs and improvements in place as of June 1, 2006?

2. What is the frequency of flooding due to the range of expected hurricane events with the system repairs and improvements in place as of June 1, 2006?

3. What are the probability distributions and annual rates of consequences that would result from failure of the hurricane protection system as defined in terms of life loss and economic impact?

4. What is the uncertainty in these estimates?

The condition of the system has been degraded by the effects of hurricane Katrina. Flood walls and levees may have been overtopped, damaged by impacts from debris, saturated, submerged and/or breached. Permanent repairs on these elements have been accomplished since the hurricane that may have different material strength parameters than the original feature. This difference in strengths is considered in the analyses of component reliability. The pumping system was also damaged and shut down or submerged. The post Katrina reliability of the levees, flood walls and pumping stations will be considered in the risk assessment. The reliability of the various elements of the protection system will be determined using analytical and expert elicitation methods.

The term reliability is intended to mean the conditional probability of a component or system performing intended function. This result can also be used to determine the conditional probability of failure. System failure refers to the failure of the HPS to provide protection from flooding in one or more protected areas and can also be thought of as the occurrence of flood inundation. The effectiveness of the protection system is also dependent upon how well the operational elements of the system performed. Elements such as road closure structures, gate operations and pumping plants, etc. that requires human operation and proper installation during a flood fight can dramatically impact flood levels. The lessons learned concerning the performance of these elements during Katrina will be considered in the analysis.

The changed demographics of the local areas protected by the system will be considered when determining the consequences. In some areas, many homes and much of the infrastructure were destroyed by the hurricane and some may not be rebuilt. Therefore the pre-Katrina populations and property values will be impacted and must be considered in the post-Katrina analysis.

Risk is generally calculated by combining the probability of system failure with the consequences associated with that failure. For New Orleans, the post Katrina risks will be lower primarily due to reduced population and economic activity. In order to better compare the adequacy of pre and post Katrina HPS, probability of failure and inundation mapping will be used as the primary metric by which to measure the effectiveness of repairs and improvements.

Background

Decisions about natural hazards are best made by explicitly and quantitatively considering risks. Implementation of risk analysis to the hurricane protection system (HPS) of New Orleans and S.E. Louisiana is difficult because the system serves a large geographical region and our capability to accurately model hurricanes in regions as complex as the Mississippi delta is limited. Nonetheless, modeling capabilities have improved enough in recent years to make risk analysis an important tool for decision making as the New Orleans HPS is restored.

It is important to note that detailed knowledge of the New Orleans HPS and the engineering parameters that influence its performance or of the hurricane characteristics is limited. For example, we do not know with certainty the properties of foundation soils underlying the extensive levee system, or even the frequency with which hurricanes occur. Hurricane models can predict winds, waves and surges only with limited precision, and reliability models of levee performance when subjected to hurricane forces are similarly limited. Hence, the risks of hurricane-induced flooding cannot be established with certainty. Therefore a risk analysis must include not just a best estimate of risk, but also an estimate of the uncertainty in that best estimate.

The reliability and risk analyses relate the performance of individual features (floodwalls, levees, pumps, levee closures, etc.) located throughout the hurricane protection system to the overall performance of the integrated system and the impact of that performance on economics and public safety. The reliability of all structural features also considers the varying foundation conditions that exist throughout the hurricane protection system. The risk analysis covers three states that represent the condition of the hurricane protection system.

- The system as it existed before the arrival of Hurricane Katrina. This state is the baseline for estimating risk.

- After Hurricane Katrina with repairs made prior to the 2006 hurricane season.

- During the interim recovery period after the hurricane protection system has been strengthened and improved, but prior to longer-term increases in the authorized level of protection.

Risk analysis examines potential life and property losses posed by the as-built hurricane protection system prior to Katrina and by the system after Katrina in its repaired or improved condition. Reliability analysis examines the engineering performance of various elements of the system. The reliability results are used in conjunction with the consequences associated with that performance to estimates the corresponding risks. The reliability of the various elements of the protection system is determined using analytical and expert elicitation methods.

During the risk studies several key issues were considered:

- Defining the physical features of the system required an accurate inventory of all components that provide protection against storm surge and waves. It was important to model not only the cross sections and strength parameters of these components but also transitions between elements, differences in the top elevation along a reach of similar components and varying foundation conditions. The characterization of the physical features of the protection system was, however, limited by the available information and the resources available to process that information under IPET. These limitations are expressed in the analyses as uncertainties that are characterized and communicated so that they can be accounted for in decisions making.

- At many locations, the hurricane protection system has been degraded by Hurricane Katrina. Levees and floodwalls may have been overtopped or otherwise damaged. The impacts of these events upon the condition of the features is not necessarily apparent by visual inspection. The possibility of such weakening has been considered in the current condition of features of the system that survived Katrina in order to estimate the risk for the 2006 hurricane season.

- Emergency repairs of breached elements were accomplished after Hurricane Katrina, and permanent repairs have subsequently been completed. The structural/geotechnical strength of the repairs have been considered.

- The pumping system is an important element that controls flooding during and after a storm. Pumping plant reliability and capacity have therefore been considered.

- The consequences of pre- and post-Katrina flooding are different due to changes in population and economic activity. Task 10 has relied on the Task 9 Team to define post-Katrina exposure scenarios and to quantify the consequences of HPS failures.

- The effectiveness of the protection system depends on human factors as well as engineered systems (e.g., timely road and railroad closures, gate operations, functioning of pumping stations, and so on). Lessons learned from Katrina and other natural disasters will be used in modeling human performance.

Appendix A lists key terminology and definitions used in this report.

Analysis Boundaries

An important initial step in the analysis is to clearly define the bounds of the study. These bounds included defining the geographic bounds of the study region and the elements of the hurricane protection system, the resolution of information and analyses to be performed, and analysis constraints or assumptions associated with the IPET analysis. These areas are defined in the following subsections and in detail in the Appendices.

Study Region and Hurricane Protection System

At a macro scale, this analysis examines risks to New Orleans and the South East Louisiana area associated with the performance of the hurricane protection system (HPS). Figure J-1 identifies the region to be considered and the major features of the hurricane protection system.

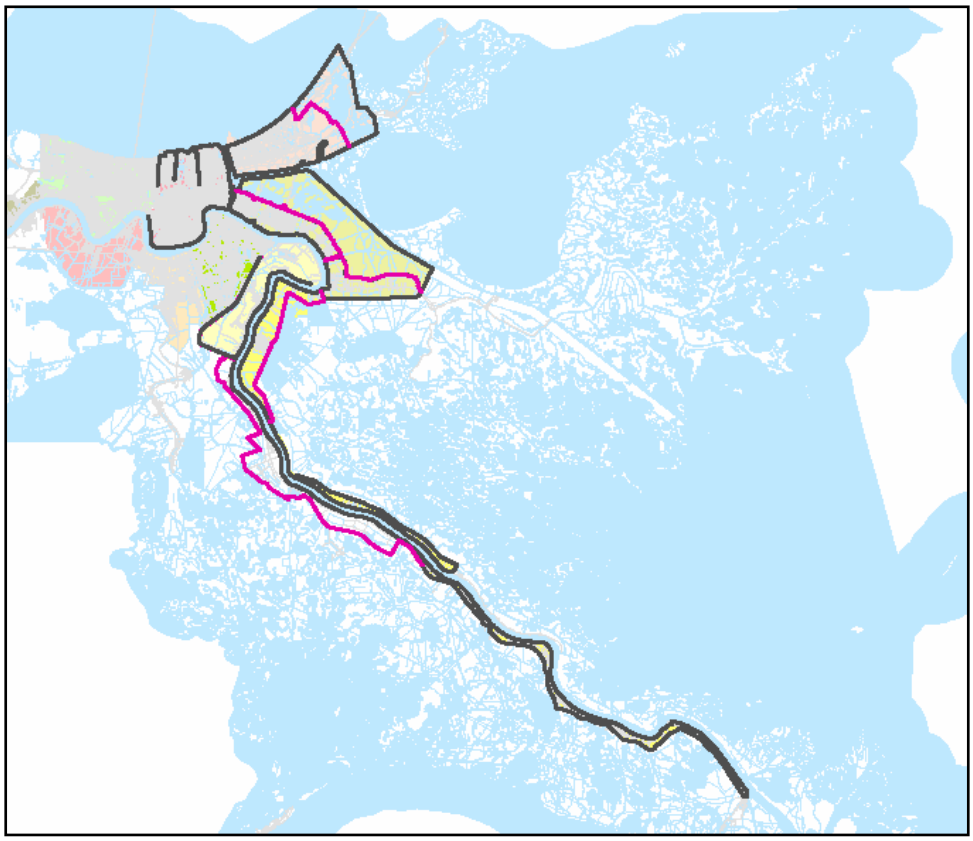

Figure J-1. Map of the New Orleans and the south east Louisiana area, the geographic bounds of the study region considered in the risk analysis and the primary features of the hurricane protection system

The hurricane protection system is comprised of a variety of subsystems, structures and components which include: earthen levees, floodwalls, foundation conditions, pumping stations, canals, wall closures, power supply systems, operations personnel. The system is also a combination of several sub-systems (polders) which are independently maintained and operated by local parishes and levee boards. Data collected by Teams 1 and 6, and during a site visit is used to define characteristics of the polders and their interdependence for use in the risk model.

Appendices B through F contain a complete inventory of the structures, systems and components that were considered in the risk analysis. The information provided in the appendices was obtained from a number of the IPET teams. The reader should note that all of the structures, systems and components listed may not have been included in the risk analysis model. Some items may

have been screened out of the analysis, whereas others may not have been included since they do not play a role in the performance of the hurricane protection system or the consequences that result in the event of a failure.

Analysis Assumptions and Constraints

As part of the process of developing the risk analysis model, it was necessary to identify key assumptions and analysis constraints. Constraints refer to events or factors that were not modeled or considered explicitly in the analysis. The assumptions and constraints are provided at the appropriate location in subsequent sections.

The following table lists the analysis limitations or constraints of the risk analysis.

No.	Limitation or Constraint
1.	Model procedures that existed prior to Katrina
2.	Geographic area limited to elements of the hurricane protection system in the 5 parishes
3.	Hazards and thus consequences not considered in the risk analysis are: a. Wind Damage to buildings b. Fire c. Civil unrest d. Effect of a release of hazardous materials
4.	The performance of the evacuation system in New Orleans was not explicitly modeled in the risk analysis. Its consideration was limited to a parametric consideration of the variation of the sensitivity of the risk analysis results to the relative effectiveness of evacuation.

Risk Analysis Methodology

Overview

The following sections describe the overall risk analysis methodology of the hurricane protection system. Sections that follow discuss individual parts of the analysis (hurricane hazard analysis, levee and floodwall vulnerability or fragility analysis) as they relate to the overall risk analysis methodology. The basic elements of the risk analysis methodology are illustrated in Figure J-2. The analysis is represented in terms of a series of modules which interface to provide a risk model for the New Orleans HPS.

Contributing Factors and Their Relationships

The development of a risk analysis model was facilitated by the preparation of an influence diagram. The process of creating an influence diagram helped establish a basic understanding of the elements of the hurricane protection system and their relationship to the overall system performance during a hurricane event and the analysis of consequences and risks.

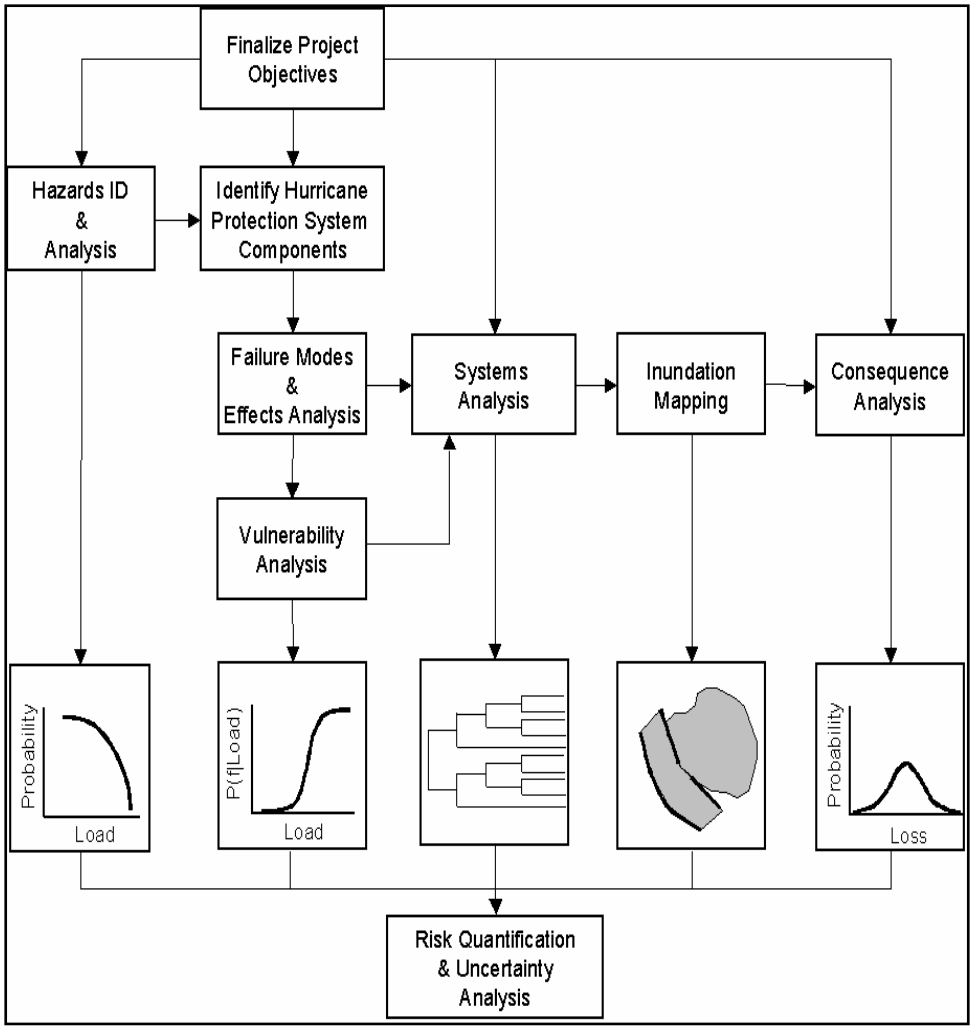

Figure J-2. Risk analysis logic diagram

Figure J-3 shows the influence diagram for the hurricane protection system and the analysis of consequences. There are four parts to the diagram influence diagram:

- Value nodes (rounded-corner box)
- Chance nodes (circular areas)
- Decision nodes (square-corner boxes)
- Factors and dependencies in the form of arrows.

The influence diagram shown in Figure J-3 was used to develop an event (or probability) tree for the hurricane protection system. Figure J-4 shows an initial probability tree derived from the influence diagram in Figure J-3. The top events across the tree identify the random events whose state following the occurrence of the hurricane could contribute to flooding in a protected area. The tree begins with the initiating event, a hurricane that generates a storm surge, winds and rainfall in the region.

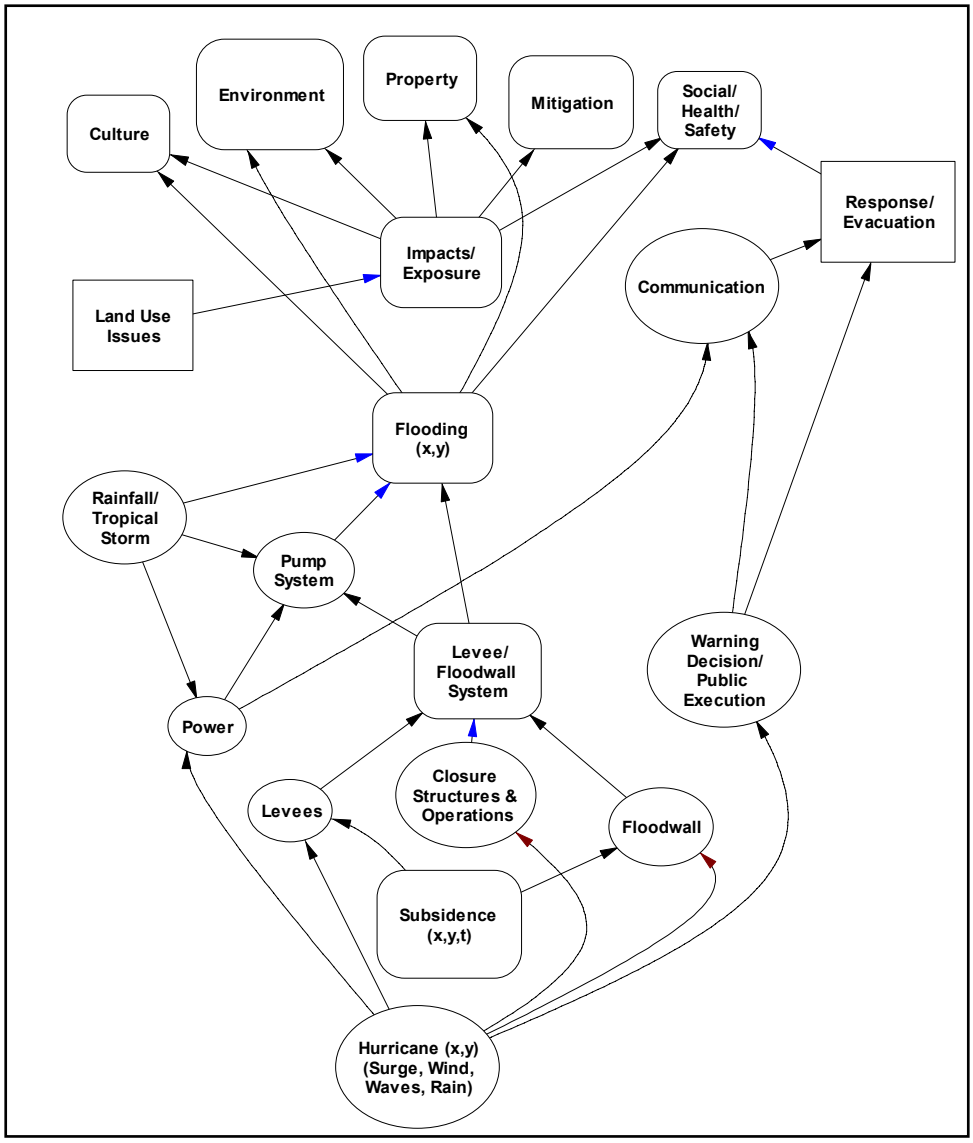

Figure J-3. Influence Diagrams for Risk Analysis

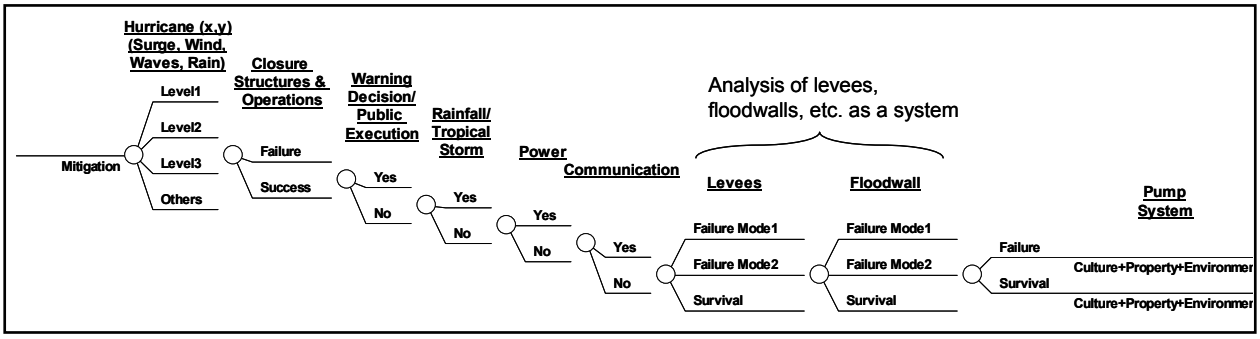

Figure J-4. Probability Tree for the Hurricane Protection System

Hurricane Protection System

The entire hurricane protection system is provided in Figure J-1. The hurricane protection system (HPS) considered in the reliability and risk analysis task is schematically shown in Figure J-5. The system consists of polders, sub-polders and reaches. The definition of these polders, sub-polders and reaches are based on the following considerations:

- Local jurisdiction,
- Floodwall type and cross section,
- Levee type and cross section,
- Engineering parameters defining structural performance,
- Soil strength parameters,
- Foundations parameters, and
- Surge and wave levels.

Reaches (R) of each polder is uniquely identified using sequential numbers as shown in the figure. The figure also shows the approximate locations of pumping stations.

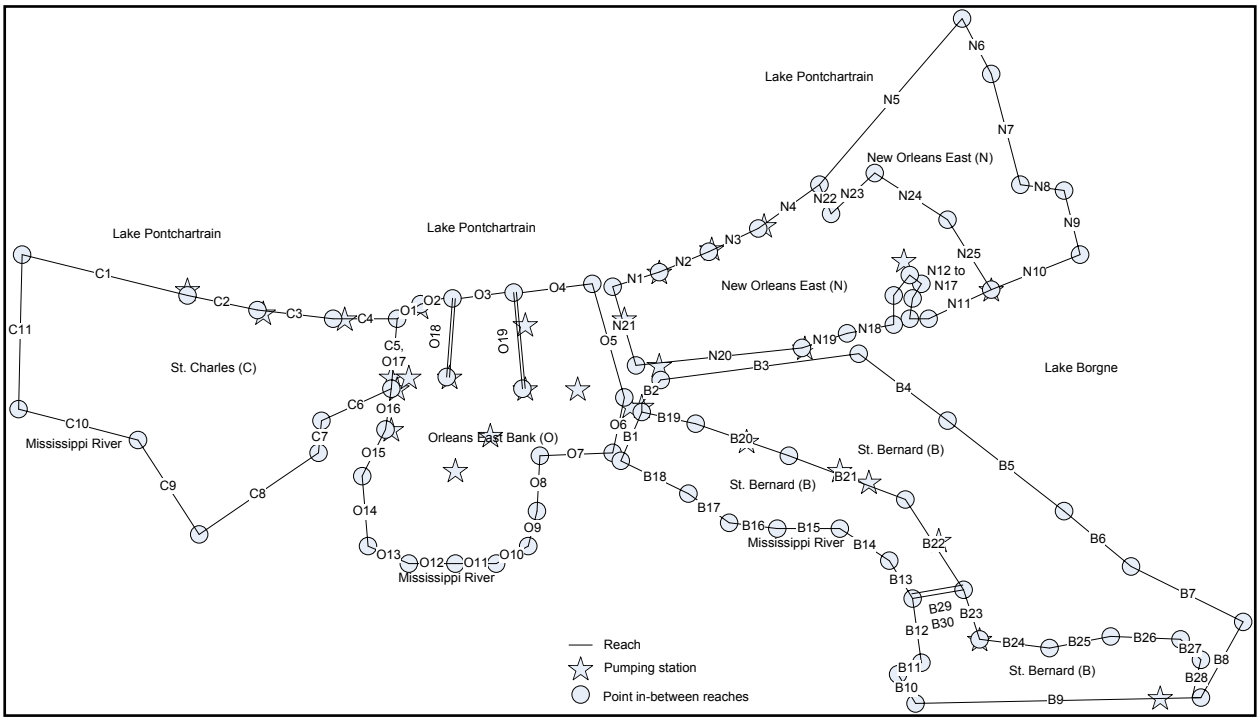

Figure J-5. Hurricane Protection System Defined by Polders and Reaches

Probabilistic Risk Model

Risk associated with the hurricane protection system is quantified through the hurricane rate (λ) and the probability $P(C > c)$ with which a consequence

measure C exceeds different levels c. The loss exceedance probability per event is evaluated as

$$P(C > c) = \sum_i \sum_j P(h_i) P(S_j \mid h_i) P(C > c \mid h_i, S_j) \tag{J-1}$$

An annual loss exceedance rate can be estimated as follows

$$\lambda(C > c) = \sum_i \sum_j \lambda P(h_i) P(S_j \mid h_i) \times P(C > c \mid h_i, S_j) \tag{J-2}$$

where $P(h_i)$ is the probability of hurricane events of type i, $P(S_j|h_i)$ is the probability that the system is left in state j from the occurrence of h_i, and $P(C > c \mid h_i, S_j)$ is the probability that the consequence C exceeds level c under (h_i, S_j). Summation is over all hurricane types i and all system states j in a suitable discretization. Simulation studies of hurricanes for risk analysis require the use of representative combinations of hurricane parameters and their respective probabilities. The outcome of this process is a set of hurricane simulation cases and their respective conditional probabilities $P(h_i)$.

Evaluation of the hurricane rate λ and the probability $P(h_i)$, the conditional probabilities $P(S_j \mid h_i)$, and the conditional probabilities $P(C > c \mid h_i, S_j)$ is the main objective of the hurricane model, the system model, and the consequence model, respectively. The probability $P(S_j \mid h_i)$ should cover the states of the components of the HPS, such as closure structure and operations, precipitation levels, electric power availability, failures modes of levees and floodwalls, and pumping station reliability. To assess the state of the HPS given a hurricane event requires an evaluation of the reliability of individual structures, systems and components (e.g., levees, floodwalls, pump systems) when they are exposed to the loads and effects of the hurricane (e.g., the peak surge, wave action) and the relationship of these elements to the overall function of the system to prevent flooding in protected areas.

If point estimates of consequences (i.e., $(c \mid h_i, S_j)$) are available instead of $P(C > c \mid h_i, S_j)$, order statistics can be used to construct the exceedance probability $P(C > c \mid h_i, S_j)$ as provided in Appendix G.

The hurricane loss provided by Eq. J-1 can be used to compute a cumulative distribution function (CDF) $F_S(s)$ as 1-$P(C > c)$. The CDF of the accumulated damage (loss) during a non-random time interval [0, t] is given by

$$F(s;\ \ t, \lambda) = \sum_{n=0}^{\infty} e^{-\lambda t} \frac{(\lambda t)^n}{n!} F_S^{(n)}(s) \tag{J-3}$$

where $F_S^{(n)}$(s) is the n-fold convolution of F_S(s).

Conceptual Event Tree

The probability tree of Figure J-4 can be simplified by determining the frequency of flooding levels and displaying the results as contours within the polders. Consequences were determined with Task 9 and are simplified by grouping communication, warning decision and public execution into an *exposure factor* parameter applied to lives and property at risk. The resulting event tree appropriately branched out is shown in Figure J-6. This tree is used as a basis for developing the risk analysis methodology. The events of the tree are defined in Table J-1.

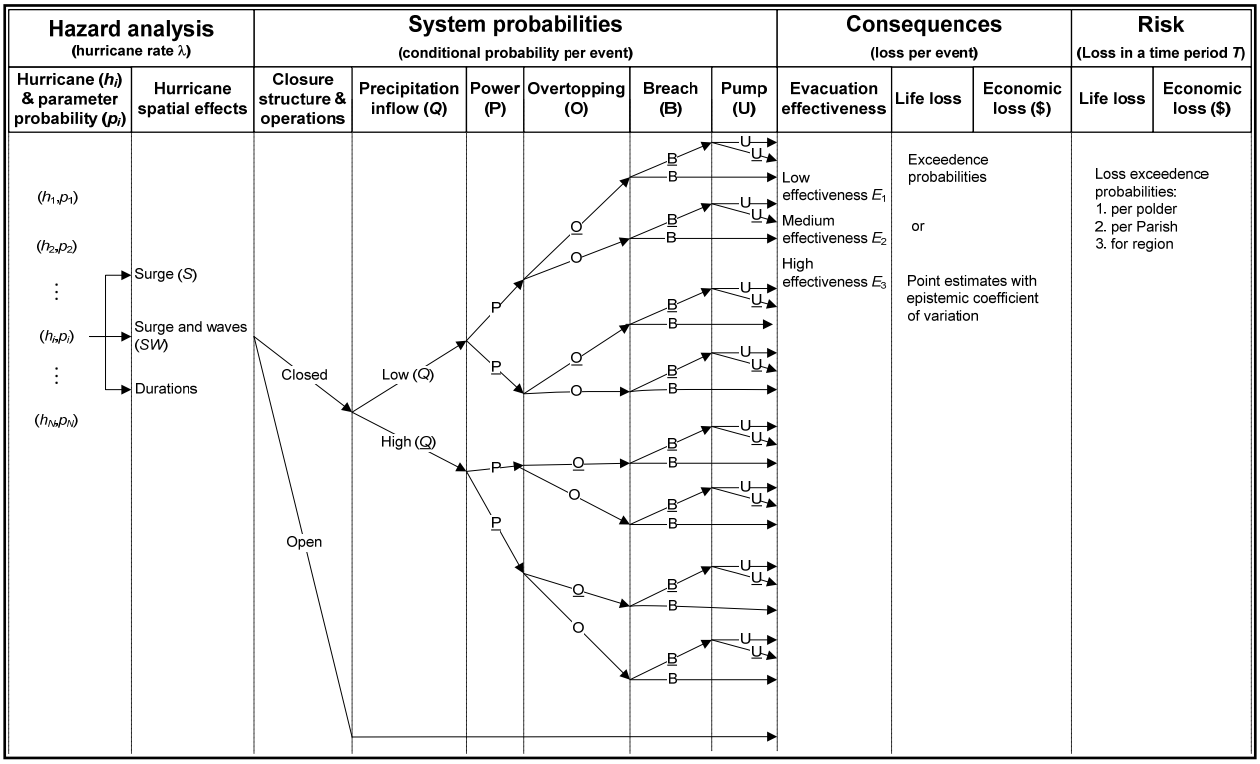

Figure J-6. Conceptual Event Tree for Risk Analysis Underlined events (i.e., $\underline{Q}$, $\underline{P}$, $\underline{O}$, $\underline{B}$, and $\underline{U}$) are the complements of the respective events (i.e., Q, P, O, B, and U).

Table J-1. Summary of the Event Tree Top Events	
Top Event	**Description**
Hurricane initiating event	The hurricane initiating event is mapping of the peak flood surge with waves in the study area with a hurricane rate λ. This event can be denoted, $h_i(x,y)$, and has a probability of occurrence, $P(h_i(x,y))$ and a rate of occurrence of $\lambda P(h_i(x,y))$.
Closure structure and operations	This event models whether the hurricane protection system closures have been sealed prior to the hurricane. This event depends on a number of factors as illustrated in the influence diagram. The closure structures are treated in groups in terms of probability of being closed in preparation for the arrival of a hurricane.
Precipitation inflow (*Q*)	This event corresponds to the rainfall that occurs during a hurricane event.
Power (*P*)	This event models the availability of power (normal) power for the pump systems. This event is modeled in the event tree to represent a common mode of failure for the pump systems, and is included in developing a model for drainage and pumping efficiency or lack thereof including backflow through pumps.
Overtopping (*O*)	This event models the failure of the enclosure/protection system due to overtopping, given that failure has not occurred by some other (non-overtopping) failure mode. If failure (breach) does not occur, some flooding due to overtopping could result.
Breach (*B*)	This event models the failure of the enclosure/protection system (e.g., levees/floodwalls, closures) during the hurricane, exclusive of overtopping failures). This event includes all other failures and it models all 'independent' levee/floodwall sections.
Pump System (*U*)	This event models the availability of the pump system and its ability to handle a particular floodwater volume. This event is treated in aggregate with drainage effectiveness and power reliability including backflow through pumps.

Risk Quantification

Functional Modeling and Computational Considerations. A hurricane protection system (HPS) has the primary function of keeping water away from protected areas. The HPS breaks down the protected areas into polders. Some polders are divided internally into sub-polders. This partitioning is based on the internal drainage and pumping system within each polder. Figure J-5 illustrates the New Orleans East polder and the two sub-polders for illustration purposes. Polders and sub-polders are divided into sections, or reaches, that have similar cross-sections, material strength parameters and foundation conditions. Table J-2 shows a table constructed for a reach belonging to a polder. For each reach, the following items are defined:

1. start and end stations
2. reach length
3. protection height
4. polder and sub-polder membership designation

The table shows other items that are needed and referenced in subsequent sections.

The quantification of risk associated with a hurricane protection system requires quantifying its performance or lack thereof. A measure of the lack of performance is the amount of water that is expected to reach the protected areas for a particular hurricane, i.e., a given hurricane run. The water enters protected areas as a result of one or more of the following two cases:

1. overtopping volumes and associated probabilities and epistemic uncertainties

2. breach elevations and associated probabilities and epistemic uncertainties

The risk quantification framework has, therefore, the objective of obtaining these estimates.

The conceptual event tree presented in Figure J-6 can be reconfigured to facilitate the computations of overtopping volume and breach elevation with associated probabilities and epistemic uncertainties as provided in Figure J-7. The figure shows the two quantities of interest in boxes as the post-surge elevation that would result in cases of breach, and the water volume that results in cases of overtopping (OT), precipitation, open closures, leaks from joints, and backflow from pumping stations.

The subsequent sections describe the computational details needed to quantify risk. They are presenting in a manner that correspond to the events shown in Figure J-7, and a level of details needed to construct a spreadsheet to perform the computations. The sections that follow provide the background information and basis behind the approaches used for these computations.

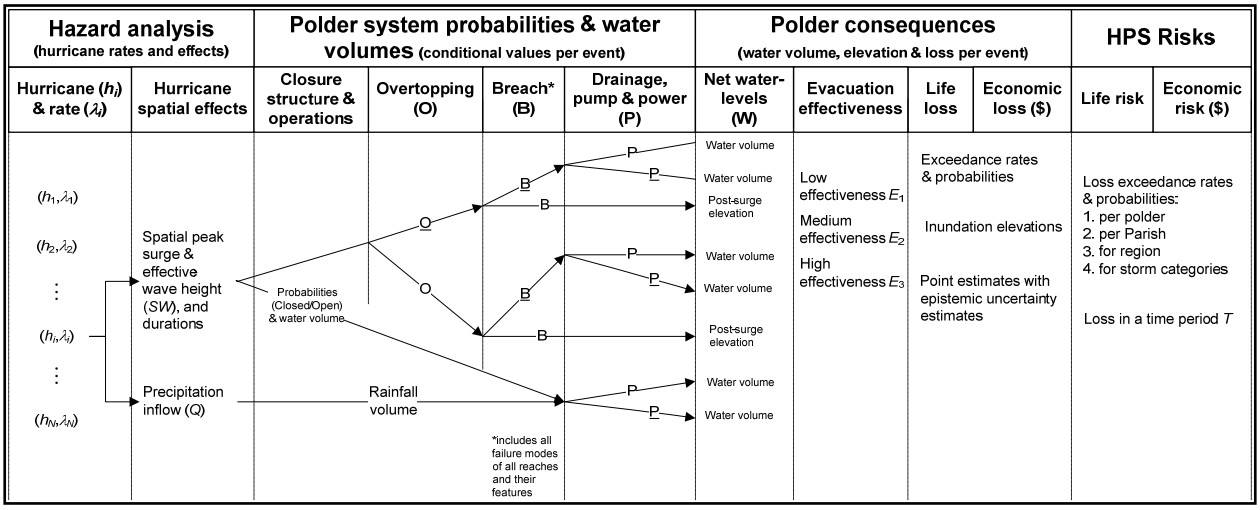

Figure J-7. Event Tree for Quantifying Risk. Underlined events (i.e., $\underline{P}$, $\underline{O}$, and $\underline{B}$) are the complements of the respective events (i.e., P, O, and B).

Table J-2. System Definition, Hurricane Hazard, and Overtopping (OT) Results

Reach	Reach 1
Reach start-end stations	To be provided
Reach coordinates	To be provided
Equal allocation to Sub-Polder(s)	1
Reach length (ft)	2000
Reach elevation (ft)	16
Mean (Weir Coeff.)	3.33
COV (Weir Coeff.)	0.15

*Not used (needed for breaches)

Hurricane Runs			Reach 1										
Run	Rate (R)		Surge+Waves		Duration		Post-surge elevation*		OT Length		OT Probability	OT Volume (Weir Eq)	
i	Mean	StD	Hs		T		Hps		L		P(OT)	V|OT	
			Mean	StD	Mean	StD	Mean	StD	Mean	StD		Mean	StD
ID	event/yr	event/yr	ft	ft	sec	sec	ft	ft	ft	ft		ft^3	ft^3
1	5.00E-04	1.00E-04	25	1	3600	720	8	1	2000	0	1.00E+00	6.549E+08	1.637E+08
2	5.00E-04	1.00E-04	24	1	3600	720	8	1	2000	0	1.00E+00	5.311E+08	1.328E+08
3	7.50E-04	1.50E-04	23	1	4320	864	8	1	2000	0	1.00E+00	5.107E+08	1.277E+08
4	1.00E-03	2.00E-04	22	1	3600	720	8	1	2000	0	1.00E+00	3.365E+08	8.412E+07
5	1.00E-03	2.00E-04	21	1	5400	1080	8	1	2000	0	1.00E+00	3.930E+08	9.825E+07
6	1.50E-03	3.00E-04	20	1	5400	1080	8	1	2000	0	1.00E+00	3.008E+08	7.520E+07
7	2.00E-03	4.00E-04	19	1	3600	720	8	1	2000	0	9.99E-01	1.505E+08	3.762E+07
8	2.00E-03	4.00E-04	18	1	3600	720	8	1	2000	0	9.82E-01	1.103E+08	2.758E+07
9	2.00E-03	4.00E-04	17	1	5400	1080	8	1	1000	200	8.42E-01	5.906E+07	1.891E+07
10	2.00E-03	4.00E-04	16	1	5400	1080	8	1	1000	200	4.88E-01	4.082E+07	1.307E+07
11	3.50E-03	7.00E-04	15	1	5400	1080	8	1	1000	200	1.58E-01	2.714E+07	8.688E+06
12	5.00E-03	1.00E-03	14	1	5400	1080	8	1	1000	200	2.82E-02	1.719E+07	5.504E+06
13	5.00E-03	1.00E-03	13	1	5400	1080	8	1	1000	200	3.06E-03	1.025E+07	3.280E+06
14	5.00E-03	1.00E-03	12	1	5400	1080	8	1	1000	200	2.33E-04	5.637E+06	1.805E+06
15	5.00E-03	1.00E-03	11	1	5400	1080	8	1	1000	200	1.49E-05	2.781E+06	8.903E+05
16	5.00E-03	1.00E-03	10	1	5400	1080	8	1	1000	200	9.60E-07	1.171E+06	3.749E+05
17	5.00E-03	1.00E-03	9	1	5400	1080	8	1	1000	200	7.62E-08	3.840E+05	1.229E+05

Hurricane Hazard Analysis. The joint probability (JP) of hurricane parameters is used for the purpose of generating hurricane runs. This method parameterizes hurricanes using a vector $\underline{\theta}$ of characteristics at landfall (central pressure drop, radius of maximum wind, etc.). From the values of $\underline{\theta}$ for historic events, one estimates the recurrence rate density $\lambda(\underline{\theta}) = \lambda f(\underline{\theta})$ where λ is the rate of hurricane events in a neighborhood of the region of interest and $f(\underline{\theta})$ is the joint probability density function of $\underline{\theta}$ in that neighborhood. These runs produce combined wind, surge and wave M that are computationally demanding. To reduce the number of runs of M, a response surface approach can be used. In this approach one selects a relatively small number m of vectors $\underline{\theta}_i$ and uses M to calculate the corresponding surge and wave levels at the sites of interest. Then one fits a response surface model to each response variable (surge or wave level at a specific site) in terms of $\underline{\theta}$. Finally, one uses a refined discretization $\{\underline{\theta}_i\}$ of parameter space with the response surface as a proxy model in place of M to represent the hurricane hazard. The outcomes of these computations are combined surge and effective wave values (called surge/wave values) at particular locations of interest along the hurricane protection system, e.g., representative values at the reaches. These values are denoted as h_i in Figure 3-6.

The water elevation need for the risk analysis as a loading can be taken as the surge elevation plus the effective wave height if waves are present, called the surge/wave elevation. Surge only, therefore, need not to be considered as a separate loading condition.

Hurricane rate modeling and prediction methods are then used to compute the corresponding exceedance rates to h_i values, and are denoted as λ_i in Figure J-7. Also, surge duration and post-surge elevation, i.e., applicable lake or river water level, are needed. The epistemic uncertainties in both the surge/wave elevation and the rates are represented in the form of standard deviation of respective biases in prediction methods and practices. Table J-2 shows a summary of such results as they appear in a spreadsheet under development for this purpose. The values provided in this table are for illustration purposes, and are shown in Figure J-8.

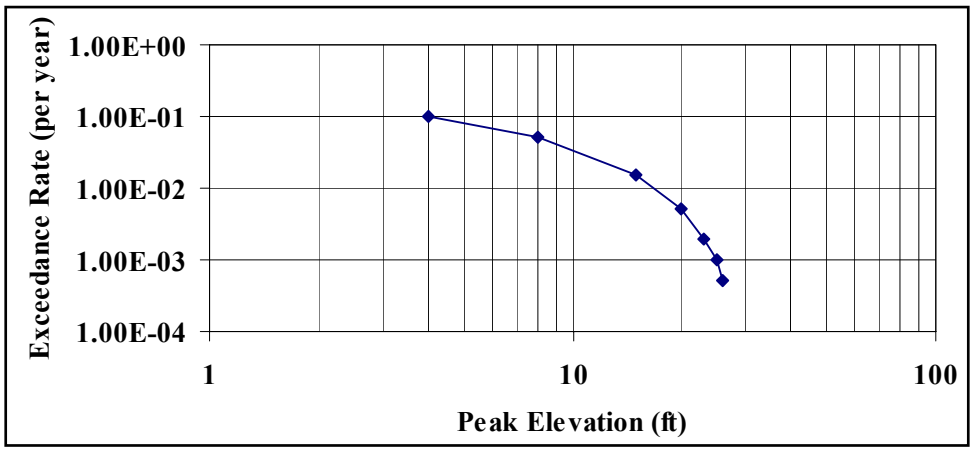

Figure J-8. Surge and wave Exceedance Curve Corresponding to Table J-2

Overtopping Flow Rate and Volume Models, and Probabilities.

Deterministic Models. The overtopping rate can be computed using the rectangular weir formulae (Daugherty, et al. 1985). The overtopping water flow has the elevation H and width L. If the water is assumed to be the ideal liquid, it can be shown using the energy conservation law that the flow rate Q (L^3/T) is given by the following equation:

$$Q = \frac{2}{3}(2g)^{1/2} LH^{3/2} \tag{J-4}$$

where g is the acceleration of gravity. The actual flow over the weir is known to be less than ideal (Daugherty, et al. 1985) because the effective flow area is considerably smaller than the product LH.

The model can be enhanced further for engineering applications by replacing the term $\frac{2}{3}(2g)^{1/2}$ in Eq. J-4 by the empirical coefficient, known as the weir coefficient C_w, so that Eq. J-4 takes on the following form:

$$Q = C_W LH^{3/2} \tag{J-5}$$

where

$$C_W = \begin{cases} 3.33 & \text{if } L \text{ and } H \text{ are given in English units} \\ 1.84 & \text{if } L \text{ and } H \text{ are given in SI units} \end{cases} \quad \text{(J-6)}$$

Note that the C_w for the ideal fluid case is $\frac{2}{3}(2g)^{1/2}$ which is equal to 2.95 m/s^2. This coefficient is assumed to have a coefficient of variation (COV) of 0.15.

For the application considered, the volume of the overtopping (OT) water V for a given reach can be calculated as

$$V(L,T,H_s,H_p) = C_W LT(H_s - H_p)^{3/2} \quad \text{(J-7)}$$

where L is OT length taken as a fraction of the reach length, H_s is surge elevation, H_p is the top the protection for a reach elevation, T is surge duration, and the evaluation is constrained by the inequality that $H_s > H_p$. The resulting volume is the conditional volume *given* overtopping.

Uncertainty Analysis. For a particular hurricane run, the values of L, H_s, and T can be estimated. These point estimates involve epistemic uncertainty. The OT volume as given by Eq. J-7 is, therefore, a random variable that is a function of the following random variables: L, H_s, and T, assuming H_p deterministic. For specified probabilistic characteristics of L, H_s, and T, the probabilistic characteristics of V can be evaluated. Assuming L, H_s, and T, to be non-correlated, the mean value and the standard deviation of V can be evaluated using Monte Carlo simulation and nonlinear curve fitting based on least squares.

The uncertainty analysis of the OT flow rate can be assessed using Monte Carlo simulation based on a normally distributed epistemic uncertainty of the H_s at a reach for a particular hurricane run. Using Eq. J-5, the OT rate for a unit width (i.e., $L = 1$) is

$$q = 3.33H^{3/2} \quad \text{(J-8)}$$

where $H = H_s - H_p$ with the constraint that $H_s > H_p$, which reflects the deterministic nature of Eq. J-8. A truncated distribution resulting from such a formulation requires the use of Monte Carlo simulation. The simulation was performed using 100 cycles for mean H values incremented from -6 to 10 ft using an increment of 0.01 ft, and standard deviation (S) values of 0, 1, and 2 ft as shown in Figure J-9a. Figure J-9b shows the differential increase in flow rate due to the standard deviation of water Head. Regression analysis was performed to obtain the mean and standard deviation of the conditional OT rate as follows:

$$\overline{q} = \left(\overline{H} + 10\right)^{3.87577} \exp\left(0.01916 S_H - 6.92066\right) \quad \text{(J-9a)}$$

$$S_q^2 = 80.65\left(\overline{H} + 10\right) + 165.67 S_H^2 - 1344.26 \quad if \geq 0; \quad otherwise \quad S_q^2 = 0 \quad \text{(J-9b)}$$

The respective multiple correlation coefficients are 0.996 and 0.870. The respective plots of simulated and predicted values are shown in Figures J-10 and J-11. The coefficient of variation of the flow rate ($COV(q)$) can be computed as $COV(q) = S_q / \overline{q}$. Equations J-9a and J-9b can be adjusted to account for various weir coefficients, such as 2.6 for levees and 3.0 for floodwalls. Similar models can be used for flow through open closures.

Equation J-9a is a substitute of Eq. J-8 in the case of random water elevation, which at least assumes that it is applicable for $S_H > 0$. Physically, Eq. J-9a shows that water overtopping is possible even when $H_s < H_p$, i.e., when the water elevation is negative.

The coefficient of variation of the OT volume as given by Eq. J-7 can be evaluated using first-order approximation of a Taylor series expansion at the mean to produce the following estimate:

$$COV_V \cong \sqrt{COV_{C_W}^2 + COV_T^2 + COV_q^2 + COV_L^2} \quad \text{(J-10)}$$

The above equation is based on the assumption of independence for the random variables representing the epistemic uncertainty, and the $COV(H_p)$=0.

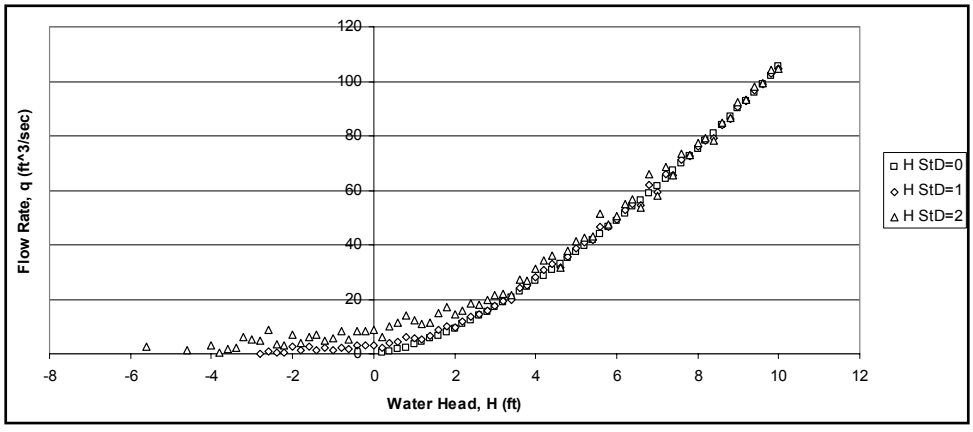

Figure J-9a. Simulated Flow Rate

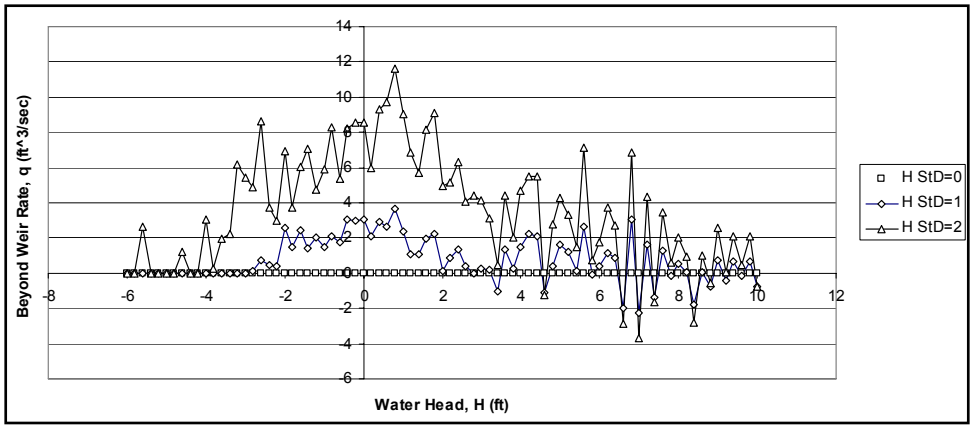

Figure J-9b. Differential Increase in Flow Rate Due to Standard Deviation of Water Head

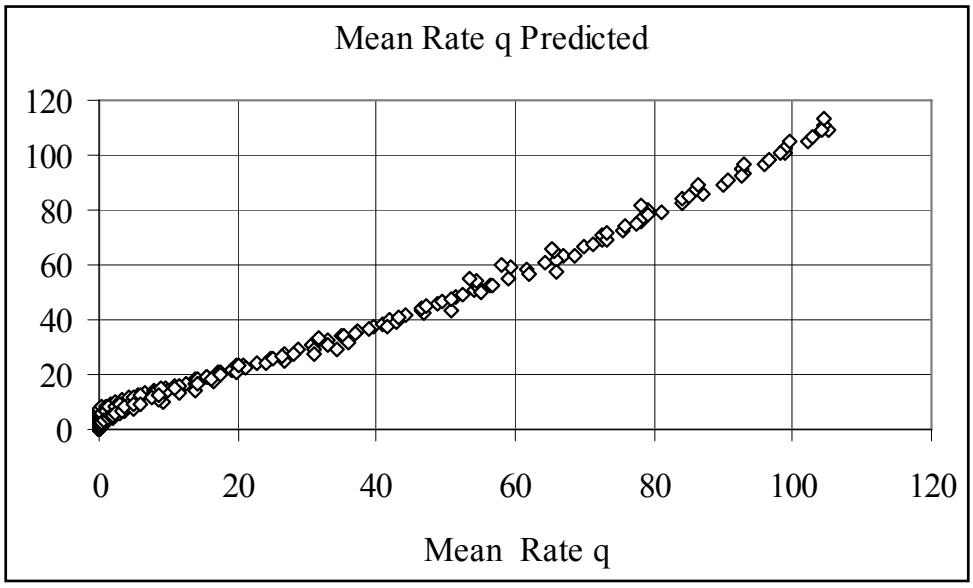

Figure J-10. Mean Rate

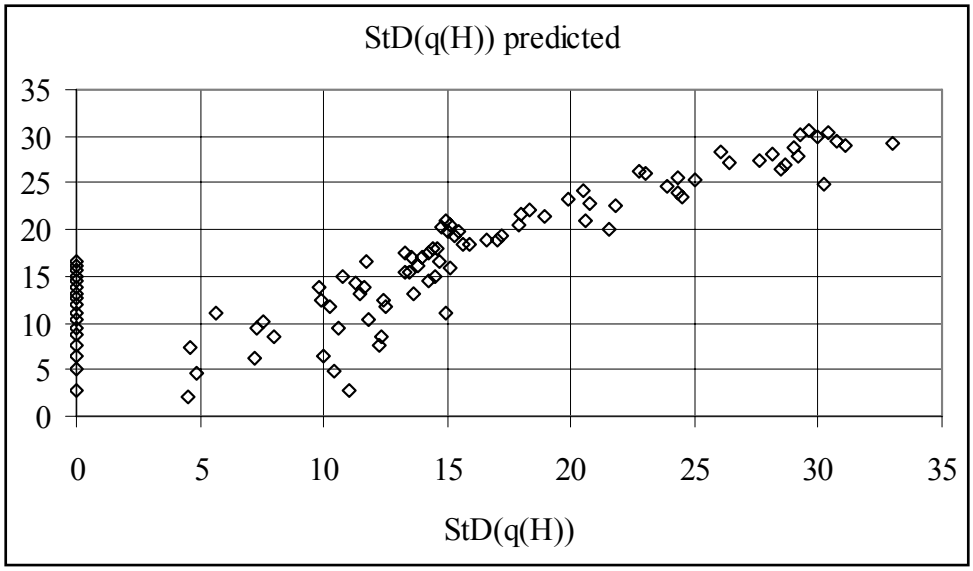

Figure J-11. Standard Deviation of Rate

Overtopping Probability. Probabilities of overtopping can be computed based on a performance function as commonly used in structural reliability assessment (see for example Ayyub 2003; Ayyub and McCuen 2003) as given by

$$Z = R - L \tag{J-11}$$

where Z = performance function, R = strength (resistance) and L = loading in the structure. In this case the resistance is provided by the hurricane protection elevation, and the loading is provided by the surge/wave elevation. The non-performance probability can be computed as

$$P = \text{Prob}\ (g < 0) \tag{J-12}$$

The reliability index for normally distributed random variables is

$$\beta = \frac{\mu_R - \mu_L}{\sqrt{\sigma_R^2 + \sigma_L^2}} \tag{J-13a}$$

where μ_R = mean value of strength R, μ_L = mean value of the load effect L, σ_R = standard deviation of strength R, and σ_R = standard deviation of the load effect L.

The reliability index for lognormally distributed random variables is

$$\beta = \frac{\ln\left(\frac{\mu_R}{\mu_L}\sqrt{\frac{\delta_L^2+1}{\delta_R^2+1}}\right) - \mu_L}{\sqrt{\ln\left(\left(\delta_R^2+1\right)\left(\delta_L^2+1\right)\right)}} \quad \text{(J-13b)}$$

where d = coefficient of variation. Equation J-13b is used in this study. The relationship between the reliability index β and the probability of failure is given by

$$P_f = 1 - \Phi(\beta) \quad \text{(J-14)}$$

where $\Phi(.)$ = cumulative probability distribution function of the standard normal distribution. Additional information on reliability assessment methods including non-normal and correlated random variables is provided by Ayyub (2003), and Ayyub and McCuen (2003).

The cumulative distribution function (CDF) of the total volume for a polder of n reaches can be computed as follows:

$$F_V = \sum_{i=1}^{n} p_i F_{V_i} \quad \text{(J-15)}$$

where p_i = a branch probability in an event tree, and F = CDF. In case of point estimates of flooding per reach, computations can be based on order statistics. Once the total volume is obtained from all overtopping and breach cases, the net volume (as a random variable) needed for consequence analysis can be computed as follows:

$$\text{Net Volume} = \text{Total Volume} + \text{Precipitation} - \text{Pumping Volume} + \text{Pumping Backflow} \quad \text{(J-16)}$$

The pumping volume and backflow are considered as a multiplier called the pumping factor.

Illustrations. As was stated previously, Table J-2 provides typical results for a reach. Four hypothetical reaches were used to construct overtopping results that were aggregated by sub-polders as illustrated in Table J-3. In this example, the polder is assumed to contain only one sub-polder. The overtopping results for this polder include the overtopping (OT) probability, i.e., P(OT), and the overtopping volume based on an overtopping condition, i.e., V|OT. The epistemic uncertainty for the V|OT is also provided. The epistemic uncertainty for the P(OT) is not provided and might not be necessary. Figures J-12 and J-13 show the exceedance rate curves of the P(OT) and V|OT for reach 1 and sub-polder 1, respectively.

Table J-3
Aggregation of Overtopping Volume by Sub-polders and Polders

Summary by Sub-Polders		
1	2	3
To be provided	To be provided	To be provided

Sub-Polder	1			Sub-Polder	2			Sub-Polder	3		
OT Probability		OT Volume (Weir Eq)		OT Probability		OT Volume (Weir Eq)		OT Probability		OT Volume (Weir Eq)	
P(OT)		V|OT		P(OT)		V|OT		P(OT)		V|OT	
Mean	StD	Mean	StD	Prob.	Prob.	Mean	StD	Prob.	Prob.	Mean	StD
Prob.	Prob.	ft^3	ft^3	Prob.	Prob.	ft^3	ft^3	Prob.	Prob.	ft^3	ft^3
1.00E+00	NA	1.893E+09	2.484E+08		TBD		TBD		TBD		TBD
1.00E+00	NA	1.557E+09	2.038E+08		TBD		TBD		TBD		TBD
1.00E+00	NA	1.521E+09	1.985E+08		TBD		TBD		TBD		TBD
1.00E+00	NA	1.020E+09	1.328E+08		TBD		TBD		TBD		TBD
1.00E+00	NA	1.216E+09	1.578E+08		TBD		TBD		TBD		TBD
1.00E+00	NA	9.522E+08	1.232E+08		TBD		TBD		TBD		TBD
1.00E+00	NA	4.893E+08	6.311E+07		TBD		TBD		TBD		TBD
1.00E+00	NA	3.430E+08	4.644E+07		TBD		TBD		TBD		TBD
9.98E-01	NA	2.647E+08	4.066E+07		TBD		TBD		TBD		TBD
9.14E-01	NA	1.488E+08	2.434E+07		TBD		TBD		TBD		TBD
5.39E-01	NA	1.045E+08	1.705E+07		TBD		TBD		TBD		TBD
1.67E-01	NA	7.094E+07	1.156E+07		TBD		TBD		TBD		TBD
3.24E-02	NA	4.622E+07	7.531E+06		TBD		TBD		TBD		TBD
4.95E-03	NA	2.864E+07	4.680E+06		TBD		TBD		TBD		TBD
7.25E-04	NA	1.667E+07	2.746E+06		TBD		TBD		TBD		TBD
1.20E-04	NA	8.957E+06	1.500E+06		TBD		TBD		TBD		TBD
2.60E-05	NA	4.340E+06	7.475E+05		TBD		TBD		TBD		TBD

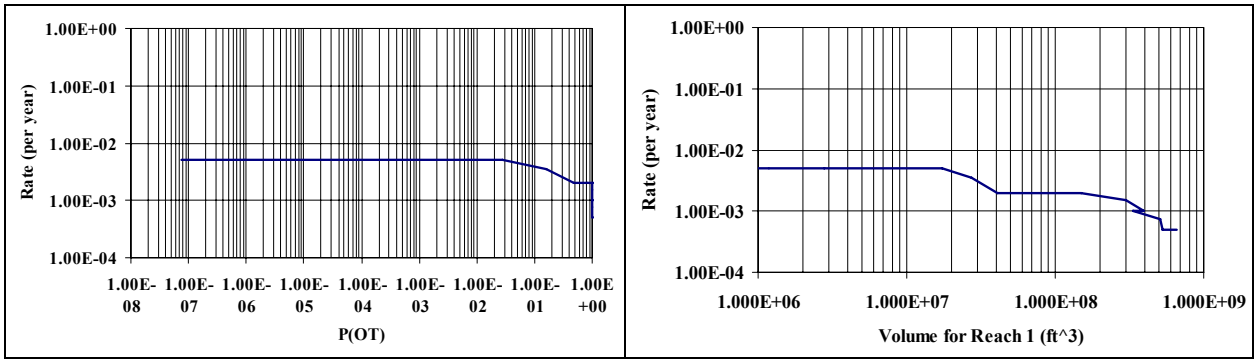

(a) Overtopping Probability (P(OT)) (b) Overtopping Volume (V|OT)

Figure J-12. Exceedance Rate Curves for Reach 1

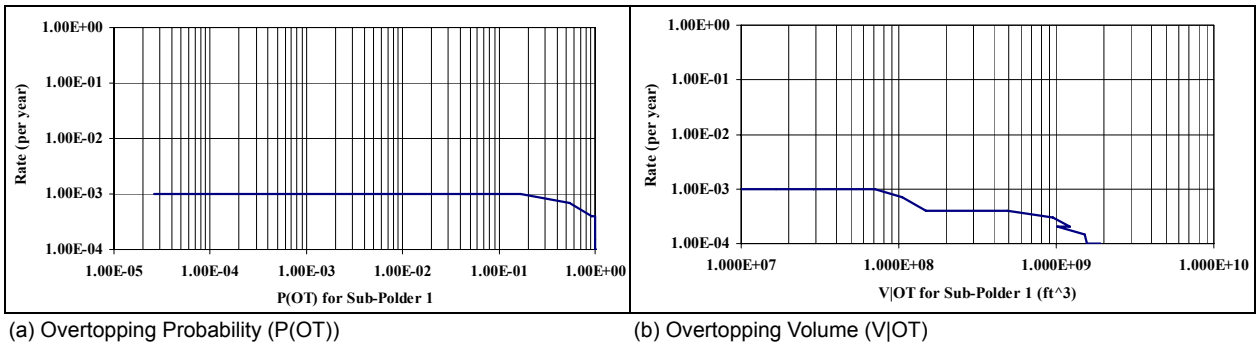

(a) Overtopping Probability (P(OT)) (b) Overtopping Volume (V|OT)

Figure J-13. Exceedance Rate Curve for Sub-Polder 1

Water Volumes from Other Features of the Protection System. The hurricane protection system includes other features that could contribute to water volume making its way to the protected areas during a hurricane. These features include:

1. closure structures that are left open or failed to close
2. localized changes in levee or floodwall elevations that create a gap in the HPS

These features are identified within each reach and assigned to sub-polders in case of nonperformance. For the closure structures case, the water volume resulting from the closure structure for a given hurricane can be computed based on respective closure closing probabilities, width of the closure structure, elevation of the bottom of the structure, and Eqs. J-9a and J-9b. The water volume associated with the localized changes in levee or floodwall elevations requires identifying the changes in elevation and the lengths over which the elevation varies. Sample computations are shown in Table J-4.

Table J-4. Water Volumes from Other Features

Feature	Closures including gates				Feature	Water-tight joints			
Reach number	1	2			Reach number	1			
Sub-Polder allocation	1	1			Sub-Polder allocation	1			
Feature number(s)	1, 2	3, 4, 5			Count	100			
Total width (ft)	100	200							
Feature bottom elevation (ft)	15	14							
Open probability*	0.1	0.5			Failure probability*	0.01			
*COV =	0.15				*COV =	0.15			

Hurricane Runs			Expected Water Volume from Open Closures						Expected Water Volume from Failed Joints				
Run	Rate (R)						Closure Water Volume					Joint Water Volume	
i	Mean	StD					V(C)					V(J)	
			Water Volume|Open		Water Volume|Open		Mean	StD				Mean	StD
ID	event/yr	event/yr	Mean	StD	Mean	StD	ft^3	ft^3				ft^3	ft^3
1	5.00E-04	1.00E-04	3.99E+07	9.99E+06	5.91E+07	1.48E+07	3.353E+07	8.688E+06				3.000E+07	6.000E+06
2	5.00E-04	1.00E-04	3.27E+07	8.19E+06	4.87E+07	1.22E+07	2.762E+07	7.161E+06				3.000E+07	6.000E+06
3	7.50E-04	1.50E-04	3.19E+07	7.97E+06	4.77E+07	1.19E+07	2.702E+07	7.010E+06				3.000E+07	6.000E+06
4	1.00E-03	2.00E-04	2.13E+07	5.32E+06	3.20E+07	8.01E+06	1.815E+07	4.712E+06				3.000E+07	6.000E+06
5	1.00E-03	2.00E-04	2.52E+07	6.31E+06	3.83E+07	9.57E+06	2.167E+07	5.631E+06				3.000E+07	6.000E+06
6	1.50E-03	3.00E-04	1.97E+07	4.91E+06	3.01E+07	7.52E+06	1.700E+07	4.422E+06				3.000E+07	6.000E+06
7	2.00E-03	4.00E-04	1.00E+07	2.51E+06	1.55E+07	3.88E+06	8.753E+06	2.278E+06				3.000E+07	6.000E+06
8	2.00E-03	4.00E-04	7.52E+06	1.88E+06	1.18E+07	2.94E+06	6.634E+06	1.729E+06				3.000E+07	6.000E+06
9	2.00E-03	4.00E-04	8.28E+06	2.65E+06	1.31E+07	3.28E+06	7.383E+06	1.933E+06				3.000E+07	6.000E+06
10	2.00E-03	4.00E-04	5.91E+06	1.89E+06	9.50E+06	3.04E+06	5.343E+06	1.693E+06				3.000E+07	6.000E+06
11	3.50E-03	7.00E-04	4.08E+06	1.31E+06	6.69E+06	2.14E+06	3.754E+06	1.192E+06				3.000E+07	6.000E+06
12	5.00E-03	1.00E-03	2.71E+06	8.69E+05	4.55E+06	1.46E+06	2.547E+06	8.101E+05				3.000E+07	6.000E+06
13	5.00E-03	1.00E-03	1.72E+06	5.50E+05	2.96E+06	9.49E+05	1.654E+06	5.276E+05				3.000E+07	6.000E+06
14	5.00E-03	1.00E-03	1.02E+06	3.28E+05	1.83E+06	5.86E+05	1.018E+06	3.257E+05				3.000E+07	6.000E+06
15	5.00E-03	1.00E-03	5.64E+05	1.80E+05	1.06E+06	3.38E+05	5.845E+05	1.878E+05				3.000E+07	6.000E+06
16	5.00E-03	1.00E-03	2.78E+05	8.90E+04	5.56E+05	1.78E+05	3.059E+05	9.880E+04				3.000E+07	6.000E+06
17	5.00E-03	1.00E-03	1.17E+05	3.75E+04	2.58E+05	8.25E+04	1.406E+05	4.575E+04				3.000E+07	6.000E+06

Breach Elevation and Volume Models.

Three Cases of Breach Failure of Reaches. The risk quantification can be effectively performed by examining three cases of breach failure that correspond to branches presented in the event tree of Figure J-7. The three cases are:

1. breach given overtopping
2. breach given no overtopping
3. breach due to feature failures

The first case of breach given overtopping is primarily driven by erosion resulting from overtopping water flow. The computations of breach failure probability for this case can be performed using Eqs. J-13 and J-14 by considering *R* as *time to breach* and *L* as the *duration of overtopping* provided in

Table J-2. The time to breach is a random variable that can be quantified by its mean and standard deviation, and is a function of water flow and speed, and characteristics of the protection side of the hurricane protection system. Sample computations are shown in Table J-5. The water level in this case is the post-surge level in an adjacent water body. The results should be aggregated by sub-polder using system reliability modeling as discussed in the subsequent sections.

The second case of breach given no overtopping is driven by all applicable failure modes of the levees and walls as discussed in Chapter 5. Sample computations are shown in Table J-6. The water level in this case is the post-surge level in an adjacent water body. The results should be aggregated by sub-polder using system reliability modeling as discussed in the subsequent sections. All failure modes were considered, and exclusions are justified and reported in the reliability analysis chapter. All failure modes for a reach are aggregated into one failure probability as a function of water elevation (i.e., a fragility curve) that accounts for correlations associated with the length of the reach. Therefore, failure probabilities of the reaches can be treated as corresponding to independent events. The epistemic uncertainty in these failure probabilities can be computed that accounts for all the epistemic uncertainties on the strength parameters and modeling aspect of the reliability models.

The third case of breach due to failed features requires computing additional breach probabilities associated with instability of drainage structures and failure of transitions due to erosion. The resulting water levels from these breaches are the post-surge water elevations determined by an adjacent water body on the unprotected side.

Table J-5. Computations Relating to Breach given Overtopping

Reach			Reach 1				Reach 2				Reach 3				Reach 4			
Reach start-end stations			To be provided				To be provided				To be provided				To be provided			
Reach coordinates			To be provided				To be provided				To be provided				To be provided			
Equal allocation to Sub-Polder(s)			1				1				1				1			
Reach length (ft)			2000				1800				2200				2200			
Reach elevation (ft)			16				14				13				13			
Time to breach (sec)*			7200				10800				10800				6000			
COV(time to breach) =		0.5																
Hurricane Runs			Reach 1				Reach 2				Reach 3				Reach 4			
Run	Rate (R)		Surge+Waves		Post-surge elevation		Surge+Waves		Post-surge elevation		Surge+Waves		Post-surge elevation		Surge+Waves		Post-surge elevation	
i	Mean	StD	P(B|OT)		Hps		P(B|OT)		Hps		P(B|OT)		Hps		P(B|OT)		Hps	
			All Modes		Mean	StD	All Modes		Mean	StD	All Modes		Mean	StD	All Modes		Mean	StD
ID	event/yr	event/yr	Mean	StD	ft	ft	Mean	StD	ft	ft	Mean	StD	ft	ft	Mean	StD	ft	ft
1	5.00E-04	1.00E-04	0.12026	0.02405	8	1	0.0247	0.00494	8	1	0.0247	0.00494	8	1	0.2067	0.04135	8	1
2	5.00E-04	1.00E-04	0.12026	0.02405	8	1	0.0247	0.00494	8	1	0.0247	0.00494	8	1	0.2067	0.04135	8	1
3	7.50E-04	1.50E-04	0.20675	0.04135	8	1	0.0538	0.01075	8	1	0.0538	0.01075	8	1	0.3221	0.06442	8	1
4	1.00E-03	2.00E-04	0.12026	0.02405	8	1	0.0247	0.00494	8	1	0.0247	0.00494	8	1	0.2067	0.04135	8	1
5	1.00E-03	2.00E-04	0.35119	0.07024	8	1	0.1203	0.02405	8	1	0.1203	0.02405	8	1	0.4896	0.09791	8	1
6	1.50E-03	3.00E-04	0.35119	0.07024	8	1	0.1203	0.02405	8	1	0.1203	0.02405	8	1	0.4896	0.09791	8	1
7	2.00E-03	4.00E-04	0.12026	0.02405	8	1	0.0247	0.00494	8	1	0.0247	0.00494	8	1	0.2067	0.04135	8	1
8	2.00E-03	4.00E-04	0.12026	0.02405	8	1	0.0247	0.00494	8	1	0.0247	0.00494	8	1	0.2067	0.04135	8	1
9	2.00E-03	4.00E-04	0.35119	0.07024	8	1	0.1203	0.02405	8	1	0.1203	0.02405	8	1	0.4896	0.09791	8	1
10	2.00E-03	4.00E-04	0.35119	0.07024	8	1	0.1203	0.02405	8	1	0.1203	0.02405	8	1	0.4896	0.09791	8	1
11	3.50E-03	7.00E-04	0.35119	0.07024	8	1	0.1203	0.02405	8	1	0.1203	0.02405	8	1	0.4896	0.09791	8	1
12	5.00E-03	1.00E-03	0.35119	0.07024	8	1	0.1203	0.02405	8	1	0.1203	0.02405	8	1	0.4896	0.09791	8	1
13	5.00E-03	1.00E-03	0.35119	0.07024	8	1	0.1203	0.02405	8	1	0.1203	0.02405	8	1	0.4896	0.09791	8	1
14	5.00E-03	1.00E-03	0.35119	0.07024	8	1	0.1203	0.02405	8	1	0.1203	0.02405	8	1	0.4896	0.09791	8	1
15	5.00E-03	1.00E-03	0.35119	0.07024	8	1	0.1203	0.02405	8	1	0.1203	0.02405	8	1	0.4896	0.09791	8	1
16	5.00E-03	1.00E-03	0.35119	0.07024	8	1	0.1203	0.02405	8	1	0.1203	0.02405	8	1	0.4896	0.09791	8	1
17	5.00E-03	1.00E-03	0.35119	0.07024	8	1	0.1203	0.02405	8	1	0.1203	0.02405	8	1	0.4896	0.09791	8	1

Table J-6. Computations Relating to Breach given No Overtopping

Reach			Reach 1				Reach 2				Reach 3				Reach 4			
Reach start-end stations			To be provided				To be provided				To be provided				To be provided			
Reach coordinates			To be provided				To be provided				To be provided				To be provided			
Equal allocation to Sub-Polder(s)			1				1				1				1			
Reach length (ft)			2000				1800				2200				2200			
Reach elevation (ft)			16				14				13				13			
Additional parameter			To be provided				To be provided				To be provided				To be provided			
Hurricane Runs			Reach 1				Reach 2				Reach 3				Reach 4			
Run	Rate (R)		Surge		Post-surge elevation		Surge		Post-surge elevation		Surge		Post-surge elevation		Surge		Post-surge elevation	
i	Mean	StD	P(B|NOT)		Hps		P(B|NOT)		Hps		P(B|NOT)		Hps		P(B|NOT)		Hps	
			All Modes		Mean	StD	All Modes		Mean	StD	All Modes		Mean	StD	All Modes		Mean	StD
ID	event/yr	event/yr	Mean	StD	ft	ft	Mean	StD	ft	ft	Mean	StD	ft	ft	Mean	StD	ft	ft
1	5.00E-04	1.00E-04	0.1	0.05	8	1	0.1	0.05	8	1	0.1	0.05	8	1	0.1	0.05	8	1
2	5.00E-04	1.00E-04	0.2	0.1	8	1	0.2	0.1	8	1	0.2	0.1	8	1	0.2	0.1	8	1
3	7.50E-04	1.50E-04	0.1	0.05	8	1	0.1	0.05	8	1	0.1	0.05	8	1	0.1	0.05	8	1
4	1.00E-03	2.00E-04	0.1	0.1	8	1	0.1	0.1	8	1	0.1	0.1	8	1	0.1	0.1	8	1
5	1.00E-03	2.00E-04	0.1	0.1	8	1	0.1	0.1	8	1	0.1	0.1	8	1	0.1	0.1	8	1
6	1.50E-03	3.00E-04	0.05	0.1	8	1	0.05	0.1	8	1	0.05	0.1	8	1	0.05	0.1	8	1
7	2.00E-03	4.00E-04	0.2	0.1	8	1	0.2	0.1	8	1	0.2	0.1	8	1	0.2	0.1	8	1
8	2.00E-03	4.00E-04	0.2	0.1	8	1	0.2	0.1	8	1	0.2	0.1	8	1	0.2	0.1	8	1
9	2.00E-03	4.00E-04	0.2	0.2	8	1	0.2	0.2	8	1	0.2	0.2	8	1	0.2	0.2	8	1
10	2.00E-03	4.00E-04	0.2	0.05	8	1	0.2	0.05	8	1	0.2	0.05	8	1	0.2	0.05	8	1
11	3.50E-03	7.00E-04	0.2	0.05	8	1	0.2	0.05	8	1	0.2	0.05	8	1	0.2	0.05	8	1
12	5.00E-03	1.00E-03	0.2	0.05	8	1	0.2	0.05	8	1	0.2	0.05	8	1	0.2	0.05	8	1
13	5.00E-03	1.00E-03	0.2	0.05	8	1	0.2	0.05	8	1	0.2	0.05	8	1	0.2	0.05	8	1
14	5.00E-03	1.00E-03	0.2	0.05	8	1	0.2	0.05	8	1	0.2	0.05	8	1	0.2	0.05	8	1
15	5.00E-03	1.00E-03	0.2	0.05	8	1	0.2	0.05	8	1	0.2	0.05	8	1	0.2	0.05	8	1
16	5.00E-03	1.00E-03	0.2	0.05	8	1	0.2	0.05	8	1	0.2	0.05	8	1	0.2	0.05	8	1
17	5.00E-03	1.00E-03	0.2	0.05	8	1	0.2	0.05	8	1	0.2	0.05	8	1	0.2	0.05	8	1

Polder Reliability Analysis. Failure modes, performance functions, basic random variables, and computational procedures of failure probability are provided in the reliability analysis chapter. The failure probabilities of n failure modes for all reaches in a polder are denoted as $p_1, p_2, \ldots, p_n$. The breach failure probability for a polder (P_B) can be computed as

$$P_B(Polder) = 1 - \prod_{i=1}^{n} (1 - p_i) \tag{J-17}$$

Equation J-17 can be used for the cases of probability of breach given overtopping, the probability of breach given non-overtopping, and the probability of breach of features.

Water Elevation and Volume. The hurricane runs are expected to produce the level of flood inundation within a polder after a hurricane surge. The surge hydrograph produced by a hurricane is used to compute the water volume entering a polder during levee overtopping or breaching, and the post-surge water elevation (H_{ps}) within the polder. In the case of levee overtopping, H_{ps} within a polder is based on a water volume computed using the duration of overtopping. If a breach occurs and the invert of the breach is below the final elevation of the adjacent body of water, H_{ps} is the elevation of that body of water. If the breach invert is above the final elevation of the adjacent body of water, H_{ps} is based on a water volume entering the polder computed using the duration that the surge is above the breach invert. The topography of the polder, and the drainage and pumping models provided by Tasks 2,3 and 8 are used to construct such a relationship. An example of this relationship was provided in the 2000

unwatering plan of the greater metropolitan area of New Orleans, LA prepared the District which has figures that relate stage elevation to storage. Figure J-14 shows such a stage-storage plot for the New Orleans East (Citrus). Regression analysis was used to fit a model for this plot. The resulting model with a multiple correlation coefficient of 0.998 is

$$V = 1.8690 \times 10^{7} \left(E + 7.5\right)^{2} + 2.9492 \times 10^{8} \left(E + 7.5\right) \qquad \text{(J-18)}$$

where V = storage volume (ft^3), E = stage elevation (ft), and E domain of -7.5 to 15 ft. These relationships were provided by Tasks 2 and 3 for the risk analysis.

These computations become more complicated when a polder has two or more sub-polders in which flooding is controlled by separate pumping and drainage systems. For the two sub-polder case as an example, the computations of the final volumes can be assessed as follows:

Let

V_1 inflow to sub-polder 1

V_2 inflow to sub-polder 2

V_{1f} final water volume in sub-polder 1

V_{2f} final water volume in sub-polder 2

V_{12f} final water volume for combined sub-polders 1 and 2

C_{12} capacity of sub-polder 1 for water flowing from sub-polder 1 to sub-polder 2

C_{21} capacity of sub-polder 2 for water flowing from sub-polder 2 to sub-polder 1

Figure J-14. Stage-Storage Relationship of New Orleans (Citrus)

The final volumes can be computed as shown in Table J-7.

Table J-7. Polder Inflow Volumes		
Condition	**Model**	**Comments**
Case 1 $V_1 < C_{12}$ and $V_2 < C_{21}$	$V_{1f} = V_1$ and $V_{2f} = V_2$	Provide elevations
Case 2 $V_1 \geq C_{12}$ and $V_2 \geq C_{21}$	Develop and use V_{12f}	Provide elevations
Case 3 $V_1 \geq C_{12}$ and $V_2 < C_{21}$ Case 3.1 $\Delta V_1 = V_1 - C_{12}$ $\Delta V_1 + V_2 < C_{21}$ Case 3.2 $\Delta V_1 = V_1 - C_{12}$ $\Delta V_1 + V_2 \geq C_{21}$	Use $V_{1f} = C_{12}$ and $V_{2f} = V_2 + \Delta V_1$ Use V_{12f}	Provide elevations Provide elevations
Case 4 $V_1 < C_{12}$ and $V_2 \geq C_{21}$ Case 4.1 $\Delta V_2 = V_2 - C_{21}$ $\Delta V_2 + V_1 < C_{12}$ Case 4.2 $\Delta V_2 = V_2 - C_{21}$ $\Delta V_2 + V_1 \geq C_{12}$	Use $V_{2f} = C_{21}$ and $V_{1f} = V_1 + \Delta V_2$ Use V_{12f}	Provide elevations Provide elevations

Water Level and Probability Aggregation Prior to Drainage, Pumping and Backflow. The results from overtopping and breach analysis can be aggregated and summarized in terms of water volume, post-surge elevation, associated probabilities, and epistemic uncertainties. A sample summary is shown in Table J-8.

Table J-8a. Illustrative Water Level and Probability Aggregation for Overtopping Failures

Parameters	
Polder Name	Polder X
Sub-Polder number	1
Sub-Polder Population at Risk	xxxxx
Additional parameter	
Additional parameter	
Additional parameter	

Hurricane Runs			Water Volume (ft^3)											
Run	Rate (R)		Overtopping			Precipitation		Water from Closures&Joints		NOT Subtotal water volume		OT Subtotal water volume	
i	Mean	StD	Probability	Overtopping Volume (V|OT)		Rainfall volume		Water volume		Water volume		Water volume	
			P(OT)	Mean	StD	Mean	StD	Mean	StD	Mean	StD	Mean	StD
ID	event/yr	event/yr		ft^3	ft^3	ft^3	ft^3	ft^3	ft^3	ft^3	ft^3	ft^3	ft^3
1	5.00E-04	1.00E-04	1.000E+00	1.893E+09	2.484E+08	5.000E+07	1.500E+07	6.353E+07	1.056E+07	1.135E+08	1.834E+07	2.006E+09	2.491E+08
2	5.00E-04	1.00E-04	1.000E+00	1.557E+09	2.038E+08	6.000E+06	1.800E+06	5.762E+07	9.342E+06	6.362E+07	9.514E+06	1.620E+09	2.040E+08
3	7.50E-04	1.50E-04	1.000E+00	1.521E+09	1.985E+08	6.000E+06	1.800E+06	5.702E+07	9.227E+06	6.302E+07	9.401E+06	1.584E+09	1.988E+08
4	1.00E-03	2.00E-04	1.000E+00	1.020E+09	1.328E+08	6.000E+06	1.800E+06	4.815E+07	7.629E+06	5.415E+07	7.839E+06	1.074E+09	1.330E+08
5	1.00E-03	2.00E-04	1.000E+00	1.216E+09	1.578E+08	6.000E+06	1.800E+06	5.167E+07	8.228E+06	5.767E+07	8.423E+06	1.273E+09	1.580E+08
6	1.50E-03	3.00E-04	1.000E+00	9.522E+08	1.232E+08	6.000E+06	1.800E+06	4.700E+07	7.453E+06	5.300E+07	7.668E+06	1.005E+09	1.235E+08
7	2.00E-03	4.00E-04	1.000E+00	4.893E+08	6.311E+07	6.000E+06	1.800E+06	3.875E+07	6.418E+06	4.475E+07	6.666E+06	5.340E+08	6.346E+07
8	2.00E-03	4.00E-04	1.000E+00	3.430E+08	4.644E+07	6.000E+06	1.800E+06	3.663E+07	6.244E+06	4.263E+07	6.498E+06	3.856E+08	4.689E+07
9	2.00E-03	4.00E-04	9.977E-01	2.647E+08	4.066E+07	6.000E+05	1.800E+05	3.738E+07	6.304E+06	3.798E+07	6.306E+06	3.027E+08	4.115E+07
10	2.00E-03	4.00E-04	9.142E-01	1.488E+08	2.434E+07	6.000E+05	1.800E+05	3.534E+07	6.234E+06	3.594E+07	6.237E+06	1.847E+08	2.512E+07
11	3.50E-03	7.00E-04	5.390E-01	1.045E+08	1.705E+07	6.000E+05	1.800E+05	3.375E+07	6.117E+06	3.435E+07	6.120E+06	1.388E+08	1.812E+07
12	5.00E-03	1.00E-03	1.670E-01	7.094E+07	1.156E+07	6.000E+05	1.800E+05	3.255E+07	6.054E+06	3.315E+07	6.057E+06	1.041E+08	1.305E+07
13	5.00E-03	1.00E-03	3.237E-02	4.622E+07	7.531E+06	6.000E+05	1.800E+05	3.165E+07	6.023E+06	3.225E+07	6.026E+06	7.848E+07	9.645E+06
14	5.00E-03	1.00E-03	4.949E-03	2.864E+07	4.680E+06	6.000E+05	1.800E+05	3.102E+07	6.009E+06	3.162E+07	6.012E+06	6.026E+07	7.619E+06
15	5.00E-03	1.00E-03	7.246E-04	1.667E+07	2.746E+06	6.000E+05	1.800E+05	3.058E+07	6.003E+06	3.118E+07	6.006E+06	4.785E+07	6.604E+06
16	5.00E-03	1.00E-03	1.204E-04	8.957E+06	1.500E+06	6.000E+05	1.800E+05	3.031E+07	6.001E+06	3.091E+07	6.004E+06	3.986E+07	6.188E+06
17	5.00E-03	1.00E-03	2.597E-05	4.340E+06	7.475E+05	6.000E+05	1.800E+05	3.014E+07	6.000E+06	3.074E+07	6.003E+06	3.508E+07	6.049E+06

Table J-8b. Illustrative Water Level and Probability Aggregation for Breach Failures

Parameters	
Polder Name	
Sub-Polder number	
Sub-Polder Population at Risk	
Additional parameter	
Additional parameter	
Additional parameter	

Hurricane Runs			**Breaches**													
Run	Rate (R)		Reaches		Reaches		Drainage Structures		Transitions		Breach Probability			Post-surge Elevation		
i	Mean	StD	P(B|OT)		P(B|NOT)		P(DS)		P(Transition)		P(B)					
			Mean	StD	Mean	StD	Mean	StD	Mean	StD	Mean	StD		Mean	StD	
ID	event/yr	event/yr	Prob.	Prob.	Prob.	Prob.	Prob.	Prob.	Prob.	Prob.	Prob.	Prob.		ft	ft	
1	5.00E-04	1.00E-04	3.362E-01	4.834E-02	3.439E-01	1.000E-01	1.000E-04	2.000E-05	1.000E-04	2.000E-05	3.36E-01	1.11E-01		8		1
2	5.00E-04	1.00E-04	3.362E-01	4.834E-02	5.904E-01	2.000E-01	1.000E-04	2.000E-05	1.000E-04	2.000E-05	3.36E-01	2.06E-01		8		1
3	7.50E-04	1.50E-04	5.185E-01	7.805E-02	3.439E-01	1.000E-01	1.000E-04	2.000E-05	1.000E-04	2.000E-05	5.19E-01	1.27E-01		8		1
4	1.00E-03	2.00E-04	3.362E-01	4.834E-02	3.439E-01	2.000E-01	1.000E-04	2.000E-05	1.000E-04	2.000E-05	3.36E-01	2.06E-01		8		1
5	1.00E-03	2.00E-04	7.437E-01	1.252E-01	3.439E-01	2.000E-01	1.000E-04	2.000E-05	1.000E-04	2.000E-05	7.44E-01	2.36E-01		8		1
6	1.50E-03	3.00E-04	7.437E-01	1.252E-01	1.855E-01	2.000E-01	1.000E-04	2.000E-05	1.000E-04	2.000E-05	7.44E-01	2.36E-01		8		1
7	2.00E-03	4.00E-04	3.362E-01	4.834E-02	5.904E-01	2.000E-01	1.000E-04	2.000E-05	1.000E-04	2.000E-05	3.36E-01	2.06E-01		8		1
8	2.00E-03	4.00E-04	3.362E-01	4.834E-02	5.904E-01	2.000E-01	1.000E-04	2.000E-05	1.000E-04	2.000E-05	3.36E-01	2.06E-01		8		1
9	2.00E-03	4.00E-04	7.437E-01	1.252E-01	5.904E-01	4.000E-01	1.000E-04	2.000E-05	1.000E-04	2.000E-05	7.44E-01	4.19E-01		8		1
10	2.00E-03	4.00E-04	7.437E-01	1.252E-01	5.904E-01	1.000E-01	1.000E-04	2.000E-05	1.000E-04	2.000E-05	7.31E-01	1.60E-01		8		1
11	3.50E-03	7.00E-04	7.437E-01	1.252E-01	5.904E-01	1.000E-01	1.000E-04	2.000E-05	1.000E-04	2.000E-05	6.73E-01	1.60E-01		8		1
12	5.00E-03	1.00E-03	7.437E-01	1.252E-01	5.904E-01	1.000E-01	1.000E-04	2.000E-05	1.000E-04	2.000E-05	6.16E-01	1.60E-01		8		1
13	5.00E-03	1.00E-03	7.437E-01	1.252E-01	5.904E-01	1.000E-01	1.000E-04	2.000E-05	1.000E-04	2.000E-05	5.96E-01	1.60E-01		8		1
14	5.00E-03	1.00E-03	7.437E-01	1.252E-01	5.904E-01	1.000E-01	1.000E-04	2.000E-05	1.000E-04	2.000E-05	5.91E-01	1.60E-01		8		1
15	5.00E-03	1.00E-03	7.437E-01	1.252E-01	5.904E-01	1.000E-01	1.000E-04	2.000E-05	1.000E-04	2.000E-05	5.91E-01	1.60E-01		8		1
16	5.00E-03	1.00E-03	7.437E-01	1.252E-01	5.904E-01	1.000E-01	1.000E-04	2.000E-05	1.000E-04	2.000E-05	5.91E-01	1.60E-01		8		1
17	5.00E-03	1.00E-03	7.437E-01	1.252E-01	5.904E-01	1.000E-01	1.000E-04	2.000E-05	1.000E-04	2.000E-05	5.91E-01	1.60E-01		8		1

Net Water Level Due to Drainage, Pumping and Backflow. The summary results from Table J-8 can be used in conjunctions with drainage and pumping efficiency, and any backflow potential through the pumps that are functions of water volume and elevations to compute net water volumes. A sample summary is shown in Table J-9.

Table J-9. Illustrative Net Water Level Computations

Parameters		
Polder Name	Polder X	Polder X
Sub-Polder number	1	2
Sub-Polder Population at Risk	xxxxx	xxxxx
Additional parameter		
Pumping factor COV	0.2	0.2
Mean capacity of sub-Polder (ft^3)	??	
StD Capacity of Sub-Polder (ft^3)	??	

Hurricane Runs			Water Volume (ft^3)						Water Volume (ft^3)					
Run	Rate (R)		Overtopping	OT Subtotal water volume		Pumping	Net water volume		Overtopping	OT Subtotal water volume		Pumping	Net water volume	
i	Mean	StD	Probability			Factor			Probability			Factor		
			P(OT)	Mean	StD	(including	Mean	StD	P(OT)	Mean	StD	(including	Mean	StD
ID	event/yr	event/yr		ft^3	ft^3	backflow)	ft^3	ft^3		ft^3	ft^3	backflow)	ft^3	ft^3
1	5.00E-04	1.00E-04	1.000E+00	2.006E+09	2.491E+08	8.000E-01	1.605E+09	3.778E+08	0.000E+00	0.000E+00	0.000E+00	8.000E-01	0.000E+00	TBD
2	5.00E-04	1.00E-04	1.000E+00	1.620E+09	2.040E+08	1.200E+00	1.944E+09	4.595E+08	0.000E+00	0.000E+00	0.000E+00	1.200E+00	0.000E+00	TBD
3	7.50E-04	1.50E-04	1.000E+00	1.584E+09	1.988E+08	1.000E+00	1.584E+09	3.739E+08	0.000E+00	0.000E+00	0.000E+00	1.000E+00	0.000E+00	TBD
4	1.00E-03	2.00E-04	1.000E+00	1.074E+09	1.330E+08	6.000E-01	6.444E+08	1.516E+08	0.000E+00	0.000E+00	0.000E+00	6.000E-01	0.000E+00	TBD
5	1.00E-03	2.00E-04	1.000E+00	1.273E+09	1.580E+08	6.000E-01	7.639E+08	1.798E+08	0.000E+00	0.000E+00	0.000E+00	6.000E-01	0.000E+00	TBD
6	1.50E-03	3.00E-04	1.000E+00	1.005E+09	1.235E+08	6.000E-01	6.031E+08	1.416E+08	0.000E+00	0.000E+00	0.000E+00	6.000E-01	0.000E+00	TBD
7	2.00E-03	4.00E-04	1.000E+00	5.340E+08	6.346E+07	6.000E-01	3.204E+08	7.454E+07	0.000E+00	0.000E+00	0.000E+00	6.000E-01	0.000E+00	TBD
8	2.00E-03	4.00E-04	1.000E+00	3.856E+08	4.689E+07	6.000E-01	2.314E+08	5.415E+07	0.000E+00	0.000E+00	0.000E+00	6.000E-01	0.000E+00	TBD
9	2.00E-03	4.00E-04	9.977E-01	3.027E+08	4.115E+07	6.000E-01	1.816E+08	4.392E+07	0.000E+00	0.000E+00	0.000E+00	6.000E-01	0.000E+00	TBD
10	2.00E-03	4.00E-04	9.142E-01	1.847E+08	2.512E+07	6.000E-01	1.108E+08	2.680E+07	0.000E+00	0.000E+00	0.000E+00	6.000E-01	0.000E+00	TBD
11	3.50E-03	7.00E-04	5.390E-01	1.388E+08	1.812E+07	6.000E-01	8.331E+07	1.989E+07	0.000E+00	0.000E+00	0.000E+00	6.000E-01	0.000E+00	TBD
12	5.00E-03	1.00E-03	1.670E-01	1.041E+08	1.305E+07	6.000E-01	6.245E+07	1.474E+07	0.000E+00	0.000E+00	0.000E+00	6.000E-01	0.000E+00	TBD
13	5.00E-03	1.00E-03	3.237E-02	7.848E+07	9.645E+06	6.000E-01	4.709E+07	1.105E+07	0.000E+00	0.000E+00	0.000E+00	6.000E-01	0.000E+00	TBD
14	5.00E-03	1.00E-03	4.949E-03	6.026E+07	7.619E+06	6.000E-01	3.616E+07	8.555E+06	0.000E+00	0.000E+00	0.000E+00	6.000E-01	0.000E+00	TBD
15	5.00E-03	1.00E-03	7.246E-04	4.785E+07	6.604E+06	6.000E-01	2.871E+07	6.977E+06	0.000E+00	0.000E+00	0.000E+00	6.000E-01	0.000E+00	TBD
16	5.00E-03	1.00E-03	1.204E-04	3.986E+07	6.188E+06	6.000E-01	2.392E+07	6.055E+06	0.000E+00	0.000E+00	0.000E+00	6.000E-01	0.000E+00	TBD
17	5.00E-03	1.00E-03	2.597E-05	3.508E+07	6.049E+06	6.000E-01	2.105E+07	5.558E+06	0.000E+00	0.000E+00	0.000E+00	6.000E-01	0.000E+00	TBD

Sub-Polder and Polder Event Trees. The event tree according to Figure J-7 can be evaluated as shown in Table J-10 for the sub-polders. The water volume and elevation capacities of sub-polders should be determined in order to develop logic rules for water flow among sub-polders. Figures J-15 and J-16 illustrate the resulting risk profiles. Epistemic uncertainty propagation is presently under development and will provide bounds on the results. Non-parametric methods for uncertainty propagation will also be examined.

Table J-10. Risk Profiles of Sub-polders and Polders

Parameters	
Polder Name	Polder X
Sub-Polder number	1
Sub-Polder Population at Risk	xxxxx
Additional parameter	
Additional parameter	
Additional parameter	
Additional parameter	

Hurricane Runs			Water Volume (ft^3)			Breach								
Run	Rate (R)		Overtopping	Net water volume		Breach Rate		Post-surge Elevation		Evacuation Effectiveness	Life Risk		Economic Risk	
i	Mean	StD	Rate			λ.P(B)=λ.(P(B|OT)+P(B|NOT))								
			λ(1-P(B))*P(OT)	Mean	StD	Mean	StD	Mean	StD					
ID	event/yr	event/yr		ft^3	ft^3	Prob	Prob	ft	ft		Mean	StD	Mean	StD
1	5.00E-04	1.00E-04	3.318E-04	1.605E+09	3.778E+08	1.68E-04	6.49E-05	8	1	TBD	TBD	TBD	TBD	TBD
2	5.00E-04	1.00E-04	3.318E-04	1.944E+09	4.595E+08	1.68E-04	1.08E-04	8	1	TBD	TBD	TBD	TBD	TBD
3	7.50E-04	1.50E-04	3.609E-04	1.584E+09	3.739E+08	3.89E-04	1.23E-04	8	1	TBD	TBD	TBD	TBD	TBD
4	1.00E-03	2.00E-04	6.636E-04	6.444E+08	1.516E+08	3.36E-04	2.16E-04	8	1	TBD	TBD	TBD	TBD	TBD
5	1.00E-03	2.00E-04	2.561E-04	7.639E+08	1.798E+08	7.44E-04	2.79E-04	8	1	TBD	TBD	TBD	TBD	TBD
6	1.50E-03	3.00E-04	3.842E-04	6.031E+08	1.416E+08	1.12E-03	4.18E-04	8	1	TBD	TBD	TBD	TBD	TBD
7	2.00E-03	4.00E-04	1.327E-03	3.204E+08	7.454E+07	6.73E-04	4.33E-04	8	1	TBD	TBD	TBD	TBD	TBD
8	2.00E-03	4.00E-04	1.327E-03	2.314E+08	5.415E+07	6.73E-04	4.33E-04	8	1	TBD	TBD	TBD	TBD	TBD
9	2.00E-03	4.00E-04	5.118E-04	1.816E+08	4.392E+07	1.49E-03	8.89E-04	8	1	TBD	TBD	TBD	TBD	TBD
10	2.00E-03	4.00E-04	4.923E-04	1.108E+08	2.680E+07	1.46E-03	4.34E-04	8	1	TBD	TBD	TBD	TBD	TBD
11	3.50E-03	7.00E-04	6.164E-04	8.331E+07	1.989E+07	2.36E-03	7.33E-04	8	1	TBD	TBD	TBD	TBD	TBD
12	5.00E-03	1.00E-03	0.000E+00	6.245E+07	1.474E+07	3.08E-03	1.01E-03	8	1	TBD	TBD	TBD	TBD	TBD
13	5.00E-03	1.00E-03	0.000E+00	4.709E+07	1.105E+07	2.98E-03	9.98E-04	8	1	TBD	TBD	TBD	TBD	TBD
14	5.00E-03	1.00E-03	0.000E+00	3.616E+07	8.555E+06	2.96E-03	9.96E-04	8	1	TBD	TBD	TBD	TBD	TBD
15	5.00E-03	1.00E-03	0.000E+00	2.871E+07	6.977E+06	2.95E-03	9.95E-04	8	1	TBD	TBD	TBD	TBD	TBD
16	5.00E-03	1.00E-03	0.000E+00	2.392E+07	6.055E+06	2.95E-03	9.95E-04	8	1	TBD	TBD	TBD	TBD	TBD
17	5.00E-03	1.00E-03	0.000E+00	2.105E+07	5.558E+06	2.95E-03	9.95E-04	8	1	TBD	TBD	TBD	TBD	TBD

Risk Profile by Polders, Storm Categories, and for the region. The risk profiles for polders, storm categories and the region can be evaluated by performing the corresponding aggregation similar to what is done for the sub-polders, and results can be displayed using similar curves to the ones provided in Figures J-15 and J-16.

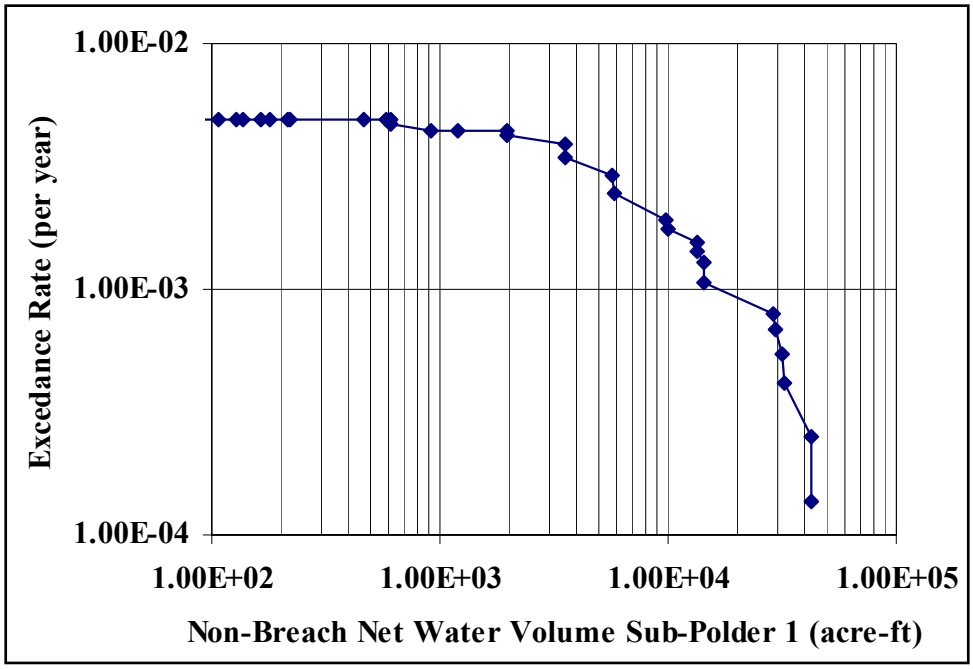

Figure J-15. Overtopping Risk Profile for Sub-Polder 1

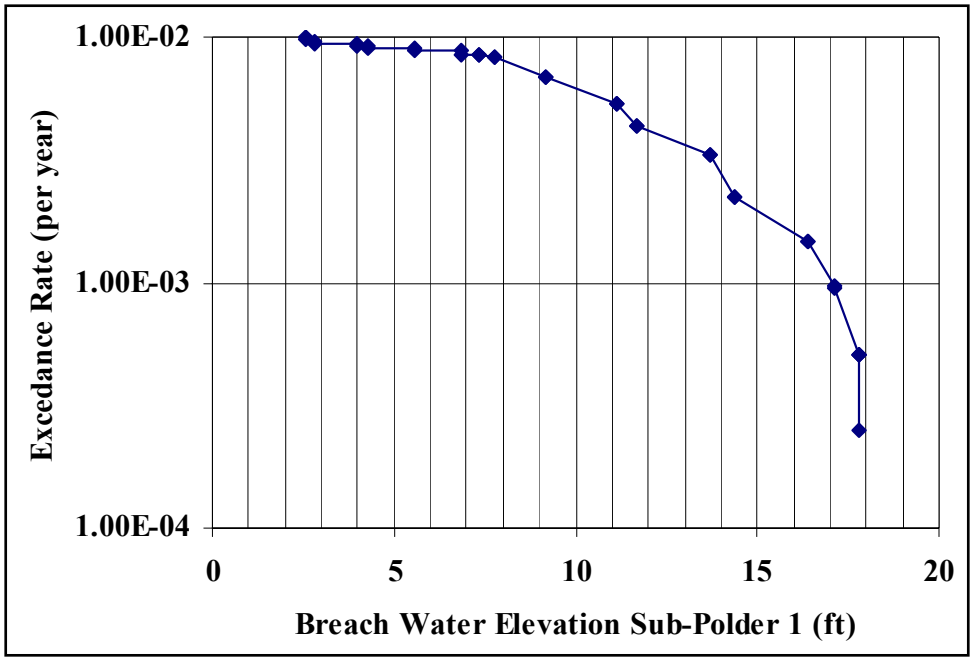

Figure J-16. Breach Risk Profile for Sub-Polder 1

Hazard Analysis and Initiating Events

Several methods have been developed to quantify hurricane hazard, typically in the context of wind-related risk. These methods are classified into three main types: historic (HI), joint-probability (JP), and Monte Carlo simulation (MC) methods.

Historic Methods

Historic (HI) methods quantify the hazard based on the rate at which the effect of interest, L, (e.g. L = wind speed or surge or loss) has occurred in the historical record. These methods are fundamentally nonparametric, i.e. they do not assume a parametric form for the recurrence rate of the hurricanes or their effects. One problem with purely nonparametric historic approaches is the "granularity" of the results that reflects the small number of significant events in the historical record and the sensitivity of the results to unusual occurrences ("outliers") during the observation period. To reduce these effects, some HI approaches include smoothing procedures. For example, the empirical simulation technique (EST) of Sheffner et al. (1996) "smears" the influential historical hurricanes by replacing them with a sweep of hypothetical events with somewhat different characteristics, typically with different landfall locations. Other smoothing methods fit a parametric distribution to the hurricane effects L_i calculated from the historic events. An example of the latter type is the 1987 version of the National Hurricane Center Risk Analysis Program HURISK (Neumann, 1987). The EST method has been extensively used by the USACE and FEMA to identify design events with relatively low return periods, up to

100 years. Confidence intervals on the results are usually obtained through bootstrapping (resampling) techniques.

Joint Probability (JP) Methods

Joint probability (JP) methods make a parametric representation of hurricanes, typically based on their characteristics $\underline{\Theta}$ at landfall and the filling rate after landfall. For example, $\underline{\Theta}$ might include the location and velocity vector, the central pressure deficit, the radius to maximum winds and possibly a few other parameters at landfall. The historic record is used to estimate the recurrence rate $\lambda(\underline{\Theta})$. One then calculates the effects of interest, say $L(\underline{\Theta})$, for a suitable set of $\underline{\Theta}$ values and, by combining $\lambda(\underline{\Theta})$ and $L(\underline{\Theta})$, one obtains the recurrence rate $\lambda(L)$.

The values of $\underline{\Theta}$ for which $L(\underline{\Theta})$ is calculated may form a regular (factorial) discretization of a critical region in parameter space. Alternatively, one may use Monte Carlo simulation or importance sampling to generate a set of values $\{\underline{\Theta}_i\}$ from that region. Factorial discretization and importance sampling are generally preferred when interest is in the tail distribution of L, whereas straight MC simulation is more efficient for short return periods. The MC and importance sampling versions of the JP method may be seen as procedures that replace the actual historical catalog with a much larger synthetic catalog. The JP approach with MC simulation is perhaps the most frequently used method for hurricane wind hazard; see for example Russell (1971), Batts et al. (1980), Georgiou et al. (1983), and Vickery and Twisdale (1995a). If the number of events $\underline{\Theta}_i$ is too large to evaluate the responses L_i with high accuracy, one may use coarser analysis procedures to rank the events or to interpolate the results for a subset of events.

Monte Carlo Simulation Methods

Monte Carlo (MC) simulation methods use a stochastic representation of the origin and temporal evolution of hurricanes in the general region of interest, in this case the North Atlantic region. The random trajectory and parameter evolution are typically represented through Markov processes of suitable order, discrete in time but continuous in state. The state-transition parameters vary spatially and are estimated from the historical record. A large number of hurricane events are simulated using this random dynamic model. The sample is trimmed to retain only the events that are significant to the region and the effects of interest and the retained events are treated like the historical sample in the HI methods. As in the JP method, when the number of retained events is too large to evaluate the responses L_i with high accuracy, one must use parsimonious high-accuracy runs in combination with less accurate methods. The MC simulation method was first proposed by Vickery et al. (2000). More recent studies that use MC simulation are Huang et al. (2001) and Powell et al. (2005).

Choice of a Method

The attractiveness of a method depends in general on the amount of data and computational resources available as well as the objective of the analysis. Regarding the latter, it matters whether (1) interest is in frequent or rare events, (2) the objective is to identify design events with given return periods (return-period analysis) or find the rate at which certain consequences are exceeded (risk analysis), and (3), in the case risk analysis, whether the losses occur in a small geographical region that may be considered uniformly impacted by any given hurricane or over an extended region where spatial homogeneity of the hurricane loads cannot be assumed. For flood hazard, return-period analysis is generally easier than risk analysis because hurricane severity may be ranked using surrogate quantities (such as a rough estimate of maximum surge) that are much easier to calculate than the flooding conditions themselves.

Since medium to long return periods are of interest, historical methods are discarded. Both JP and MC methods can handle such return periods. MC approaches face the problem of sorting out the potentially damaging events from large suites of simulated hurricane scenarios. This is not a trivial problem for the geographically extended and differently vulnerable system we are considering. For these reasons, the joint probability approach has been selected. This approach is further described in the following few sections.

To implement a JP method for hurricane hazard, it is convenient to describe hurricanes at landfall through the parameter vector $\underline{\Theta} = [\Delta P, R_{\max}, X, \theta, V, B]$, where

- ΔP (mB) = central pressure deficit at landfall
- $R_{\max}$ (km) = radius to maximum winds at landfall
- X (km) = longitudinal landfall location relative to downtown New Orleans (positive if east of New Orleans)
- θ (degrees) = direction of storm motion at landfall, ($\theta = 0$ for tracks pointing north, increasing clockwise)
- V (m/s) = storm translation speed at landfall
- B = Holland's radial pressure profile parameter at landfall (Holland, 1980)

While the variation of these parameters before and after landfall is also of interest, our primary characterization of hurricanes is in terms of their properties at landfall. Hence the main tasks of hazard quantification are the estimation of the recurrence rate $\lambda(\underline{\Theta})$ and the evaluation of the environmental loads $L(\underline{\Theta})$ over a suitable range of $\underline{\Theta}$ values. These tasks are described below, together with other issues such as the discretization of $\underline{\Theta}$ space for risk analysis, the treatment of pre- and post-landfall conditions, the use of strategies to reduce the computational effort, and the assessment of epistemic uncertainty.

Hurricane Recurrence at Landfall

The recurrence law for $\underline{\Theta}$ may be written as

$$\lambda(\underline{\Theta}) = \lambda_o f(\underline{\Theta}) \tag{J-19}$$

where $\lambda(\underline{\Theta})$ is the rate density function for $\underline{\Theta}$, meaning that $\lambda(\underline{\Theta})dV$ is the rate of hurricanes with parameters in an infinitesimal volume dV around $\underline{\Theta}$, λ_o is the total occurrence rate in a suitable region of parameter space, and $f(\underline{\Theta})$ is the joint PDF of $\underline{\Theta}$ inside that region.

Information used to estimate λ_o and $f(\underline{\Theta})$ includes historical data sets (mainly NOAA's HURDAT data for λ_o, ΔP, X, θ and V and data on $R_{\max}$ from Ho et al., 1987) as well as published distribution results. The HURDAT data set (Jarvinen et al., 1984, and recent updates) has been used to extract values of (ΔP, X, θ, V) at landfall over the stretch of coastline between longitudes 85W and 95W. For recurrence analysis, we have considered only storms of hurricane strength at landfall (defined as those having measured or estimated $\Delta P \geq 25$ mb) since 1890. Earlier events have been neglected because prior to 1890 the historical record is severely incomplete and less accurate. The HURDAT data set has been used also to analyze pre-landfall conditions.

Information on the structure and parameterization of $f(\underline{\Theta})$ is provided in various references, including Holland (1980), Ho et al. (1987), Vickery and Twisdale (1995a,b), Chouinard et al. (1997), Vickery et al. (2000), Huang et al. (2001), Willoughby and Rahn (2004), and Powell et al. (2005). For the coastal area of interest here, the main findings of these studies are:

- The distribution of ΔP may be assumed to be either lognormal or Weibull. The Weibull distribution tends to give better fits to the data when all tropical storms not just hurricanes are included, whereas the lognormal model is appropriate when only hurricanes are considered; see Vickery and Twisdale (1995a). Using the lognormal model and a locally weighted maximum-likelihood procedure, Chouinard et al. (1997) found that along the Louisiana Coast the standard deviation of ΔP is almost constant at 21 mb, whereas the mean value of ΔP increases eastward from about 32 mb near the Texas border to about 38 mb near the Mississippi border. This trend is attributed to the sea temperature anomaly of the Loop Current.

- Depending on coastal location, the distribution of θ is generally found to be normal or a mixture of two normal distributions, one for easterly storms and the other for westerly storms (Vickery and Twisdale, 1995a; Huang et al., 2001).

- Vickery et al. (2000) found that V may be taken to be lognormally distributed, with mean value about 6 m/s and standard deviation about 2.5 m/s. V has a mild dependence on θ, increasing as θ increases (Vickery and Twisdale, 1995a).

- $R_{\max}$ decreases with increasing hurricane intensity ΔP and its conditional distribution given ΔP may be taken to be lognormal (Vickery and Twisdale, 1995a; Powell et al., 2005). Using data from Ho et al. (1987), Vickery et al. (2000) fitted several linear and quadratic models to $\ln R_{\max}$ against ΔP and latitude. A simple one, with coefficient of determination $R^2 = 0.28$, is $\ln R_{\max} = 2.636 - 0.00005086\Delta P^2 + 0.03949 Lat$. Willoughby and Rahn (2004) obtained qualitatively similar results when regressing $\ln R_{\max}$ against latitude and maximum wind speed. Their logarithmic standard deviation is 0.66.

- B varies with $R_{\max}$ and possibly ΔP or maximum wind speed $V_{\max}$ and latitude (Holland, 1980, Vickery et al., 2000, Willoughby and Rahn, 2004, Powell et al., 2005). For storms of hurricane strength, Vickery et al. fitted several relations using data from different flight height ranges. Their recommended mean value relation is $B = 1.38 + 0.00184\Delta P - 0.00309 R_{\max}$. Willoughby and Rahn (2004) studied the dependence of B on $R_{\max}$, $V_{\max}$, and latitude. These found that the distribution of B is nearly symmetrical and somewhat flatter and shorter-tailed than a normal distribution (in part because their estimation algorithm searches for optimal values between 0.5 and 2.5). Although Willoughby and Rahn estimate a linear dependence of B on $ln\, R_{\max}$, the slope coefficient is only marginally significant. The regression residual has standard deviation 0.36. The data analyzed by Powell et al. (2005) is a subset of that of Willoughby and Rahn. The Powell et al. subset uses selection criteria (high winds, low-level flights, and geographical location) that are relevant also to the present study. Powell et al. find that a good fit for (B| $R_{\max}$, Lat) is given by a truncated normal distribution with mean value 1.881 – 0.0109Lat –0.00557 $R_{\max}$, standard deviation 0.286 (before truncation), and range between 0.8 and 2.2.

The above observations have been used in the modeling of $\lambda(\underline{\Theta})$. However, dependencies, distribution types and parameter values have been sometimes modified based on further data analyses. Two data sets are used: a broad longitude (BL) data set, which includes HURDAT data at landfall for all hurricanes at landfall ($\Delta P \geq 25$ mb) since 1890 that made landfall between longitudes 85W and 95W. The narrow longitude (NL) data set is the subset with landfall locations between 87.5W and 92.5W. The BL and NL data sets include 62 and 32 events, respectively.

- ***Location X and recurrence rate*** λ_o**.** Within both latitude ranges, landfall is approximately uniformly distributed (the uniform distribution easily passes various statistical tests). Using the BL data sets one obtains λ_o = 5.7×10^{-4} per longitude-km per year, with a coefficient of variation of 0.18.

- ***Approach angle*** θ**.** The distribution of θ for both longitude ranges is very nearly normal (tests of normality pass with P around 0.5 with no evidence of bimodality). For the BL data set, which is preferred for statistical accuracy, the normal distribution fit is shown in Figure J-17.

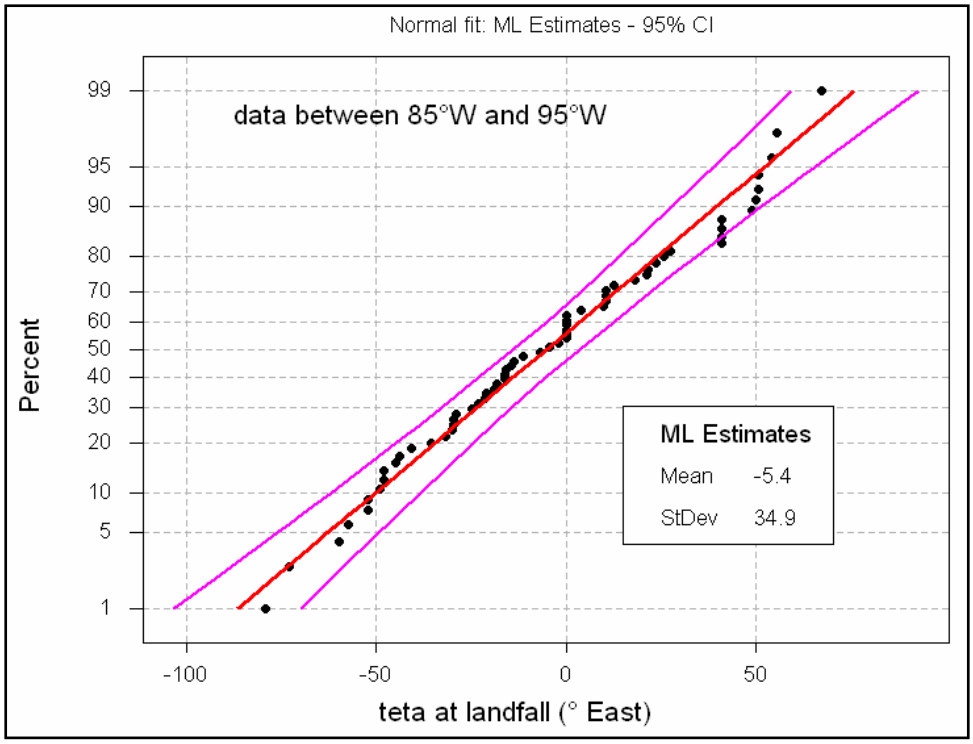

Figure J-17. Normal distribution fit for the approach angle θ

- ***Central pressure deficit ΔP.*** For $\Delta P > 34$ mb, which is the range of interest to us, the BL and NL data are fitted well by nearly identical shifted lognormal distributions, with shift parameter 18 mb, i.e. $(\Delta P - 18)$ has lognormal distribution for $\Delta P > 34$ mb. The four largest values of ΔP in the data set are associated with hurricanes Camilla, Katrina, Carmen, and Betsy. All four hurricanes have occurred inside the narrow longitude range. The slightly more conservative fit obtained from the NL data set, which is the one we prefer, is shown in Figure J-18. The local trend in the mean value of ΔP observed by Chouinard et al. (1997) is small and statistically not significant; hence it is ignored.

- ***Translational speed V.*** The often-used lognormal model is not well supported by our data. Better fits are obtained with a Weibull distribution model. The Weibull fit to the NL data is shown in Figure J-19.

- $\boldsymbol{R_{max}}$. For R_{max} we use the model in Eq. 9 of Vickery et al. (2000), which for Lat = 30N gives

$$\ln(R_{max}) = 3.962 - 0.00567\Delta P + \varepsilon_R \qquad \text{(J-20)}$$

where ε_R is a normal variable with zero mean and standard deviation 0.313.

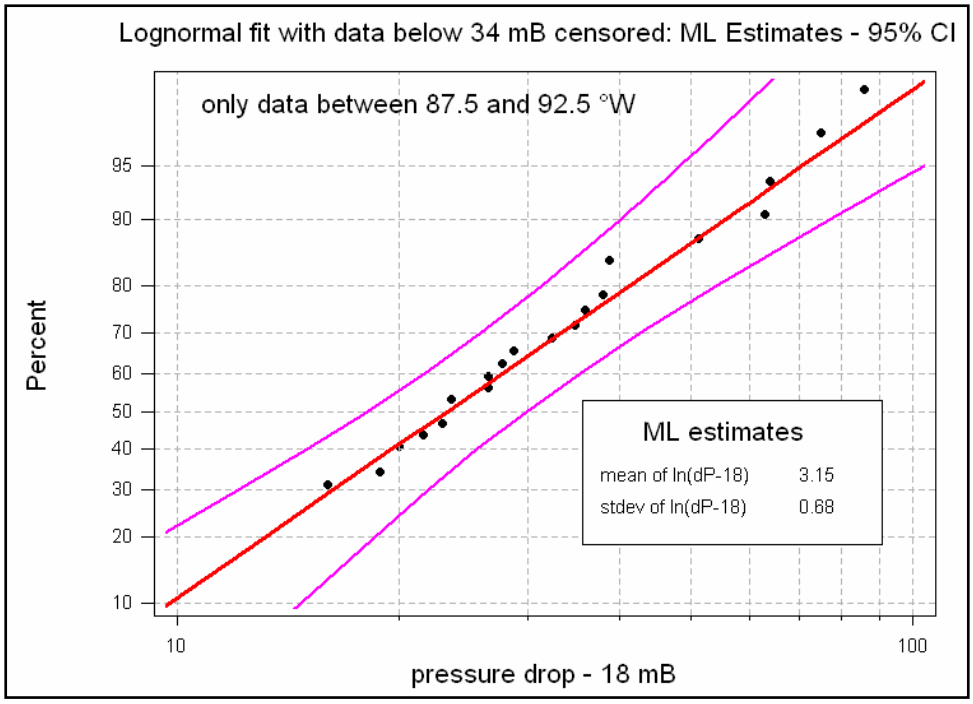

Figure J-18. Lognormal distribution of $(\Delta P - 18)$ fitted to ΔP values above 34 mb in the narrow longitude range

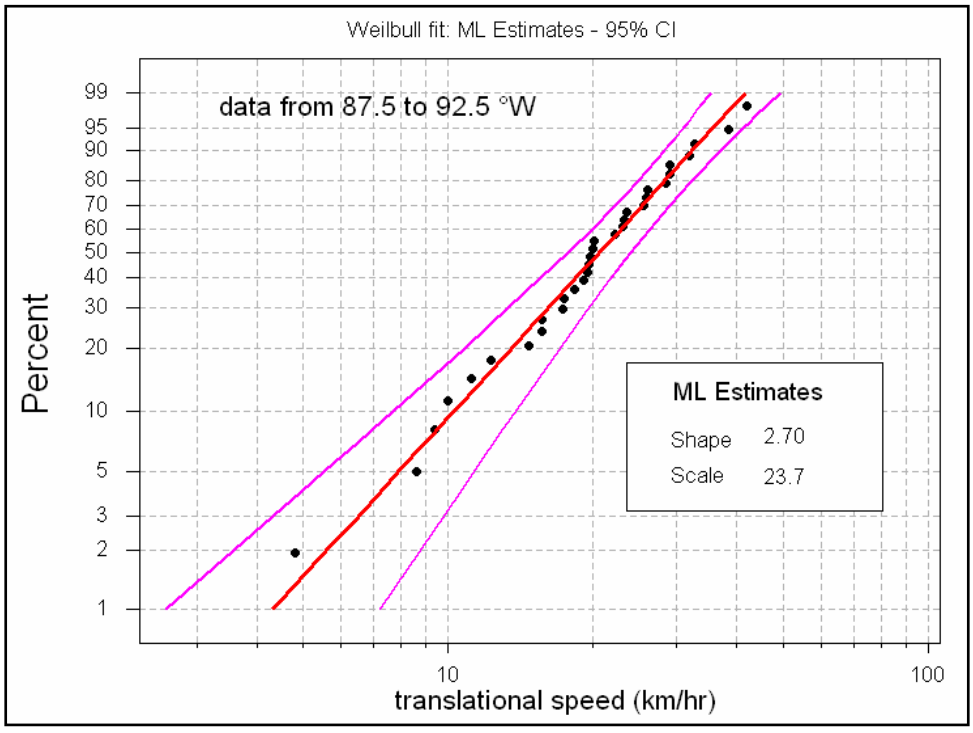

Figure J-19. Weibull fit to storm speed data in the WL data set

- **Holland's *B***. For *B* Powell et al.'s (2005) model is used, which for Lat = 30*N* gives

$$B = 1.554 - 0.00557 R_{\max} + \varepsilon_B \qquad \text{(J-21)}$$

where ε_B is a normal variable with zero mean and standard deviation 0.286.

Pre- and Post-Landfall Parameter Variation

The $\underline{\Theta}$ parameterization concerns exclusively the hurricane characteristics at landfall. One possibility, which has often been used in hurricane hazard analysis, is to assume straight paths and constant values of ΔP, $R_{\max}$, V and B prior to landfall; see for example Russell (1971), Batts et al. (1980), Georgiou et al. (1983), Neumann (1991), and Vickery and Twisdale (1995a). A more refined approach is used for the hurricane path and the pre-landfall variability of these parameters, as described in the following sections.

Pre-Landfall Parameter Variation. All tropical storms (not just hurricanes) after 1890 in the HURDAT record that made landfall within latitudes 85W and 95W are used to estimate the mean hurricane path for landfall angles θ around $-60^\circ, -30^\circ, 0, 30^\circ, 60^\circ$. Results are shown in Figure J-20, where the dots represent average locations at 12 hour intervals relative to the time of landfall. These θ-dependent paths are used in all the hurricane analyses.

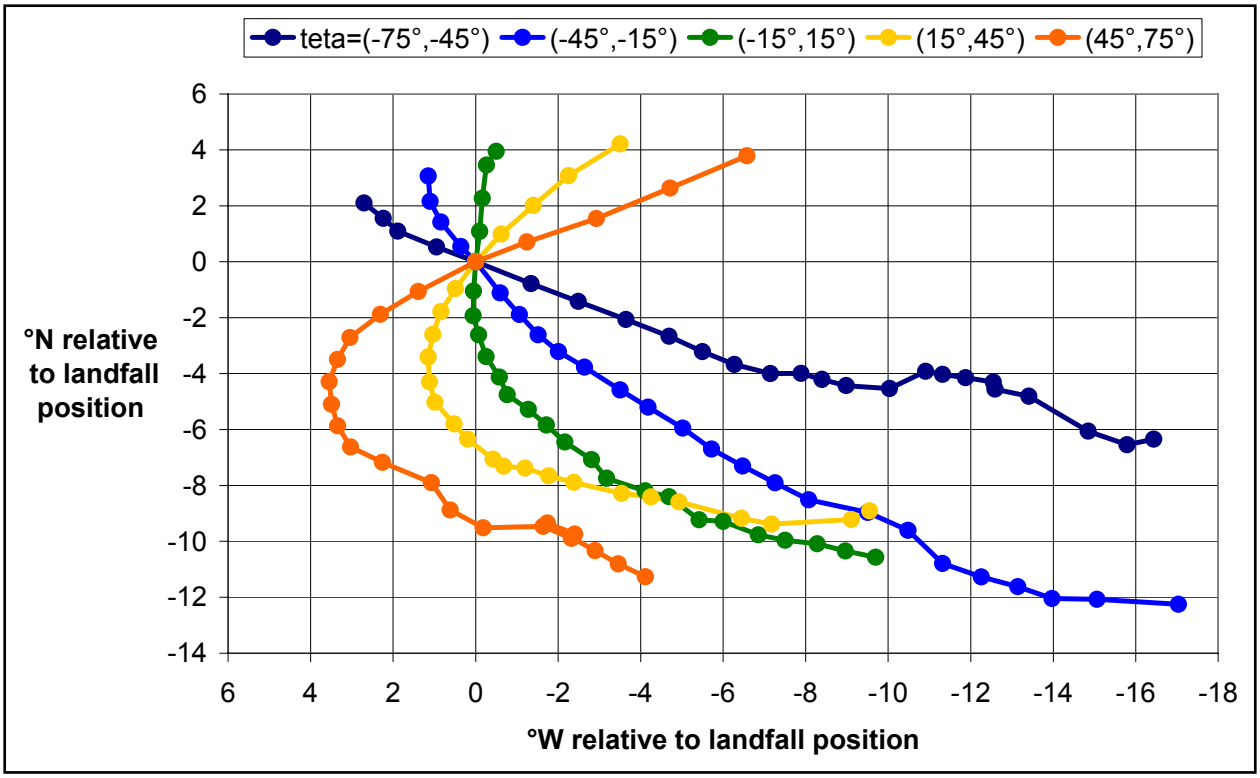

Figure J-20. Mean hurricane path depending on landfall angle θ

The temporal variation of ΔP and V is considered through the ratios

$$\Delta P_R(t) = \frac{\Delta P(t)}{\Delta P}$$
$$V_R(t) = \frac{V(t)}{V} \qquad \text{(J-22)}$$

where t is time before landfall and ΔP and V are the values at landfall (the values for $t = 0$). Dependence of $\Delta P_R(t)$ and $V_R(t)$ on the parameters $\underline{\Theta}$ at landfall has been investigated. While the statistics of $\Delta P_R(t)$ may be taken to be independent of $\underline{\Theta}$, $V_R(t)$ varies significantly with V (and to a negligible extent on the storm direction at landfall, θ). Since the ratios in Eq. J-22 have significant temporal correlation, one may represent their uncertain evolution in time by assuming perfect dependence. Under perfect dependence, one may connect the P-quantile values of $\Delta P_R(t)$ and $V_R(t)$ at different times t to produce single time series, $\Delta P_{R,P}(t)$ and $V_{R,P}(t)$, for each probability P. Figure J-21 shows empirical and smoothed estimates of $\Delta P_{R,P}(t)$ for $P = 0.25$, 0.5 and 0.75. Notice the tendency for ΔP to decrease during the 12 hours prior to landfall. This decrease is likely due to temperature gradients in the Gulf due to the Loop Current and its eddies and perhaps more importantly to the effect of land on the peripheral hurricane winds prior to landfall. In some cases (including hurricane Katrina), this intensity decay is rather pronounced, whereas in others (like

hurricane Camille), it is not. The $\Delta P_R(t)$ profile for Katrina, which is shown in Figure J-21 for comparison, lies within the inter-quartile range and is close to the upper 75% profile during the 18 hours prior to landfall.

Figure J-22 shows similar results for $V_{R,P}(t)$. Since $V_{R,P}(t)$ depends significantly on V at landfall, results are shown separately for $V < 15$ km/h, V between 15 and 25 km/h, and $V > 25$ km/h (the empirical mean values of V within these ranges are close to the values of V used in the analysis; see Section 4).

The temporal profiles of translational speed in Figure J-22 reflect the fact that $V(t)$ is close to a stationary process (with ergodicity in the mean). This is why, for large t, $V(t)$ looses memory of its value at landfall and $V_R(t)$ is small (large) for V large (small).

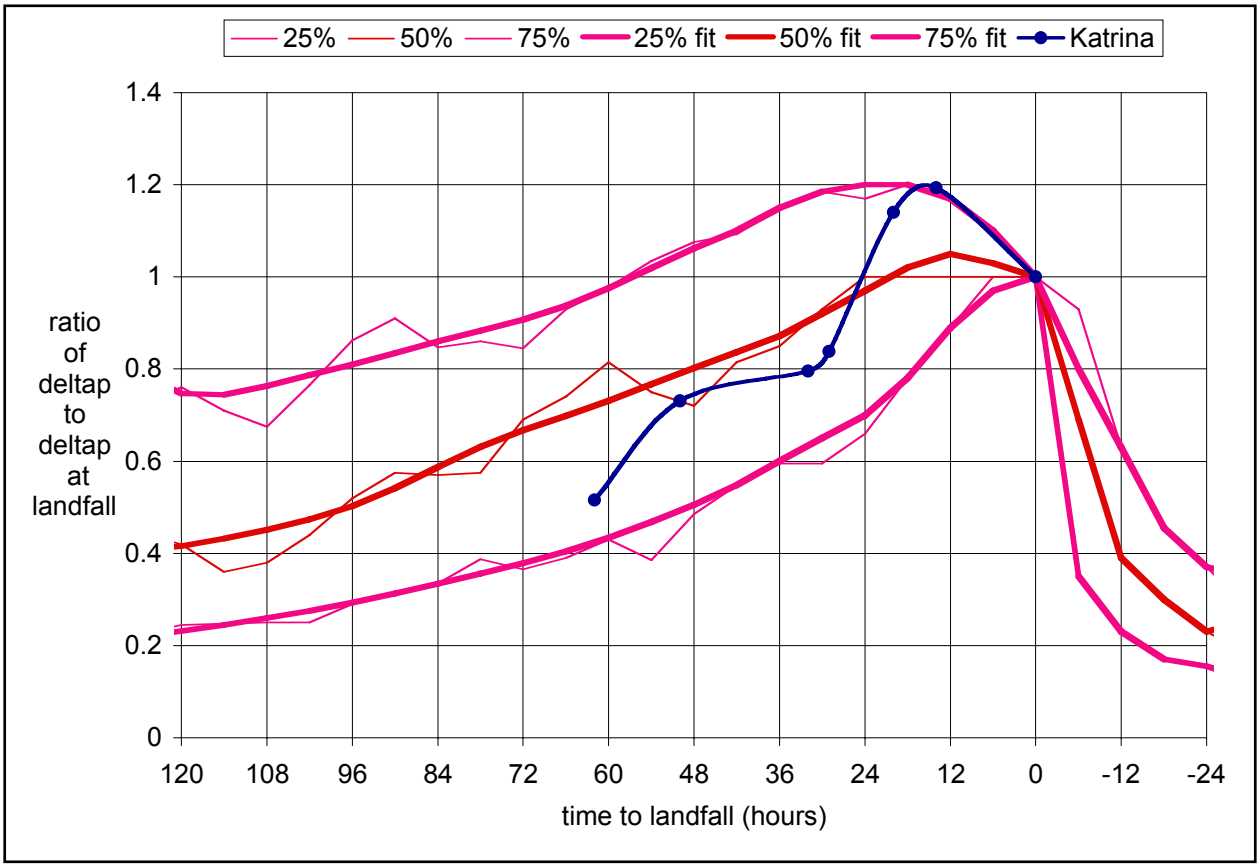

Figure J-21. Pressure deficit ratios $\Delta P_{R,P}(t)$ for P = 0.25, 0.5 and 0.75

HURDAT does not include information on $R_{\max}$ and B. For $R_{\max}$, we use the model in Eq. 7 of Vickery et al. (2000), which gives

$$R_{\max}(t) \propto e^{-0.00005086\Delta P(t)^2 + 0.03949 Lat(t)} \qquad \text{(J-23)}$$

as a first-order adjustment to the value at landfall using $\Delta P(t)$ and $Lat(t)$ along the track.

For B, Powell et al.'s (2005) model is used, which gives the dependence of $B(t)$ on $R_{\max}(t)$ and $Lat(t)$ as

$$B(t) = const. - 0.0109 Lat(t) - 0.00557 R_{\max}(t) \qquad \text{(J-24)}$$

The factor in Eq. J-23 and the constant in Eq. J-24 are adjusted to reproduce the values of $R_{\max}$ and B at landfall. Both equations give a mean-trend corrections along the track. No random temporal fluctuation of $R_{\max}$ or B is considered.

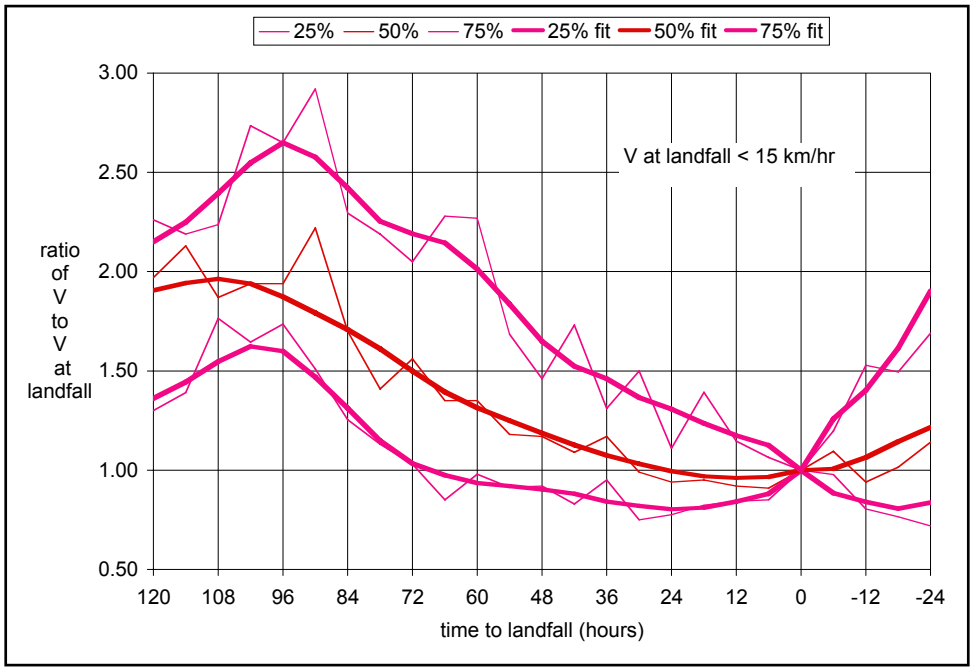

(a) V < 15 km/h

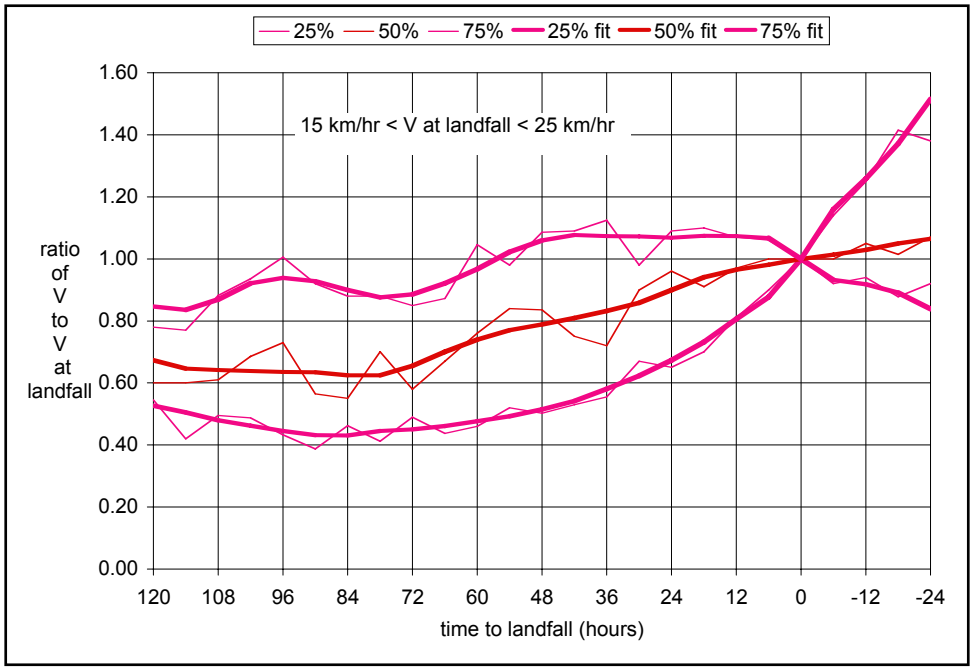

(b) 15 km/r < V < 25 km/h

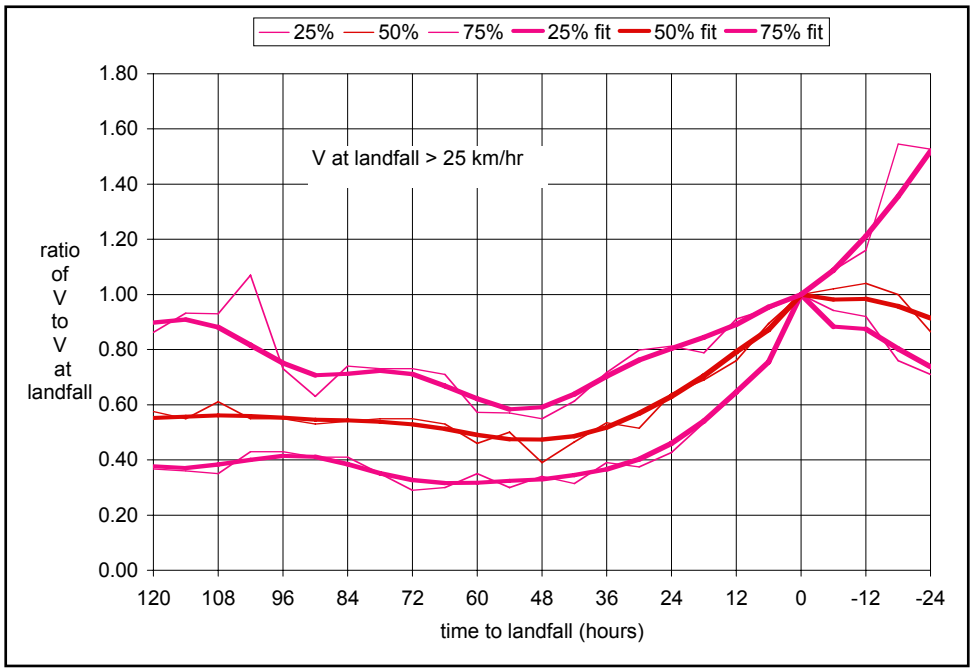

(c) *V > 25 km/h*

Figure J-22. Storm speed ratios $V_{R,P}(t)$ for *P* = 0.25, 0.5 and 0.75 and (a) *V* < 15 km/h, (b) *V* between 15 and 25 km/h, and (c) *V* > 25 km/h

All of the analyses described below in Sections 4.6.2 and 4.6.3 are performed using the mean tracks in Figure J-20, the median ratios $\Delta P_{R,0.5}(t)$ and $V_{R,0.5}(t)$ in Figures J-20 and J-21, and the mean temporal evolutions of $R_{\max}$ and B in

Eqs. J-23 and J-24. The ratios $\Delta P_{R,P}(t)$ and $V_{R,P}(t)$ for $P = 0.25$ and 0.75 in Figures J-21 and J-22 are used to assess uncertainty on the environmental loads due to variability in the pre-landfall values of ΔP and V.

Post-landfall Conditions. After landfall, several hurricane parameters undergo significant changes. For example, the pressure deficit ΔP decreases in an approximately exponential way and the radius of maximum winds $R_{\max}$ tends to increase. The only change that may have significant effect on surges and waves is the temporal decay of ΔP, which generally has the form

$$\Delta P(t) = \Delta P\, e^{-\alpha t} \tag{J-25}$$

where t is time after landfall, ΔP is pressure deficit at landfall, and α is a decay parameter. For t in hours and ΔP in mb, Vickery and Twisdale (1995b) found that for the Gulf of Mexico α has mean value $0.035 + 0.0005\,\Delta P$ and standard deviation 0.0355. These statistics are consistent with data in our narrower longitude range; see quantile plots in Figure J-21 for $t < 0$. Since α is not a sensitive parameter for waves and surges, we use this mean value expression in Eq. J-25 and neglect the variability.

Parameter Discretization for Risk Analysis

Hurricane risk is evaluated by considering a large number of possible scenario hurricanes, each associated with one value of $\underline{\Theta}$. These scenario events are selected considering the joint density $f(\underline{\Theta})$ as well as the potential for induced damage.

For the parameters X and ΔP, which have a generally monotonic effect on the environmental loads, ranges have been that produce moderate to intense effects at the polders. Specifically, for the quantity $X\cos(\theta)$, which measures the minimum distance of the hurricane track from downtown New Orleans, the range [-130, +110] km is used. This choice is based on preliminary sensitivity runs, which indicate that hurricanes at greater distances from New Orleans do not dominate the risk. For the pressure deficit ΔP, we have used the range [41, 130] mb, where 41 mb is a representative value for Cat-2 hurricanes and 130 mb is well into the high Cat-5 range.

The other parameters have effects the sign and magnitude of which depends on location. We have generally varied them within their central 80% or 90% confidence intervals (i.e. the intervals that contain the value of the parameter with probability 0.8 or 0.9), obtained from the recurrence model. For parameters that depend significantly on other parameters, conditional rather than marginal ranges have been used.

The above ranges define a region in parameter space. A possible discretization of this region is given by all combinations of the parameter values listed in Table J-11.

The parameters above the dashed line in Table J-11 refer to conditions at landfall and those below the dashed line are for conditions before or after landfall. The first 3 values of ΔP in Table J-10 are representative of hurricane Categories 2, 3 and 4 whereas the last 3 values represent various levels within Category 5. The values of V approximate the 5%, 25%, 50%, 75%, 95% Weibull quantiles in Figure J-19. Finally notice that smooth $V_{R,0.5}(t)$ curves are shown in Figure J-22 only for some ranges of V. Curves for specific values of V are obtained by first finding the average value of V for each range in Figure J-19 (these average values are close to 8, 21, and 36 km/h) and then interpolating the curves for other values of V of interest.

Table J-11
Parameter levels that may be considered for risk analysis

Parameter	Levels for risk analysis
ΔP (mb)	41, 59, 80, 100, 115, 130
V (km/h)	8, 15, 21, 27, 36
$X\cos(\theta)$ (km)	-130, -90, -50, -10, 30, 70, 110
θ □□□□□□□□	-60, -30, 0, 30, 60
$R_{\max}$	10%, 50%, 90% quantiles from Eq. J-20
B	5%, 25%, 50%, 75%, 95% quantiles from Eq. J-21
----------	----------
$\Delta P_R(t)$	smooth $\Delta P_{R,0.5}(t)$ curve in Figure J-21
$V_R(t)$	smooth $V_{R,0.5}(t)$ curves in Figure J-22 depending on V
$R_{\max}(t)$	from $R_{\max}$, $\Delta P(t)$ and $Lat(t)$; see Eq. J-23
$B(t)$	from B, $R_{\max}$ and $Lat(t)$; see Eq. J-24
α	$0.035 + 0.0005\,\Delta P$
No. of cases	**26,250**

Not all the 26,250 hurricane scenarios in Table J-11 need be considered for risk assessment: some may be excluded because they are exceedingly rare and others because they are unlikely to cause significant losses. For example, hurricanes with small $R_{\max}$ and large $|X|$ do not threat the New Orleans region. Also, depending on the sensitivity of the loads L to each parameter, the number of parameter levels may be reduced. Conversely, if a better representation of a parameter or a more accurate decomposition of risk is required, then the number of levels may be increased. This is especially true for ΔP.

Assessment of Hurricane Loads $L(\underline{\Theta})$

Finding the environmental loads L for each parameter vector $\underline{\Theta}$ of interest is the most challenging task of hurricane hazard characterization. Following is a description of how this is done for still water levels, waves, and rainfall intensity.

Still Water Levels and Waves. It is well known that surge and waves interact (surge affects waves and vice-versa). Therefore, one should ideally assess these loads using a coupled formulation. Sophisticated coupled programs

are currently being developed, but at the present time such programs are not at a stage that they can be routinely used.

An alternative is to follow an iterative approach, whereby one first calculates the surge H(x,y,t) without waves, then estimates the wave field W(x,y,t) given the preliminary estimate of the surge, and finally re-runs the surge code considering the calculated wave field. While the treatment of waves has not been finalized yet, the plan is use a simple wave parameterization scheme based on results obtained in previous detailed analyses. This parameterization approach should produce rather accurate results and greatly streamlines computations (Robert Dean, personal communication). Surges are calculated using the ADCIRC code (Luettich et al., 1992).

ADCIRC uses a triangular grid with spatially varying resolution, which for our application covers the entire Gulf of Mexico. The resolution increases in coastal areas, in particular near the Louisiana Coast. High-resolution grids may include millions of nodes and must be run with time steps on the order of 1 second to avoid numerical problems. Such dense grids produce accurate results and can adequately resolve topographic effects on horizontal scales of tens of meters along the coast.

Since it is not feasible to use such dense computational grids for all the parameter combinations in Table J-11, a different strategy must be adopted, in which one avoids running all cases and those that are run use computational grids at lower resolutions.

Reduction in the Number of ADCIRC Runs. To reduce the number of runs, one can take advantage of two conditions: 1. If dependence of H on a parameter A is smooth, then one may calculate H for a subset of levels of A and use interpolation for the other levels, and 2. If two parameters A and B do not interact (additively or multiplicatively), then the (additive or multiplicative) effect of varying one of them is the same irrespective of the level of the other parameter. In this case one can infer H for all combinations of A and B by varying each parameter while keeping the other parameter constant. Determination of whether either condition applies can be made using a low-resolution (LR) grid with only a few thousand nodes. Moreover, for this purpose one may run ADCIRC just once, ignoring the effect of waves.

These considerations reduce the number of needed ADCIRC runs from about 26,000 in Table J-11 to about 1,000. However, even 1,000 hurricane scenarios are too many to be run with a high-density grid. The strategy selected is to run these cases with a medium-resolution (MR) grid with approximately 90,000 nodes and use the high-resolution (HR) grid for only about 40 cases. The HR runs are then used to calibrate the MR results.

The spatial pattern of surge and waves depends primarily on [$R_{\max}$, X, θ]. Since the effect of these parameters at a given geographic location is generally non-monotonic, interpolation involving these parameters would not produce accurate results. In addition, these parameters interact among themselves. Hence, all combinations of [$R_{\max}$, X, θ] in Table J-11 must be run using the MR model.

The use of only 3 levels of $R_{\max}$ in Table J-11 reduces the computational effort in the MR runs.

The LR runs have shown that, for given [$R_{\max}$, *X, θ*], the water level *H* at each geographical location depends smoothly on ΔP, *V,* and *B*. Hence one may consider a smaller number of levels of these parameters and calculate *H* for the other levels through interpolation. This has led to the MR run plan in Table J-12.

Table J-12
Parameter levels for mid-resolution runs

Parameter	Levels for mid-resolution analysis
ΔP (mb)	41, 80, 115
V (km/h)	8, 21, 36
Xcos(θ) (km)	-130, -90, -50, -10, 30, 70, 110
θ □□□□□□□□	-60, -30, 0, 30, 60
$R_{\max}$	10%, 50%, 90% quantiles from Eq. J-20
B	5%, 50%, 95% quantiles from Eq. J-21
----------	----------
$\Delta P_R(t)$	smooth $\Delta P_{R,0.5}(t)$ curve in Figure J-21
$V_R(t)$	smooth $V_{R,0.5}(t)$ curves in Figure J-22 depending on V
$R_{\max}(t)$	from $R_{\max}$, $\Delta P(t)$ and $Lat(t)$; see Eq. J-23
$B(t)$	from B, $R_{\max}$ and $Lat(t)$; see Eq. J-24
α	0.035 + 0.0005 ΔP
No. of cases	**2835**

One may reduce the number of MR runs even further. From the LR runs, it was determined that the multiplicative effect of Holland's *B* on the surge depends mildly on ΔP and *V*. Therefore there is no need to run different values of *B* with each combination of ΔP and *V*. This produces the MR plan in Table J-13, which comprises two sub-factorials of the levels in Table J-12, with a total of only 1155 runs.

Table J-13 **Final plan for the mid-resolution runs**		
	Mid-resolution model runs	
Parameter	**Factorial 1**	**Factorial 2**
ΔP (mb) V (km/h) *Xcos(□)* (km) □□□□□□□□ $R_{\max}$ B ---------- $\Delta P_R(t)$ $V_R(t)$ $R_{\max}(t)$ $B(t)$ □	41, 80, 115 8, 21, 36 -130, -90, -50, -10, 30, 70, 110 -60, -30, 0, 30, 60 10%, 50%, 90% quantile from Eq. J-20 50% quantile from Eq. J-21 ---------- $\Delta P_{R,0.5}(t)$ from Figure J-21 $V_{R,0.5}(t)$ from Figure J-22 from Eq. J-23 from Eq. J-24 0.035 + 0.0005 ΔP	80 21 -130, -90, -50, -10, 30, 70, 110 -60, -30, 0, 30, 60 10%, 50%, 90% quantile from Eq. J-20 5%, 95% quantiles from Eq. J-21 ---------- $\Delta P_{R,0.5}(t)$ from Figure J-21 $V_{R,0.5}(t)$ from Figure J-22 from Eq. J-23 from Eq. J-24 0.035 + 0.0005 ΔP
No. of runs	**945**	**210**
Total runs	**1155**	

For the HR runs, the subset of 36 hurricanes in Table J-14 is retained. In general, the levels in Table J-14 have been chosen to maximize the accuracy of calibration of the MR results.

Table J-14 **Factorial plan for the high-resolution runs**	
Parameter	**High-resolution model runs**
ΔP (mb) V (km/h) *Xcos(□)* (km) □□□□□□□□ $R_{\max}$ B ---------- $\Delta P_R(t)$ $V_R(t)$ $R_{\max}(t)$ $B(t)$ □	80, 115 21 -90, -10, 70 -60, 0, 60 10%, 90% quantiles from Eq. J-20 50% quantile from Eq. J-21 ---------- $\Delta P_{R,0.5}(t)$ from Figure J-21 $V_{R,0.5}(t)$ from Figure J-22 from $R_{\max}$, $\Delta P(t)$ and $Lat(t)$; see Eq. J-23 from B, $R_{\max}$ and $Lat(t)$; see Eq. J-24 0.035 + 0.0005 ΔP
No. of cases	**36**

Calibration and Extension of the MR Results Using the HR Runs

For the 36 cases in Table J-14, the water levels *H* and the wave characteristics *W* are directly extracted from the HR runs. For the remainder of the cases in Table J-13, which are run only with the MR grid, corrections must be made to

reflect the bias of that coarser discretization. The bias is site-specific, as it depends on the local geometry of the coast, the topography, and the different local land coverage of the MR and HR grids. The correction further depends on the hurricane parameters $\underline{\Theta}$. For example, the correction at a given location generally depends on landfall position X, direction θ, and possibly storm intensity ΔP. Finally, one must consider that our focus is on high water and wave values. The approach that follows reflects these considerations.

Let Y be a generic response of interest, e.g. Y = water level or significant wave height. At each location of interest $k = (x_k, y_k)$ and for each of the 36 events in Table J-14, we calculate $Y_{\max,MR,kj}$ and $Y_{\max,HR,kj}$, the maximum values of Y at k from the MR and HR runs, and the calibration factor

$$\gamma_{Y_{kj}} = \frac{Y_{\max,HR,kj}}{Y_{\max,MR,kj}} \tag{J-26}$$

If $Y_{\max,MR,kj}$ and $Y_{\max,HR,kj}$ fall below some minimum value, the ratio $\gamma_{Y_{kj}}$ is considered "undefined."

Next a distance d_{ij} between any pair of parameter vectors $(\underline{\Theta}_i, \underline{\Theta}_j)$ is defined where $\underline{\Theta}_i$ is the vector for MR case i in Table J-13 and $\underline{\Theta}_j$ is the vector for HR case j in Table J-14. The distance function should reflect the sensitivity of $\gamma_{Y_{kj}}$ in Eq. J-26 to different parameters (if the loads are insensitive to a parameter, differences in that parameter level should be contributing little to d_{ij}).

Finally, the time history $Y_{MR,ki}(t)$ for hurricane i in Table J-13 is corrected using a square-distance weighting scheme. The corrected values, $\hat{Y}_{ki}(t)$, are given by

$$\hat{Y}_{ki}(t) = \left(\frac{\sum_j \gamma_{Y_{kj}} / d_{ij}^2}{\sum_j 1/d_{ij}^2} \right) Y_{MR,ki}(t) \tag{J-27}$$

where the two summations extend over the values of j for which $\gamma_{Y_{kj}}$ is defined.

The previous calibration procedure applies to locations k at which the MR grid produces realistic results. At locations where this is not so, for example along narrow canals where the MR values are not reliable or may not even exist (because the MR grid does not extend to those locations), one must use a different strategy. HR results are used to fit regression relations in terms of values along the coast where the MR solution is available. Then one uses those fitted regressions to extrapolate the estimates from Eq. J-27.

Rainfall Intensity

Rainfall is among the variables that affect the inundation of the polders. While rainfall is not of primary concern for the hurricane protection system, it is a contributor to the frequency of low-level flood losses. Hence it was decided that a relatively coarse model of hurricane-induced rainfall would suffice.

Prior to NASA's Tropical Rainfall Measuring Mission (TRMM) (Simpson et al., 1988), information on hurricane rainfall was scanty. The TRMM mission, which started in November 1997, produced vast amounts of rainfall estimates for tropical storms and hurricanes at a spatial scale of about 5 km in various tropical regions, including the Atlantic basin. These rainfall products have been analyzed statistically by Lonfat et al. (2004) and Chen et al. (2006). The model proposed below is based primarily on these two studies and on discussions with Dr. Shuyi Chen at the University of Miami.

Mean Rainfall Intensity. Hurricane rainfall intensity I (mm/h) varies with distance r from the hurricane center and azimuth β relative to the direction of motion. Moreover, the mean intensity field $m_I(r,\beta)$ varies with the central pressure deficit ΔP, the radius of maximum winds $R_{\max}$, the storm velocity V, and the vertical wind shear S (in the above quoted references, S is measured as the difference between the horizontal wind fields at the 200 and 850 hPa levels). Finally, rainfall intensity displays strong fluctuations at different scales around the mean value $m_I(r,\beta)$.

The azimuthal average of $m_I(r,\beta)$, $m_I(r)$, gives the symmetrical component of the mean rainfall field. This component has a maximum at a distance from the hurricane center close to $R_{\max}$ and decays in an approximately exponential way at larger distances. This decay is contributed by the approximately exponential decay of both the fraction of rainy area and the mean rainfall intensity at the rainy locations. The rate of exponential decay $m_I(r)$ is inversely proportional to the size of the hurricane; hence in good approximation it is inversely proportional to $R_{\max}$.

The value of $m_I(r)$ for $r = R_{\max}$ increases with increasing ΔP, approximately doubling from a Cat2 to a Cat4-5 event. Considering the Cat12 and CAT3-5 results in Lonfat et al. (2004) as representative of the Cat1-2 boundary and of Cat4, respectively, assuming linear dependence of the mean rainfall intensity at $R_{\max}$ on Δp, and fitting an exponential decay with distance as mentioned above, one obtains

$$m_I(r) = \begin{cases} 1.14 + 0.12\Delta P, & for\ r \le R_{\max} \\ (1.14 + 0.12\Delta P)e^{-0.3\left(\frac{r-R_{\max}}{R_{\max}}\right)}, & for\ r > R_{\max} \end{cases} \qquad \text{(J-28)}$$

where m_I is in mm/h and ΔP is in mb.

The asymmetric component of the mean rainfall field, i.e. the way $m_I(r,\beta)$ depends on the azimuth β, is affected mainly by the storm velocity V and the vertical wind shear S. This influence is complex, as the asymmetric pattern and its strength vary with the absolute and relative values of V and S, the relative direction of wind shear and storm motion, the distance r from the center, and the geographic location. For hurricanes in the Atlantic region, there is a general tendency for rainfall to intensify in the front-east quadrant relative to the direction of storm motion and de-intensify in the rear-west quadrant. This tendency is especially evident for fast-moving storms and away from the hurricane center, reaching about 30-40% of $m_I(r)$ for $r \approx 3R_{\max}$. The effect is stronger over land than over water.

Variability of Rainfall Intensity. For each TRMM observation of each hurricane, Lonfat et al. (2004) extracted the average rainfall intensity $\bar{I}^+(r,r+10)$ at rainy locations inside annular regions of 10 km width. Using these values, they found the empirical distribution of $\bar{I}^+(r,r+10)$ for different r and different storm intensity classes. A consistent result is that $\bar{I}^+(r,r+10)$ varies by a factor of about 7 above and below the median value. The standard deviation of $\log(\bar{I}^+(r,r+10))$ corresponds to a factor of about 2-2.5. Hence the variability of this average rainfall intensity is very large.

In addition, there is variability in the fraction of rainy area. The latter variability is not given in Lonfat et al. (2004), but it can be bounded and roughly estimated as follows. The mean fraction of rainy area, m_{F+}, is given by Lonfat et al. as a function of r and storm intensity range. Given m_{F+}, an upper bound to the variance of F^+ is obtained by assuming that F^+ is either 0 (no rain in the region) or 1 (it rains everywhere in the region). In this case $Var[F^+] = m_{F^+}(1-m_{F^+})$, with a coefficient of variation $V_{F^+} = \sqrt{\frac{1}{m_{F^+}} - 1}$. A more realistic estimate of the coefficient of variation is perhaps one half of this theoretical upper bound, or

$$V_{F^+} \approx 0.5\sqrt{\frac{1}{m_{F^+}} - 1} \qquad \text{(J-29)}$$

For distances r up to 150 km, which are those that contribute the most to intense rainfall, m_{F^+} is around 0.9 irrespective of hurricane intensity and Eq. J-29 gives $V_{F^+} \approx 0.17$. This coefficient of variation is much smaller than the coefficient of variation of rainfall intensity inside the rainy area, which is on the order of 1.0. Therefore, the variability of the rainy area may be neglected.

Assessment of Rainfall Intensity Inside the Polders. Based on the above considerations, the following simplified model of rainfall inside the polders is suggested. First the mean rainfall contribution from the symmetric component of

the mean rain field, $m_I(r)$ is selected, then asymmetric component and finally the variability of rainfall around the mean is assessed.

Denote by $m_{I_k}(r,t)$ the temporal variation of $m_I(r)$ for hurricane *k* (in our model, temporal variation is due to the variations of ΔP). The contribution of $m_{I_k}(r,t)$ to the mean rainfall intensity in polder *j* is evaluated as $m_{I_k}(r_{jk}(t),t)$, where $r_{jk}(t)$ is the distance of a representative point of polder *j* from the center of hurricane *k* at time *t*.

For hurricanes that pass to the right or near the polder, the azimuthal dependence of the rainfall field is neglected. For hurricanes that pass to the left of a polder, one may account for the asymmetric component by multiplying the above symmetric mean rainfall values by 1.5. This factor includes intensification due to land effects.

Uncertainty may be expressed by a lognormal random variable with mean value 1 and log standard deviation 0.69, which corresponds to an uncertainty factor of 2. This random factor should be applied to the entire mean rainfall time history. In reality, rainfall intensity inside a polder would display significant fluctuations in time and space, which locally could far exceed a factor of 2. However, the above random factor should adequately reflect uncertainty on the total precipitation in a polder during the passage of a hurricane.

Epistemic Uncertainty

Epistemic uncertainty (uncertainty due to limited information and knowledge) affects all aspects of the hazard characterization. While a thorough assessment of these uncertainties is beyond the scope of this project, a rough quantification of uncertainty on the hurricane rates $\lambda(\underline{\Theta})$ and the loads $L(\underline{\Theta})$ will be made.

General Considerations. The hurricane rates $\lambda(\underline{\Theta})$ are uncertain due to the limited historical sample size, possible errors in the assumed form of marginal and conditional distributions (especially in the tail regions), and the uncertain near-future hurricane activity due to fluctuations and trends associated with climate changes and multi-decadal cycles. A first-order assessment of uncertainty on $\lambda(\underline{\Theta})$ is based on the hurricane effects of global warming and shorter-term climatic fluctuations in the North Atlantic.

Causes of epistemic uncertainty on $L(\underline{\Theta})$ are hurricane model errors, for example the wind field idealization, the coefficient of friction with the water surface, the effects of waves on water level, etc. One can estimate the size of these errors from the skill at hindcasting historical events or by comparing results from different modeling assumptions.

Other epistemic uncertainties are associated with the imperfect calibration of the MR model using the sparse HR results. One may estimate the magnitude of these errors by considering the variability of the calibration factors $\gamma_{Y_{kj}}$ in

Eq. J-26 in hurricane parameter space. Finally, there are interpolation errors when estimating water heights and waves for parameters $\underline{\Theta}$ not used in the MR plan.

Climatic Effects and Their Contribution to Epistemic Uncertainty

The potential effect of global warming on the frequency, size and intensity of tropical cyclones is a hotly debated issue in the technical literature; see Pielke et al. (2005), Emanuel (2005b), and Elsner (2005) for recent reviews. Theoretical analysis, numerical modeling and historical data analysis have all been used to study the effects of climate variations on various features of tropical cyclones. The main results on hurricane frequency and intensity are summarized below. What determines hurricane size is poorly understood; hence the possible dependence of $R_{\max}$ on global warming and other climatic factors is not considered.

Frequency of Tropical Cyclones. It is possible to argue theoretically that global warming could produce either a decrease or an increase in hurricane activity; an ambiguity that is also reflected in the contradictory results produced by different global circulation models (Broccoli and Manabe, 1990; Haarsma et al., 1992; Henderson-Sellers et al., 1998; Houghton et al., 2001).

From an observational viewpoint, the frequency of tropical cyclones worldwide has remained remarkably constant during the past 100 years or more (Elsner and Kocher, 2000; Webster et al., 2005; Emanuel, 2005b). Since during this period the planet has undergone global warming and cooling, one may conclude that climatic changes of this type and magnitude have small effects on the rate of tropical cyclones at the planetary scale.

On the other hand, significant fluctuations in tropical cyclone activity at decadal and multi-decadal scales have occurred in various parts of the world. For example, hurricane activity in the North Atlantic was low in the 1970s, 1980s, and early 1990s compared with the 1940s, 1950s and early 1960s or with the decade since 1995. Changes in hurricane frequency between active and quiescent periods have been by factors of 2 or more (Goldenberg et al., 2001). The current rate in the North Atlantic is about 50% higher than the historical average rate and will likely persist at least over the next 5 years (Elsner, 2005). These fluctuations are due to well-known cycles like the El-Nino-Southern Oscillation (ENSO), which by increasing the wind shear dampens the rate and intensity of hurricanes, the tropical Atlantic sea-surface temperature (SST), with warmer temperatures usually producing higher hurricane rates, and the Atlantic multi-decadal oscillation (AMO), which is the difference in air pressure between Iceland and the Azores and is thought to affect mainly the hurricane tracks (Elsner, 2005).

Intensity of Tropical Cyclones. The effect of global warming on tropical cyclone intensity is somewhat more controversial. It has been argued that an increase in sea surface temperature would make the atmosphere more thermo-dynamically unstable and increase the maximum potential intensity (PI) of hurricanes (Emanuel, 1987; Lighthill et al., 1994; Henderson-Sellers et al.,

1998). In turn, PI has been shown to be highly correlated with the average intensity of hurricanes (Emanuel, 2000). Following this argument, increases in intensity under a warmer climate may be expected (Emanuel, 2005a).

On the other hand, it may also be argued that an increase in sea surface temperature would increase the vertical wind shear, which tends to disrupt the symmetry of tropical cyclones and reduces their intensity.

Empirical evidence of higher hurricane intensity during the past 50 years, when the sea surface temperature has increased by about 0.2 degree centigrade, is weak (Landsea et al., 1999; Bister and Emanuel, 2002; Free et al., 2004; Chan and Liu, 2004). This is in agreement with findings based on global circulation models. For example, Knutson and Tuleya (2004) and Michaels et al. (2005) predict increases in wind speed of 5% or less by the year 2080. Therefore, while future variations in intensity due to global warming are considered possible, it is generally expected that such variations will be modest and overshadowed by the multi-decadal fluctuations.

Results that contrast with this general consensus are reported in Emanuel (2005a). Using data worldwide, Emanuel found that the energy released by hurricanes has increased by about 70% over the past 30 years and attributes the phenomenon to global warming. This phenomenon is contributed by an increase of 15% in the maximum wind speed and an increase of 60% in storm duration. These findings have been contested by other researchers and must be considered preliminary pending further validation.

Epistemic Uncertainty on Future Hurricane Climate. From the preceding discussion, uncertainty on the hurricane statistics in the Gulf of Mexico during the next 50-100 years is dominated by multi-decadal oscillations. Specifically, considering that the North Atlantic is now experiencing a 50% higher-than normal activity and that this elevated activity may persist over a number of years and possibly decades, it is reasonable for the next 50-100 years to increase the average historical rate of hurricanes by 20% and allow for an additional 25% uncertainty factor around this corrected rate. The latter factor includes uncertainty on the historical rate due to the finite observation period (16%) as well as uncertainty on the future evolution of the hurricane frequency (judgmentally assessed).

Considering the general consensus and dissenting views on the effect of global warming on hurricane intensity, the historical mean pressure deficit is increased by 3% and in addition apply a 5% uncertainty factor on the increased mean value. Since the effects of different factors on hurricane frequency and intensity are poorly correlated, these components of epistemic uncertainty may be treated as independent.

Reliability Analysis

As part of the risk and reliability analysis, an evaluation must be made of the conditional probability of failure (i.e., reliability) of structures, systems and

components when they are exposed to the effects (loads) of a hurricane. The analysis has three steps:

1. Specify the structures, components, and systems constituting the hurricane protection system for each polder.

2. Define *failure* and identify failure modes for each structure, system and component; and define a limit or failure state for each failure mode.

3. Assign conditional probabilities (fragilities) of those failure states given hurricane effects.

Two conditions are being analyzed for the reliability of levees, flood walls and pumping stations: (1) pre-Katrina, and (2) post-reconstruction and repair as projected for June.

Summary approach

The reliability of the hurricane protection system (HPS) under potential water surge and wave loadings is quantified using structural and geotechnical reliability models integrated within a larger systems description of each polder. The reliability models for the HPS components are being developed based on design and construction information, and on the results of the Team Seven and Team Eight studies.

Standard reliability models are being used that combine uncertainties in structural material properties, geotechnical engineering properties, subsurface soil profile conditions, and engineering performance models of levees, floodwalls, and transition points. Uncertainties due to spatial and temporal variation (aleatory uncertainty) and due to limited knowledge (epistemic uncertainty) are tracked separately in the analysis, to provide a best estimate of frequency of failures along with a measure of the uncertainty in that frequency.

To date, the reliability model has been developed for the Orleans East (NOE) polder as a means of exercising the approach. The perimeter protection system comprises levees, flood walls, levees with floodwalls on top, and various points of transition or localized facilities such as pumping stations, drainage works, pipes penetrating the HPS, or gates. This perimeter has been divided into reaches that are deemed to be homogeneous in three aspects: structural cross-section, elevation, and geotechnical cross-section. Approximately 20 such reaches have been identified for NOE.

Geometric and engineering properties have been identified for each reach of NOE and summarized in flat-file data tables. Structural cross-sections were initially identified by review of as-build drawings, aerial photographs, and GIS overlays; and were confirmed by on-the-ground reconnaissance by Team 10 members. Elevations were initially assessed in the same reconnaissance, and were later supplemented by LIDAR data and field surveys provided to the Team. Geotechnical cross-sections and corresponding soil engineering properties were derived from the original Design Memoranda for the respective project areas of

the polder, supplemented by site characterization data collected post-Katrina at levee flood wall failure sites (cone penetrometer and laboratory measurements).

Reliability assessments are performed for individual reaches of the HPS for given water levels and loadings. This results in fragility curves for each reach by mode of failure. For each reach and mode of failure, the fragility curve gives the conditional frequency at which a failure state is exceeded. As a first step, engineering performance models and calculations have been adapted from original Design Memoranda. Engineering parameter and model uncertainties are propagated through those calculations to obtain approximate fragility curves as a function of water height on the HPS. These results will later be calibrated against the ongoing work by Task 7, which is applying more sophisticated analysis techniques to similar structural and geotechnical profiles in the vicinity of failures. Failure modes identified by Task 7 will be incorporated into the reliability analyses as those results become available.

Systems risk model. The reliability assessments for individual reaches of the polder perimeter (and possibly of interior levees or walls) are combined in a systems model which brings together the uncertainties in hurricane hazard and HPS fragility to calculate frequencies of volume and duration of flooding within the polder. The systems risk model, embedded in a software application, is structured around an event-tree description of the occurrence of hurricane events, corresponding water and wave heights, and resulting response of the HPS. This model separately tracks aleatory and epistemic uncertainties from both the hurricane hazard and the structural and geotechnical response, producing a best estimate of frequency and duration of flooding, along with measures of uncertainty in those frequencies.

Structures, components, and systems constituting the HPS

Appendices B through F contain a complete inventory of the structures, systems and components that were considered as part of the risk analysis. A list of subsystems and components of the HPS is shown in Table J-15. This is not intended to be exhaustive, but representative.

Failure definitions and limiting states

The HPS for each polder comprises four components: (1) levees, (2) I-walls (which may me atop levees), (3) T-walls (which may be atop levees), and (4) transitions and closures. The reliability analysis examines the performance of the each of these components, separately and in combination.

The following structures in the HPS were not independently evaluated for their failure modes: (1) concrete apron with some I-walls, and (2) sheetpiles with a 3 to 4 ft concrete cap. Either can be addressed with failure modes developed for I-walls.

Table J-15
Components in the Hurricane Protection System.

No.	Sub-system/Components
1	Pump System
	a. Pump and motors
	b. Power – Grid
	c. Emergency Power – Diesel Generator
	d. Diesel Fuel
	e. Pump House Structure
	f. Operators
	g. Intakes
2	Closure
	a. Closure Support Structure
	b. Closure Stop-Logs, Gate or….
	c. Crew Operations
3	Levee Sections
	a. Embankment Section - A levee section must be divided into a series of independent segments. These segments are defined on the basis of physical discontinuities (geometric, physical (e.g., at the closure-embankment juncture)), embankment material/construction characteristics (e.g., correlation lengths either inferred or measured).
	b. Foundation (could be modeled similar to the levee embankment or separate.)
4	Floodwall (Note, as with the case of levee embankments, we will have to consider whether individual wall sections are independent or correlated.)
	a. Wall Structure
	b. Wall-Wall Joint/Interface
	c. Wall Foundation (Embankment Interface)
	d. Wall-Embankment Interface
	e. Sheetpile
	f. Sheetpile-Sheetpile Joint

The following failure modes or contributing factors were not considered in the reliability analysis: (1) On-going settlement of levees or walls due to subsurface consolidation. Existing and planned elevations were used in the analysis. (2) Internal erosion (piping) of levees due to seepage. While sand boils were reported following Katrina, failures did not occur at the same locations. Available geotechnical data for levee designs, and that obtained under IPET, are insufficiently detailed to determine localized weaknesses in the soil (i.e. local sand lenses) that may exist under levees. Internal erosion may be reconsidered in later studies. (3) The effects of maintenance on the HPS capacity over time. Improper maintenance or neglect can lead to reduced capacity of the levees in particular; gates and other moving components also require maintenance. Trees, landscaping, and pools were observed on the protected (landside) embankments after Hurricane Katrina, indicating a lack of enforcement and maintenance of the levees. However, there is insufficient information at present to include maintenance considerations. (4) Impact by a barge or floating tree, or other large object, on the floodwalls or levees. (5) Failure of 3-bulb waterstop.

Component Failure. For each structure, system and component, a performance level is defined such that its occurrence corresponds to a failure to perform an intended function. The critical structures and components within the

HPS, as above, are the levees, I-walls, T-walls, and transitions and closures. These structures and components can fail in a variety of modes. For each mode of failure a limit state is defined, which, if it were to occur would result in a failure to prevent flooding. Limit states differ across the failure modes associated with levee performance and floodwall performance.

From a practical perspective, engineering models of the mechanics of structure or component performance are limited in their ability to explicitly model a 'failure' state. As a result, an analysis is usually carried out for 'incipient' failure (limiting stability). If this state is equaled or exceeded, the structure or component is expected to fail to perform as intended.

System Failure. Depending on the performance of individual structures, systems and components in the HPS, various outcomes may result. For purposes of evaluating the performance of the HPS, the outcome of most interest is whether a protected area is flooded or not.

The HPS is assumed to fail if flooding occurs in a protected area beyond that expected from rainfall and runoff. Given this definition, a failure of the HPS can occur even if the structures or components making up the system do not fail, for example, if levees or wall are overtopped but not breeched.

Flooding can occur as a result of a number of different chains of events that occur individually or in combination. Chains of events that can result in flooding are:

- Levee or floodwall breaching.
- Inflow to an area due to levee or flood wall overtopping (that does not result in breeching) and which exceeds the capacity of the pump system to discharge this inflow.
- Inflow to an area that occurs as a result of rainfall.
- Inflow to an area that occurs when the capacity of the pump system is exceeded as a result of the surge elevation in the canals, resulting in backflow through pumphouses.

From a practical perspective, the events of interest have to do with whether flooding occurs at all and if the flooding is a result of a levee breach. Flooding that occurs as a result of rainfall or overtopping in most cases will not be as consequential and may be mitigated by the pumping system (e.g., failed or not).

Methodological approach

The failure modes that lead to breach of the polder perimeters are associated with four principal failure modes:

1. levee or levee foundation failure
2. levee erosion from overtopping
3. floodwall failure

4. failure modes associated with *point* features such as transitions, junctions and closures

In the case when the perimeter of a polder is breached, it is important to understand whether the number of breaches and their location matter. The losses near a breach may be high due to the sudden release of water, but this damage may be small relative to that which occurs in the entire area inundated by the breach. The location of the breach may, however, be important if there are critical facilities near the breach. At the parish aggregation level, it may matter little how many breaches occur and where except that life loss may be highest at the breach.

A similar consideration concerns the mitigating effects of the pumping system. If the capacity of the pumping system can be exceeded by the inflow volume from a single breach then the number and location of the breaches may not matter and the pumping system can be ignored in the risk analysis.

The nature of uncertainty in reliability analysis. The uncertainties dealt with in the risk analysis are of two types:

Natural variability is associated with the "inherent" randomness of natural processes, manifesting as variability over time for phenomena that take place at a single location (temporal variability), or as variability over space for phenomena at that take place at different locations but at a single time (spatial variability), or as variability over both time and space. This is aleatory uncertainty.

Knowledge uncertainty is attributed to lack of data, lack of information about events and processes, or lack of understanding of physical laws that limits our ability to model the real world. This is epistemic uncertainty.

The adverse performance of elements of mechanical, electrical, and human elements of the HPS, such as pumps, the availability of power, and the closure of gates, is predominantly treated as random (i.e., aleatory) events.

Fragility Curves. Fragility curves summarize the probability of structures, components, or systems reaching their respective limit states (i.e., failure), conditioned on levels of hurricane loading. For example, the fragility curve of Figure J-23 schematically represents the probability of failure by deep-sliding instability of a levee section as a function of water height.

Once the fragility curve for each structure and component failure mode has been determined, an event tree can be quantified in a similar manner. For each sequence in the event tree, a 'sequence' fragility curve is determined by simply evaluating the event tree logic at each successive elevation level. Once each sequence has been evaluated, the composite or total fragility for system failure can be determined for each system performance state of interest, e.g., no flooding has occurred in any area protected by the HPS or flooding as a result of levee/floodwall failure or flooding as a result of rainfall and/or overtopping, by simply summing the fragility curves for the sequences that result in the same state.

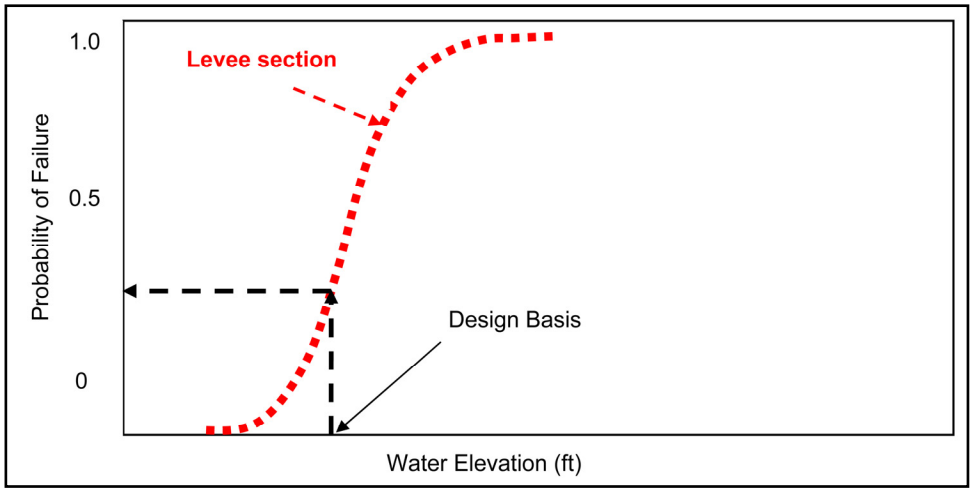

Figure J-23. Illustration of the fragility of a levee section, showing conditional probability of failure by deep-sliding within the foundation soils, as a function of the height of water on the exterior of the levee. Design basis water elevation indicates probability of failure at authorized level.

The total fragility for hurricane protection system, that is the fragility for system failure of any type provides a measure of the reliability of the entire system as a function of peak flood depth.

Fragility curves and failure probabilities

The failure modes included in the reliability analyses to model component performance in the risk analyses of the hurricane protection system (HPS) are defined for use in the appropriate branch segments of the event tree that models the HPS. The events of interest that have been selected to predict component performance are overtopping (O), breach (B), and pumping (U). Shown below are the branch segments analyzed. Where an event is underline, the event is the complement of the even, i.e., O indicates a non-overtopping event. The branch segments from the event tree are: { O, B, U ; O, B, U; O, B, U; O, B, U; O, B; O, B }.

In branches where breaching occurs, it has been assumed that the flow rate of water into the polder exceeds the capacity of the pumping stations (U). The probability of failure for the levees and floodwalls when subjected combinations of overtopping and breaching (O, B; O, B; O, B) are evaluated separately from the performance of the pumping stations.

Failure of a component has been defined as an event where flood waters enter the polder. Only a complete breach of a levee or floodwall is considered; partial breaching is not included. The expression for determining the probability of failure has been included where known in order to identify the information required. All probabilities are conditional upon the flood elevation (and associated hazards, such as wave forces, where applicable).

The following hazards are considered as component loads in the risk analysis: (1) flood elevation - storm surge plus wave setup, (2) breaking waves, (3) flood flow rate and duration for scour and erosion

Levee Failure Modes. Reliability assessments are performed for individual reaches of approximately homogeneous structural type, elevation, geotechnical conditions, and water levels and loadings. This results in fragility curves for each reach by mode of failure. Engineering performance models are adapted from the USACE original Design Memoranda. Engineering parameter and model uncertainties are propagated through those calculations to obtain approximate fragility curves as a function of water height. The geotechnical models used in the DM will be calibrated against the ongoing work by Task 7. Additional failure modes identified by Task 7 will be incorporated into the reliability analyses as they become available.

Shear sliding failure (both shallow and deep). Deep soil failure due to shear capacity of the foundation or levee material being exceeded. The shear resistance of the soils are reduce as seepage occurs until the flood-induced loads exceeds the soil shear capacity. Reliability is based on the probability that shear capacity of the saturated soils is exceeded by the loads on the levee for a given hurricane. A failure along the wedge lines of least resistance (or factor of safety) due to excess pore pressure leading to a shear failure in the soil. Reliability is based on the probability that shear resistance of a wedge is exceeded by the loads on the levee for a given hurricane.

Levee overtopped and erosion breaching. Reliability is based on the probability of overtopping causing erosion of a levee that leads to a breach. Two approaches are considered: The first approach considers flow velocities over the levee. The second approach considers flood elevation, which is an indirect parameter of flow velocity, but is estimated by the storm surge modeling.

The combinations of critical flow velocity and critical duration required to initiate erosion on the protected side of the levee and to continue for a sufficient duration to cause a breach of the levee. Possible approaches for estimating the flow velocity are (1) use of a dam spillway erosion method, or (2) a weir equation coupled with the surge inflow velocity (obtained from the storm surge analysis). Reliability is based on the probability that flow velocities experienced during overtopping exceed the erosion resistance of the soil.

$P_{E\,(x)}$ = *P[flood velocity (x) - critical velocity for soil erosion (x) > 0]*
And/or P[flood velocity duration (x) > critical duration (x)] $P_{OT(x)}$
$P_{E\,(x)}$ = *Probability of erosion failure.*

I-Wall Failure Modes. The two modes of failure due to soil or foundation failure are correlated because each mode relies on the same soil profile. A single P_f will be provided for the first mode of failure at each reach along with an estimate of the epistemic uncertainty for the soil properties and P_f.

Wall pressures failure. Deep soil failure due to shear capacity of the foundation or levee material supporting the I-wall being exceeded. Possible contributing factors: dredging canals to new depths; failure of cut-off barrier

(sheetpile) to prevent seepage under levee. The shear resistance of the soils are reduce as seepage occurs until the flood-induced loads exceeds shear capacity of the soils supporting the I-wall and/or sheetpile. Reliability is based on the probability that shear capacity of the saturated soils is exceeded by the loads on the floodwall for a given hurricane.

$$P_f = P[S_{flood\ level} - S_{capacity} > 0]\ P[flood\ level]$$
Where: P_f *= probability of failure*

Deep shear failure (wedge failure beneath sheetpile). Soil separations develop in front of the sheetpile or the levee resulting in increased hydrostatic forces on the flood side of the I-wall and the levee. If the separation is of sufficient depth, the hydrostatic forces on the wall may exceed the shear strength of the supporting soil and cause failure along wedge lines of least resistance behind the sheetpile. Reliability is based on the probability that shear resistance of a wedge is exceeded by the loads on the levee and floodwall for a given hurricane.

$$P_f = P[S_{flood\ level} - S_{wedge\ capacity} > 0]\ P[flood\ level]$$
Where: P_f *= probability of failure*

I-wall overtopped and erosion breaching.

Failure Mode B4a. Failure by rotation of I-wall, reducing I-wall elevation. This failure mode occurs after significant erosion of the protected (landside) side of the levee due to overtopping by one of the following mechanisms: Either the erosion of excess pore pressure could lead to a failure of the passive wedge behind the I-wall and sheetpile, resulting in a rotation toward the protected side and a crest elevation reduced to ground level (assuming erosion continues once flow increases over rotated I-wall).

$$P_f = P[S_{flood\ level} - S_{wedge\ capacity} > 0]\ P[flood\ level]$$
Where: P_f *= probability of failure*

Failure Mode B4b. Failure of the I-wall and/or sheetpile. A single P_f will be provided for the first mode of failure out of the three modes listed here at each reach along with an estimate of the epistemic uncertainty for the P_f.

Failure Mode B4b-1. Flexural failure of the sheetpile, induced by flood level, dynamic wave forces, and land-side erosion as cantilever length increases as shear and moment capacity are reduced. Reliability is based on the probability that the flexural strength of the sheetpile is exceeded by the moments exerted on it by the flood forces.

$$P_f = P[M_{flood\ level} - M_{sheetpile} > 0\ ]\ P[flood\ level]$$
Where: P_f *= probability of failure*

Failure Mode B4b-2 Flexural failure of the concrete at the sheetpile interface, induced by flood level, dynamic wave forces, and land-side erosion. Reliability is based on the probability that the flexural strength of the concrete is exceeded by the moments exerted on it by the flood forces.

$$P_f = P[M_{flood\ level} - M_{concrete\ section} > 0\ ]\ P[flood\ level]$$
Where: P_f *= probability of failure*

Failure Mode B4b-3. Failure of 3-bulb waterstop at I-wall panel junction, caused by differential loading and displacement between panels, developing tensile, T, and shear, S, forces in the water stop and I-wall panels. This may be due to levee erosion on flood side or dynamic flood and wave forces modifying the rotation point between I-wall panels, or to lateral displacement of the levee from a foundation shear failure. Three-bulb rubber waterstop between panels can fail in 3 modes:

1. Waterstop failure in the rubber material due to tensile or shear load
2. Waterstop pulls out of concrete due to tensile load
3. Concrete fails in tension around waterstop due to tensile or shear load

Reliability is based on the probability that the tensile or shear strength of the waterstop is exceeded by the forces exerted on it by the flood.

$$P_{fS} = P[S_{flood\ level} - S_{capacity} > 0]\ P[flood\ level]$$
Where: P_{fS} *= probability of shear failure*

$$P_{fT} = P[T_{flood\ level} - T_{capacity} > 0]\ P[flood\ level]$$
Where: P_{fT} *= probability of tensile failure*

T-wall with a Levee. T-walls are incorporated into the design for the HPS at locations where structures such as gates or drainage structures require additional foundation support. These T-walls are constructed using a reinforced concrete stem sections founded on battered prestressed concrete pile supports with a sheet pile wall cutoff to depth. These walls are designed to have much lower lateral deflections than I-walls under dynamic flood and wave forces. The T-walls were designed to handle five load conditions including varying conditions of uplift on the base. Overall, these structures performed well during Katrina and were expected to have a lower probability of failure than I-wall structures. A typical T-wall section for the INHC is shown in Figure J-24.

Failure Modes for T-walls. The T-walls were designed based on both pile forces (in both compression and tension) and deflection based on varying subgrade modulus. The design utilized the methods for battered piles presented by Hrennikoff (ASCE, 1950) and Davidson and Gill (ASCE 1963). The base and stem were designed for flexural failure using traditional reinforced concrete design techniques. Flexural failure within the T-wall (between wall and base) could be induced by flood level, dynamic wave forces, and flood-side erosion. The sections were not analyzed using a global stability analysis of the section.

Significant overtopping and erosion around both the flood and protected side of the T-walls did occur Katrina. This will be addressed in the reliability model through uplift calculation. The limit states considered for reliability purposes in this report will be the allowable pile loads (combined axial and bending), allowable deflection of the prestresed concrete piles and flexure failure in the base/stem.

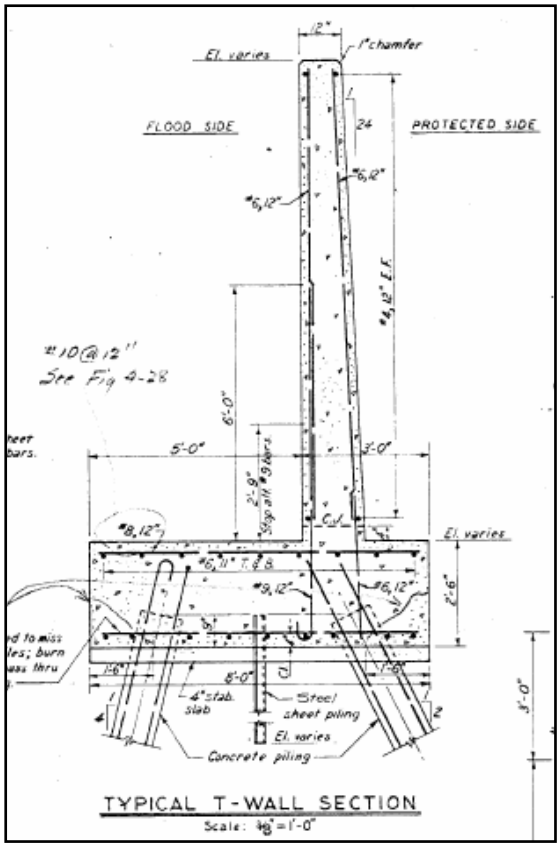

Figure J-24. Typical T-wall Section for INHC

Limit State 1 - Combined pile loads (tension and compression) – The probability of failure is based on the combined axial and bending effects in the concrete piles exceeding unity and would be based on varying pool elevations to determine the fragility curves

$$P_f = P[\frac{f_a}{F_a} + \frac{f_b}{F_b} > 1]$$

where,

f_a = axial load

F_a = allowable axial load

f_b = bending stress

F_b = allowable bending stress

Limit State 2 - Deflection at top of T-wall – The probability of failure is based in the exceedence of a set allowable deflection for the wall and would be based on varying pool elevations to determine the fragility curve. The equation for the probability of failure would be:

$$P_f = P[Y_a - y < 0]$$

where,

Y_a = allowable deflection

y = deflection

Limit State 3 - Flexural Failure – The probability of failure is based on the probability that the flexural strength of the T-wall is exceeded by the moments exerted on it by the flood forces and would be based on varying pool elevations to determine the fragility curves.

$$P_f = P[M_{\text{flood level}} - M_{\text{T-wall-in}} > 0\ ]$$

HPS Transitions and Point Structures. A number of HPS breaches were observed at transitions between HPS components. These breaches were typically at levee/I-wall, levee/T-wall or I-wall/T-wall transitions. Many of the HPS breaches were at point structures such as gates (road and railroad), pump stations, or around drainage control structures. These transitions indicate a weak link in the HPS due to the differing stiffness of the components which permit them to become areas of significant erosion during a hurricane event.

Many of these transitions zones that failed utilize a "wrap-in" levee section to a more rigid wall structure. These levee sections slope quickly away from the transition to expose the I- or T-wall. These steep slopes permit a concentrated zone for the erosion of the levee that will eventually expose the I-wall or T-wall structure to additional loading and continued eroding. This dynamic process will eventually lead to instability and collapse or damage to that transitional section of the wall. An example of a levee transition for a gate section on the east bank of the INHC is shown in Figure J-25 below.

The failure modes for these transitions zones are highly complex and dynamic. The failure modes will utilize the qualitative erosion parameters being developed by IPET Team 7 as the basis for change in the stability of components at the transition zones. Reliability models will be developed based on point structures (gates, control structures, pump stations) as determined from the system definition for each polder.

Failure Mode 1- *Scour and erosion causing point structure instability* - A levee breach may occur due to loss of the supporting I- or T-walls at a point structure and scour could create instability and collapse of the structure creating a breached area. This change in stability is due to erosion and scour around the drainage structure and the fragility curve will be based on varying the water elevation. The probability of failure is based on driving and resisting forces as:

$$P_f = P[\text{Resisting Forces} - \text{Driving Forces} < 0\}$$

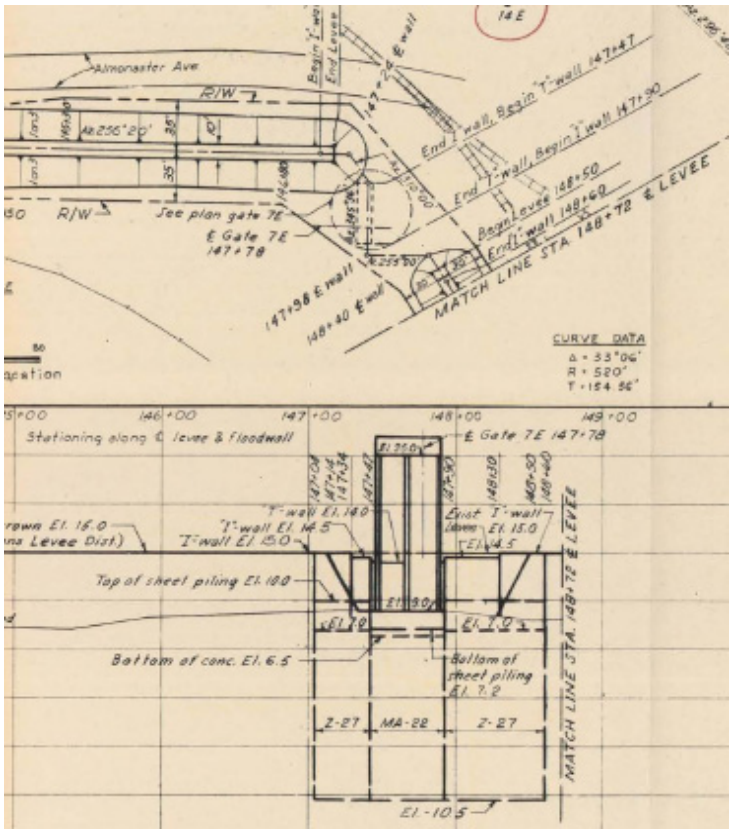

Figure J-25. Example of Transition Zone for East Bank of INHC

Failure Mode 2 - *Breach at the water stop between the I-wall and T-wall panel junction* - This failure mode may be caused by differential displacement between panels develops tensile, T, and shear, S, forces in the water stop and panels. This may be due to levee erosion on the flood side or different rotation point between panels, or to lateral displacement of the levee from a foundation shear failure. Water stops between panels can fail in 3 modes:

1. Waterstop failure in the rubber material due to tensile or shear load
2. Waterstop pulls out of concrete due to tensile load
3. Concrete fails in tension around waterstop due to tensile or shear load

The fragility curve will be based on varying the water elevation and the probability of failure is tensile and shear forces in the water stops as:

$$P_{fS} = P[S_{flood\ level} - S_{capacity} > 0]$$
$$P_{fT} = P[T_{flood\ level} - T_{capacity} > 0]$$

Failure Mode 3 - *Breach at the levee and I-wall transition* - This failure mode may occur due to levee erosion on the protected side, where the erosion starts at the end of the levee transition and progresses back toward the I-wall, until the I-wall rotates toward the protected side. Either the erosion of excess pore pressure could lead to a failure of the passive wedge behind the I-wall and sheetpile, resulting in a rotation toward the protected side and a crest elevation

reduced to ground level (assuming erosion continues once flow increases over rotated I-wall).

$$P_f = P[S_{flood\ level} - S_{wedge\ capacity} > 0]$$

Pumping Stations. The pumping stations are critical HPS system components because they maintain the flood levels on the protected side. Unfortunately, many of the pumping stations during Katrina reached and exceeded their pumping capacity shortly into the storm. Their reliability during Katrina was not exceedingly high as the stations primarily failed due to rising waters at the plants, a lack of external or backup power source, or were shut down due to inefficient pumping. These systems are designed to handle specific level of rainfall and are easily overwhelmed when the levees are overtopped by a hurricane event.

The following failure modes are possible for the pumping stations:

a. Interior flooding of station
b. Loss of power
    1. No commercial power
    2. Back up generator fails
        (a) Mechanical
        (b) Fuel unavailability
c. Pumps not functioning at time of incident
d. Mechanical failure of components
e. Operator unavailability
f. Debris blocking intakes
g. Reversed or back flow through outfall pipes

The reliability of the pumping stations will be included into the risk model as point sources. The reliability will be based on data collected on the pumping stations, performance data maintained by Task Force Hope, and information from the dewatering plan for New Orleans developed by the New Orleans District. The fragility curves for each pumping stations will need to be limited to a specific elevation or volume of water within the polder. These fragility curves will vary for each pumping station and will reflect the interior drainage areas and back flow potential.

Consequences

The primary output of the risk and reliability modeling of Team 10 will be an estimate of the probability of life loss and physical damage relating to the performance of the hurricane protection system in southeastern Louisiana. The three scenario cases which are being considered: 1) the pre-Katrina (August 28, 2005) risk, 2) the actual Katrina experience, and 3) the risk associated with conditions as of June 1, 2006. A probabilistic estimate of losses (life and property) will be provided.

Team 10 is working in close collaboration with Team 9 (Consequences) to ascertain appropriate relationships of inundation, impact and life and property loss. Team 9 is considering consequences in four areas: 1) economic consequences, including direct damage and indirect losses, at local, regional and national level; 2) environmental consequences; 3) social, cultural and historical consequences, and; 4) life safety and health consequences.

As of mid-February, the work of Team 9 has been initiated, but limited data has been collected and no firm inputs are available to the modeling effort of Team 10. Team 10 members providing liaison with Team 9 have contributed to the refinement of the flood life loss model (lifesim) and have established contact with the Louisiana State University Hurricane Center and Team Louisiana which have been tasked with the State of Louisiana to carry out forensic evaluation of the Katrina event.

Issues of interface between team activities remain a major concern. Attempts are underway to clarify the necessary input to model consequences in the categories mentioned above. It had earlier been assumed that a maximum flood elevation in each sub-folder would provide sufficient characterization of the event to generate consequence estimates. In further discussion with subgroups of Team 9, it is evident that for the case of life loss several factors are considered of critical importance including rate of inundation, duration of inundation, and velocity of flow. These factors relate to the feasibility of evacuation and rescue to prevent life loss. For physical damage, it is also possible that these characteristics will be desirable for the refinement of loss estimates. Social and demographic data is also required for the life loss estimation. This data is currently being collected but has not been analyzed to develop useful relationships for the risk model. Detailed analysis of fatality data is still required to relate socio-economic demographic information to specific risk factors for fatality. The application of the flood life loss model (lifesim) requires more detailed consideration of both evacuation and rescue procedures. That evaluation will be carried out by the Consequences team.

The Risk team is developing risk and reliability models which will be calibrated by earlier events including Katrina, but will be useful in evaluating potential variation in design, management and other risk-related factors for future events and future modification of the hurricane protection system. The establishment of valid general relationships between measurable event impacts and measurable event consequences is critical to the completion of the risk model. Currently, the Consequences team has committed to focusing its attention on two specific quantitative characterizations of consequences: 1) life loss (rather than injury, health status, mental health, etc.) and, 2) the dollar value of direct physical damage to buildings and infrastructure (rather than indirect costs such as business interruption, loss of revenue, etc.). These simplifications are necessary because of difficulties in data collection and because of time limitations imposed on the preparation of the IPET report. It should be borne in mind, that these are only representative consequences and not comprehensive. The full social, economic and culture impact of the event will be considerably greater than that represented than the two selected factors.

Liaison with Louisiana State University Hurricane Center

Team 10 liaison with the Louisiana State University Hurricane Center has provided valuable input to the understanding of Katrina consequences. The Hurricane Center at LSU has been deeply involved in assessment of previous hurricane losses and modeling of expected losses due to future hurricanes for a number of years. Of specific relevance to the consequences evaluation, the LSU hurricane center is now working with the Louisiana State Coroner's Office to analyze fatality data on the roughly 1200 confirmed fatalities (bodies recovered). Of these, approximately 700 have been identified, and circumstances and location of death have been established. LSU is currently carrying out detailed studies of fatality circumstances and has developed a GIS for the location of victims recovered and their home addresses. This material is not currently available to IPET because of privacy concerns and further negotiation will be necessary to obtain data relevant to the IPET consequences study. The LSU Hurricane Center has collaborated with the FEMA mitigation assessment team which has carried out an analysis of building damage in the affected area and this data will be available from FEMA. The work is carried out under a FEMA contract with URS. The LSU Hurricane Center includes LSU faculty members with experience and expertise in a range of relevant areas: evacuation, experts in transportation, planning and traffic management have been directly involved in the development of state evacuation policy and have played a major role in the successful evacuation of over 1 million people from New Orleans. Members of the Sociology Faculty have worked on the analysis of behavioral aspects of warning and evacuation response in various neighborhoods and populations of New Orleans. Regional economists from LSU have developed input-output modeling for the region which will provide perspective on indirect losses at the regional level. The Hurricane Center also participated in the PAM exercise organized by FEMA in advance of Katrina and documentation of the PAM exercise should provide a useful input for the consequence calculation. The FEMA contractor for the PAM exercise was Innovative Emergency Management of Louisiana.

The Hurricane Center has developed its own models for the impact of hurricanes in the New Orleans region. It has calibrated ADCIRC for Betsy (1965) experience and it provided model results of Katrina impact to the Louisiana Department of Emergency Preparedness and the Times-Picayune in advance of Katrina landfall (these model results did not include breaching of the levee and floodwall system). Data sources identified by the LSU Hurricane Center have been communicated to the Consequences team for follow-up. The clarification of required inputs and expected outputs of the Consequences team represent a major step forward. It is now necessary to communicate those input needs to other relevant IPET teams and to incorporate those expected outputs into the risk model.

Risk Profiles and Summaries

The reliability and risk analysis will relate the performance of individual features (floodwalls, levees, pumps, etc.) located throughout the hurricane protection system to the overall performance of operating the integrated system.

Storm and system performance scenarios will be studied in the risk model to determine the economic and life risks of the New Orleans hurricane protection system:

- As authorized, as a state constituting the baseline for estimating risk;
- As built, before the arrival of Hurricane Katrina;
- June 1, 2006: After Hurricane Katrina repairs have been accomplished prior to the 2006 hurricane season, nominally on June 1 2006; and
- Longer-term options for providing a greater level of protection through a strengthened and improved hurricane protection features.

The difference in relative risks among the three states will be a unified measure for fully evaluating the performance of the integrated system before Hurricane Katrina, after Hurricane Katrina, and during the interim recovery period.

The results of the risk and reliability analyses can be portrayed in various ways in order to facilitate risk communication to inform decision makers and with different public audiences. These will include narratives describing hurricane and system performance scenarios, inundation mapping based on the scenarios studied and graphic displays to portray critical components and identify significant failure modes. Also, Figure J-26 illustrates a typical risk result for economic consequences (in this case the mean frequency of exceedance for economic consequences).

Uncertainty Analysis

One of the objectives of the risk analysis is to quantitatively assess the uncertainties associated with modeling the performance of the HPS, likelihood of failure and the associated consequences of flooding. There are two fundamentally different sources of uncertainty that affect an estimation of the likelihood of future events. The first is attributed to the inherent randomness of events in nature. These events are predicted in terms of their likelihood of occurring (e.g., the chance of heads in a coin flip). This source of uncertainty is known as aleatory uncertainty and is, in principle, irreducible.

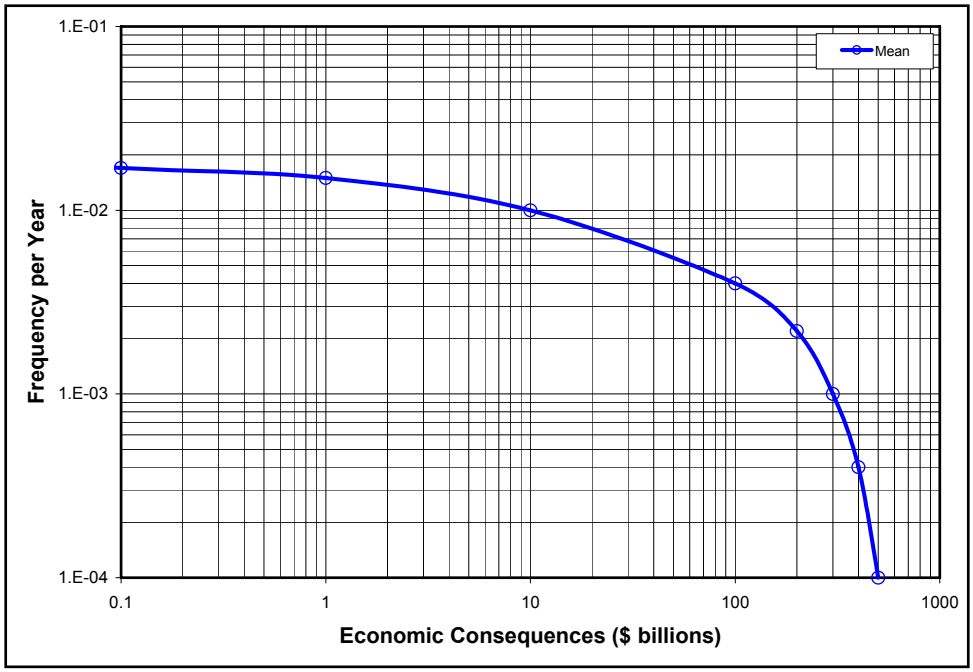

Figure J-26. Illustration of Typical Risk Analysis Results for Economic Consequences

The second source of uncertainty is attributed to our lack of knowledge or data. For example, the ability to determine the likelihood of an event (i.e., its rate of occurrence) requires that certain data be available. Depending on the volume of data that is available, the *accuracy* of the estimate of the rate of occurrence will vary. If limited data are available, the estimated rate may be quite uncertain (i.e., statistical confidence intervals on parameter estimates will be large). A second type of knowledge uncertainty is attributed to our lack of understanding (e.g., knowledge) about the physical processes that must be modeled (e.g., the meteorological processes that generate hurricane events). Often scientists and engineers have interpretations of existing data and models of physical processes of interest that often competing in the sense they lead to different results, while at the same time are consistent with observations. In these instances expert evaluations are often required to assess the current state of knowledge and to quantitatively evaluate the level of uncertainty. These sources of uncertainty are referred to *as* epistemic (knowledge-based) uncertainty.

The distinction between what is aleatory and what is epistemic uncertainty can often seem arbitrary. For example, the distinction depends on the models that are used in a particular analysis. In addition, their estimates can change in time. Nonetheless, making a distinction between the sources of uncertainty in logical manner helps insure that all uncertainties are quantified and those that can be reduced with additional data or knowledge are identified.

In principle, epistemic uncertainties are reducible with the collection of additional data or the use/development of improved models. However, in a given project, it is typically not possible to reduce these uncertainties.

Figure J-27 shows an example of where the epistemic uncertainty is manifested in the results of the HPS risk analysis. Shown is the probability density function on the estimate frequency of HPS failure (where failure is simple used here as the occurrence of inundation in one or more protected areas). The uncertainty in the estimate of the frequency of failure is an aggregation of the uncertainties in the estimate of the frequency and magnitude of hurricane storm surge and in the estimate of the reliability (or fragility) of the structures, systems and components that comprise the HPS.

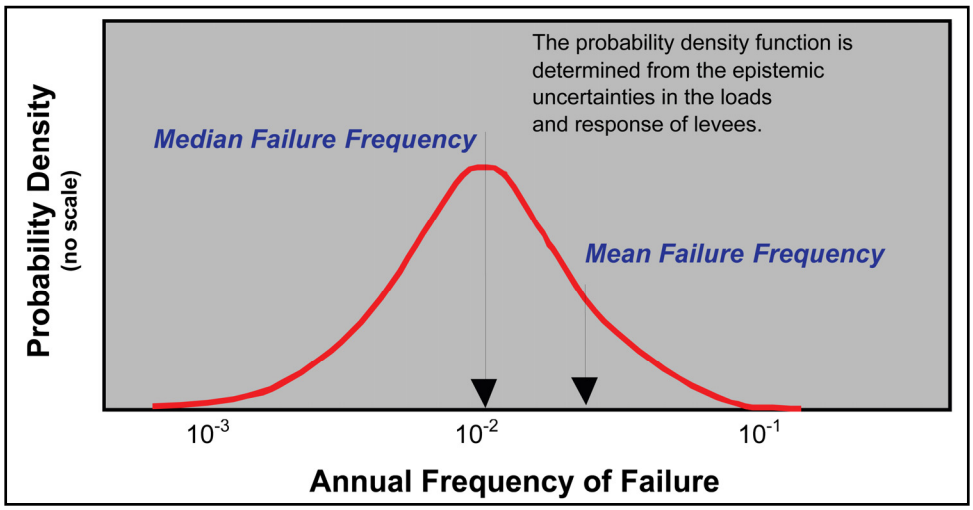

Figure J-27. Illustration of the Uncertainty in the Estimate of the Frequency HPS Failure due to Hurricane Events

In the HPS risk and reliability analysis, there will be uncertainties associated with each of the inputs to the risk model developed by other IPET teams. Sensitivity studies of the parameters used in the drainage model, failure mode models and pumping station performance models are used in order to identify critical sources of uncertainty. In addition, sensitivity studies are conducted during the development of the risk model to identify uncertainties in the input parameters synthesized by Team 10 and to identify data or analyses that could reduce uncertainties.

The effectiveness of the protection system is also dependent upon how well the operational elements of the system performed. Elements such as road closure structures, gate operations and pumping plants, etc. that requires human operation and proper installation during a flood fight can dramatically impact flood levels. The lessons learned concerning the performance of these elements during Katrina will be considered in the uncertainty analysis using parametric analysis.

Figure J-28 shows the fragility for the HPS including uncertainty and its effect on the estimate of the reliability at the authorization basis.

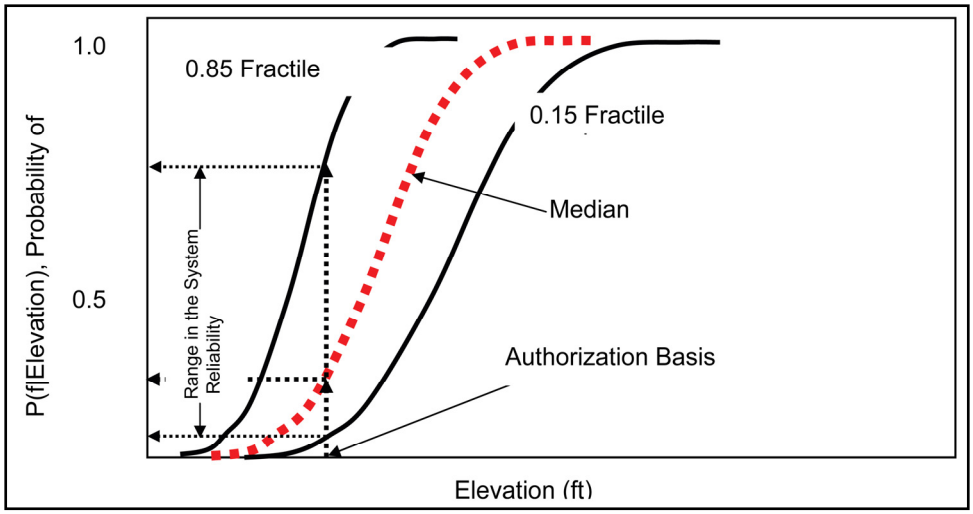

Figure J-28. Illustration of the Fragility for the HPS Including Modeling Uncertainty and the Effect at the Authorization Basis

The epistemic uncertainties in each part of the analysis lead to uncertainty in the final risk results. Propagating the uncertainties of the individual parts of the analysis through to the final result, produces a probability distribution on the frequency of exceedance of consequence metrics (e.g., economic consequences). This result is shown in Figure J-29.

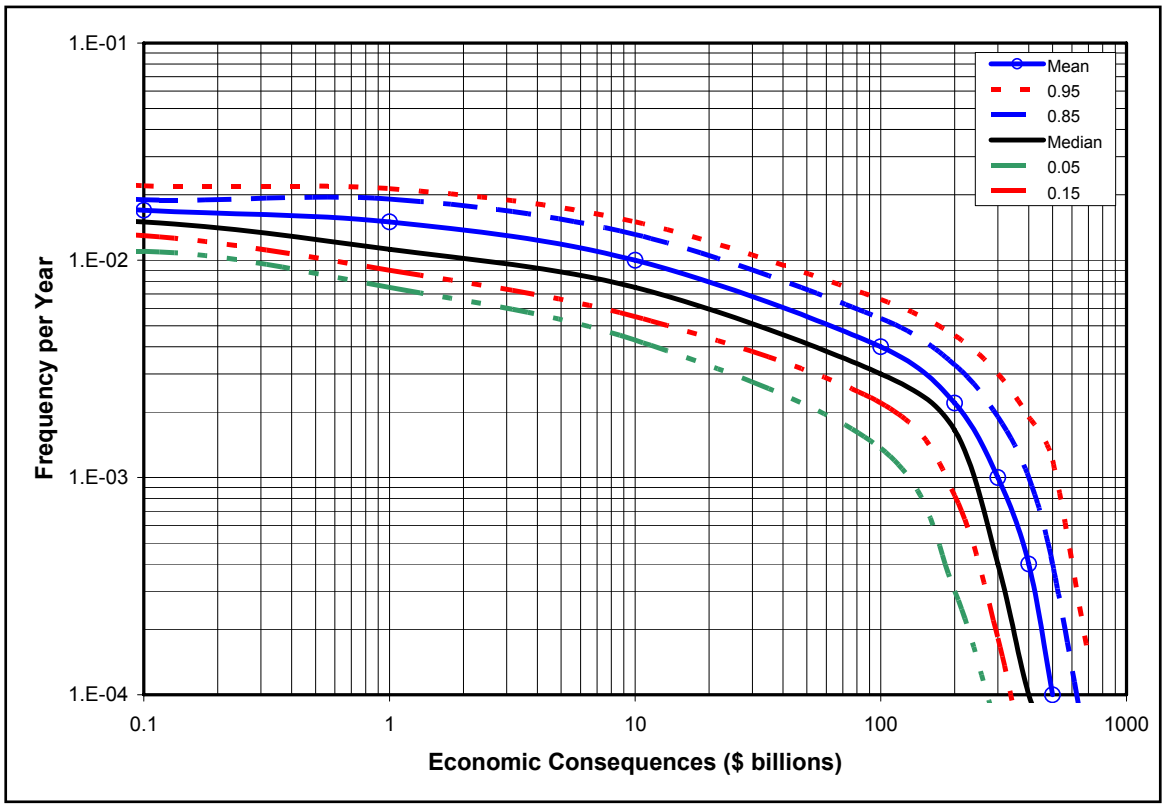

Figure J-29. Illustration of Typical Risk Analysis Results for Economic Consequences Including Uncertainty

References

Risk methodology

Ayyub, B. M., 2003. Risk Analysis in Engineering and Economics, Chapman & Hall/CRC Press, FL.

Ayyub, B. M., and McUen, R. H., 2003. Probability, Statistics and Reliability for Engineers and Scientists, Chapman & Hall/CRC Press, FL.

Daugherty, R., Franzini, J., and Finnemore E., 1985, Fluid Mechanics with Engineering Applications, 598 p., McGraw-Hill Book Co., NY.

Kumamoto, H., and Henley, E.J., 1996, Probabilistic Risk Assessment and Management for Engineers and Scientists, Second Edition, IEEE Press, New York.

Modarres, M., Kaminskiy, M., Krivstov, V., 1999. Reliability Engineering and Risk Analysis: A Practical Guide, Marcel Decker Inc., New York, NY.

USACE, 2000, Unwatering Plan of the Greater Metropolitan Area of New Orleans, LA, USACE New Orleans District.

Hurricane Methodology

Batts, M. E., Cordes, M. R., Russell, L. R., Shaver, J. R., and Simiu, E. (1980), "Hurricane Wind Speeds in the United States," *Rep. No. BSS-124,* Nat. Bureau of Standards, U.S. Department of Commerce, Washington, D.C.

Bister, M. and K. A. Emanuel (2002), "Low Frequency Variability of Tropical Cyclone Potential Intensity. 1: Interannual to Interdecadal Variability," *J. Geoph. Res.* **107**: 4801.

Broccoli, A. J. and S. Manabe (1990), "Can Existing Climate Models Be Used to Study Anthropogenic Changes in Tropical Cyclone Climate?" *Geophys. Res. Lett.* **17**: 1917-1920.

Chan, J. C. L. and S. L. Liu (2004), "Global Warming and Western North Pacific Typhoon Activity from an Observational Perspective," *J. Climate* **17**: 4590-4602.

Chen, S., M. Lonfat, J. A. Knaff, and F. D. Marks, Jr. (2006), "Effects of Vertical Wind Shear and Storm Motion on Tropical Cyclone Rainfall Asymmetries Deduced from TRMM," submitted to *Monthly Weather Review*.

Chouinard, L. E., C. Liu, and C. K. Cooper (1997), "Model for Severity of Hurricanes in Gulf of Mexico," *J. of Waterway, Port, Coastal and Ocean Engineering,* **123**(3): 120-129.

Elsner, J. B. (2005), "Hurricane Science Review: The Next 5 Years?" Dept. of Geography, Florida State University, http://garnet.fsu.edu/~jelsner/www.

Elsner, J. B. and B. Kocher (2000), "Global Tropical Cyclone Activity: A Link to the North Atlantic Oscillation," *Geophys. Res. Lett.* **27**: 129-132.

Emanuel, K. A. (1987), "The Dependence of Hurricane Intensity on Climate," *Nature* **326**: 483-485.

Emanuel, K. A. (2000), "A Statistical Analysis of Tropical Cyclone Intensity," *Mon. Wea. Rev.* **128**: 1139-1152.

Emanuel, K. A. (2005a), "Increasing Destructiveness of Tropical Cyclones Over the Past 30 Years," *Nature* **436**: 686-688.

Emanuel, K. A. (2005b), "Anthropogenic Effects on Tropical Cyclone Activity," Dept. of Earth and Planetary Sciences, MIT, http://wind.mit.edu/~emanuel/anthro2.htm.

Free, M., M. Bister, and K. A. Emanuel (2004), "Potential Intensity of Tropical Cyclones: Comparison of Results from Radiosonde and Reanalysis Data," *J. Climate* **17**: 1722-1727.

Georgiou, P. N., Davenport, A. G., and Vickery, B. J. (1983), "Design Wind Speed in Regions Dominated by Tropical Cyclones," *J. Wind Engrg. And Industrial Aerodynamics,* **13**(1): 139-152.

Goldenberg, S. B., C. W. Landsea, A. M. Mestas-Nunez, and W. M. Gray (2001), "The Recent Increase in Atlantic Hurricane Activity: Causes and Implications," *Science* **293**: 474-479.

Haarsma, R. J., J. F. B. Mitchell, and C. A. Senior (1992), "Tropical Disturbances in a GCM," *Climate Dyn.* **8**: 247-257.

Henderson-Sellers, A. H. Zhang, G. Berz, K. A. Emanuel, W. Gray, C. Landsea, G. Holland, J. Lighthill, S-L. Shieh, P. Webster, and K. McGuffie (1998): "Tropical Cyclones and Global Climate Change: A Post-IPCC Assessment," *Bull. Amer. Meteor. Soc.* **79**: 9-38.

Ho, F. P., J. C. Su, J. L. Hanevich. R. J. Smith, and F. P. Richards (1987), "Hurricane Climatology for the Atlantic and Gulf Coasts of the United States," *NOAA Technical Report NWS 38*, U.S. Department of Commerce, Washington, D.C.

Holland, G. J. (1980), "An Analytic Model of the Wind and Pressure Profiles in Hurricanes," *Monthly Weather Review,* **108**: 1212-1218.

Houghton, J. T., Y. Ding, D. J. Griggs, M. Noguer, P. J. van der Linden, and D. Xiaosu, Eds. (2001), Climate Change 2001: The Scientific Basis: Contributions of Working Group I to the Third Assessment Report of the Intergovernmental Panel on Climate Change, Cambridge University Press, 881 pp.

Jarvinen, B. R., Neumann, C. J., and Davis, M. A. S. (1984), "A Tropical Cyclone Data Tape for the North Atlantic Basin 1886-1893: Contents, Limitations and Uses," *NOAA Tech. Memo. NWS-NHC-22,* U.S. Department of Commerce, Washington, D.C.

Knutson, T. R. and R. E. Tuleya (2004), "Impact of CO_2-induced Warming on Simulated Hurricane Intensity and Precipitation: Sensitivity to the Choice of Climate Model and Convective Parameterization," *J. Climate* **17**: 3477-3495.

Landsea, C. W., R. A. Pielke Jr., A. M. Mestas-Nunez, and J. A. Knaff (1999), "Atlantic Basin Hurricanes: Indices of Climatic Changes," *Climatic Change* **42**: 89-129.

Lighthill, J., G. J. Holland, W. M. Gray, C. Landsea, K. A. Emanuel, G. Craig, J. Evans, Y. Kurihara, and C. P. Guard (1994), "Global Climate Change and Tropical Cyclones," *Bull. Amer. Meteor. Soc.* **75**: 2147-2157.

Lonfat, M., F. D. Marks, Jr., and S. S. Chen (2004), "Precipitation Distribution in Tropical Cyclones Using the Tropical Rainfall Measuring Mission (TRMM) Microwave Imager: A Global Perspective," *Mon. Wea. Rev.,* **132**: 1645-1660.

Luettich, R. A., J. J. Westerink, and N. W. Sheffner (1992), "ADCIRC: An Advanced Three-dimensional Circulation Model for Shelves, Coasts and Estuaries; Report 1: Theory and Methodology of ADCIRC-2DDI and ADCIRC-3DL," *Coastal Engineering Research Center, U. S. Army Engineer Waterways Experiment Station,* Technical Report DRP-92-6, Vicksburg, MS.

Michaels, P. J., P. C. Knappenberger, and C. W. Landsea (2005), "Comments on 'Impact of CO_2-induced Warming on Simulated Hurricane Intensity and Precipitation: Sensitivity to the Choice of Climate Model and Convective Parameterization'," *J. Climate,* in press.

Neumann, C. J. (1991), "The National Hurricane Center Risk Analysis Program (HURISK)," *NOAA Tech. Memo. NWS-NHC-38,* U.S. Department of Commerce, Washington, D.C.

Pielke, R. A. Jr., C. W. Landsea, M. Mayfield, J. Laver, and R. Pasch (2005), "Hurricanes and Global Warming," *Bull. Amer. Meteor. Soc.,* November, 2005: 1571-1575.

Powell, M., G. Soukup, S. Cocke, S. Gulati, N. Morisseau-Leroy, S. Hamid, N. Dorst, and L. Axe (2005), "State of Florida Hurricane Loss Projection Model: Atmospheric Science Component," *J. Wind Engineering and Industrial Aerodynamics,* **93**: 651-674.

Russell, L. R. (1971), "Probability Distribution for Hurricane Effects," *J. Wtrwy., Harb. And Coast. Engrg. Div., ASCE,* **97**(1): 139-154.

Scheffner, N. W., L. E. Borgman, and D. J. Mark (1996), "Empirical Simulation Technique Based Storm Surge Frequency Analyses," *J. Wtrwy., Port, Coast., and Oc. Engrg.* **122**(2): 93-101.

Vickery, P. J. and L. A. Twisdale (1995a), "Prediction of Hurricane Wind Speeds in the United States," *J. of Structural Engineering*, **121**(11): 1691-1699.

Vickery, P. J. and L. A. Twisdale (1995b), "Wind-Field and Filling Models for Hurricane Wind-Sped Predictions," *J. of Structural Engineering*, **121**(11): 1700-1709.

Vickery, P. J., P. F. Skerlj, and L. A. Twisdale (2000), "Simulation of Hurricane Risk in the U.S. Using Empirical Track Model," *J. of Structural Engineering*, **126**(10): 1222-1237.

Webster, P. J., G. J. Holland, J. A. Curry, and H.-R. Chang (2005), "Changes in Tropical Cyclone Number, Duration, and Intensity in a Warming Environment," *Science* **309**: 1844-1846.

Willoughby, H. E. and M. E. Rahn (2004), "Parametric Representation of the Primary Hurricane Vortex. Part I: Observations and Evaluation of the Holland (1980) Model," *Monthly Weather Review*, **132**: 3033-3048.

Appendix A. Terminology

Event tree analysis is an inductive analysis process that utilizes an event tree graphical construct that shows the logical sequence of the occurrence of events in, or states of, a system following an initiating event.

A *failure mode* is a way that failure can occur, described by the means by which element or component failures must occur to cause loss of the sub-system or system function.

Fault tree analysis is a systems engineering method for representing the logical combinations of various system states and possible causes which can contribute to a specified event (called the top event).

A *fragility curve* is a function that defines the probability of failure as a function of an applied load level.

A *hazard* is condition, which may result from either an external cause (e.g. earthquake, flood, or human agency) or an internal vulnerability, with the potential to initiate a failure mode. It is a source of potential harm or a situation with a potential to cause loss.

The *performance* of a system or component can be defined as its ability to meet functional requirements. The performance of an item can be described by

various elements, such as flood protection, reliability, capability, efficiency, and maintainability. The design and operation of system affects this performance.

A *system* is a deterministic entity comprising an interacting collection of discrete elements and commonly defined using deterministic models. The word *deterministic* implies that the system is identifiable and not uncertain in its architecture. The definition of the system is based on analyzing its functional and/or performance requirements. A description of a system may be a combination of functional and physical elements. Usually functional descriptions are used to identify high information levels on a system. A system can be divided into subsystems that interact. Additional details in the definition of the system lead to a description of the physical elements, components, and various aspects of the system. Methods to address uncertainty in systems architecture are available and can be employed as provided by Ayyub and Klir (1996).

Reliability can be defined for a system or a component as its ability to fulfill its design functions under designated operating and/or environmental conditions for a specified time period. This ability is commonly measured using probabilities. Reliability is, therefore, the occurrence probability of the complementary event to failure.

Consequences for a failure event, can be defined as the degree of damage or loss from some failure. Each failure of a system has some consequence(s). A failure could cause economic damage, environmental damage, injury or loss of human life, or other possible events. Consequences need to be quantified in terms of failure-consequence severities using relative or absolute measures for various consequence types to facilitate risk analysis.

Risk is the potential of losses for a system resulting from an uncertain exposure to a hazard or as a result of an uncertain event. Risk should be based on identified risk events or event scenarios. Risk can be viewed to be a multi-dimensional quantity that includes event-occurrence probability, event-occurrence consequences, consequence significance, and the population at risk; however, it is commonly measured as a pair of the probability of occurrence of an event, and the outcomes or consequences associated with the event's occurrence. Another common representation of risk is in the form of an exceedance probability function of consequences.

Probability is a measure of the likelihood, chance, odds, or degree of belief that a particular outcome will occur. A conditional probability is the probability of event occurrence based on the assumption that another event (or multiple events) has occurred.

Safety can be defined as the judgment of risk tolerance (or acceptability in the case of decision making) for the system. Safety is a relative term since the decision of risk acceptance may vary depending on the individual or the group of people making the judgment.

Risk analysis is the technical and scientific process to breakdown risk into its underlying components. Risk analysis provides the processes for identifying hazards, event-probability assessment, and consequence assessment. The risk

analysis process answers three basic questions: (1) What can go wrong? (2) What is the likelihood that it will go wrong? (3) What are the consequences if it does go wrong? Also, risk analysis can include the impact of making any changes to a system to control risks.

Risk communication can be defined as an interactive process of exchange of information and opinion among stakeholders such as individuals, groups, and institutions. It often involves multiple messages about the nature of risk or expressing concerns, opinions, or reactions to risk managers or to legal and institutional arrangements for risk management. Risk communication greatly affects risk acceptance and defines the acceptance criteria for safety.

A *scenario* is a unique combination of states that lead to an outcome of interest. A scenario defines a suite of circumstances of interest in a risk assessment. Thus there may be loading scenarios, failure scenarios or downstream flooding scenarios.

Appendix B. New Orleans East Polder

New Orleans East (NOE) Polder

NOE – Background

The New Orleans East hurricane protection system was designed as part of the Lake Pontchartrain, LA and Vicinity Hurricane Protection Project. The New Orleans East (NOE) portion of the project protects 45,000 acres of urban, industrial, commercial, and ecological lands. As designed, the levees were generally constructed with a 10-foot crown width with side slopes of 1 on 3. The height of the levees varies but was in the range of 12 - 19 feet depending upon location and design characteristics. There are also floodwall segments along the line of protection that consists of sheet-pile walls or concrete I-walls constructed on the top of sheet-pile. The line of protection was designed to provide protection from the Standard Project Hurricane (approximately a fast moving Category 3 storm). As designed, there is a total of approximately 206,000 linear feet of levees and floodwalls, 8 pump stations, 3 U.S. Fish and Wildlife Service (USFWS) pump stations, a multitude of culverts through/over the levee/ floodwall, and multiple gate closures for road and rail crossings. The NOE polder is essentially broken into two major sections, as shown in Figure J-B1. The west side of the polder is primarily residential and the east side is essentially a wetlands area. These two areas are separated by a small levee. The west side of the polder is further divided into residential and industrial areas. The area along the GIWW and IHNC is primarily industrial while the remainder of the western portion is residential in nature.

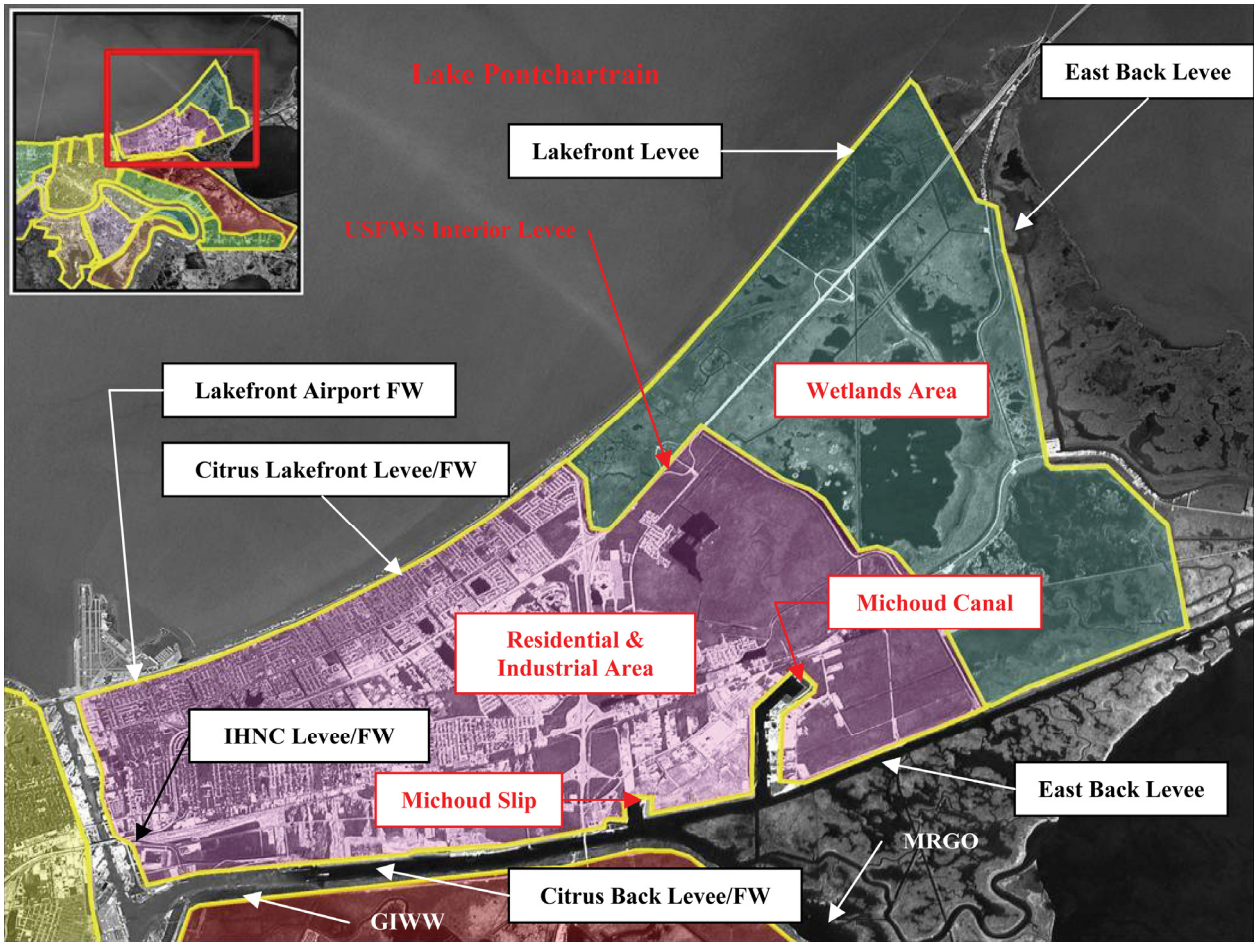

Figure J-B1. New Orleans East Polder – Major Stretches by DM

NOE – Design Memorandums

For the purposes of the IPET risk assessment, each polder must be broken into "reaches" that are defined by a combination of physical characteristics, major elevation changes, and potential consequences. Many of the basic reaches were defined initially by when individual design memorandums (DM) were completed and then constructed since different stretches of the levee/floodwall were raised at different times throughout the life of the structure. There are a total of 7 levee/floodwall major stretches separated by different DM's within NOE. These 7 are defined below and illustrated in Figure J-B1.

Lakefront Airport Floodwall
Beginning Point: Northwest corner of polder below Ted Hickey Bridge
Ending Point: End of floodwall just south of Hayne Blvd closure gate

Citrus Lakefront Levee/Floodwall
Beginning Point: Begin transition levee just south of Hayne Blvd closure
Ending Point: Levee height transition at Paris Road and USFWS levee

Lakefront Levee
Beginning Point: Levee transition at Paris Road and USFWS interior levee
Ending Point: South Point at northeast end of polder

East Levee
Beginning Point: South Point at northeast corner of polder
Ending Point: GIWW at southeast corner of polder

East Back Levee
Beginning Point: GIWW at southeast corner of polder
Ending Point: Northeast end of Michoud Canal floodwall

Citrus Back Levee/Floodwall
Beginning Point: Northeast end of Michoud Canal floodwall
Ending Point: Southwest corner of polder at IHNC

IHNC East Levee/Floodwall
Beginning Point: Southwest corner of polder at IHNC
Ending Point: Northwest corner of polder under Ted Hickey Bridge

NOE – Layout of Reaches for Risk Model by Physical Feature

Within these major stretches defined by the DM's there are reaches, which are defined by physical changes in the protection system, i.e. switching from floodwall to levee, etc…, or by changes in geotechnical parameters. Within each reach, there are specific "key points" whose reliability needs to be determined in order to calculate the effect on the overall reach being evaluated. An example of a "key point" would be a closure gate at a road or rail line crossing along a floodwall. IPET engineers reviewed existing plans, damage survey reports, and conducted field verification inspections to ensure each polder was accurately defined within the system. As a part of the field verification inspections, GPS coordinates were obtained and stationing from DM's and "as-built" plans was verified. For each polder, this information was transformed into a spread sheet and then a system map for each polder, as shown in Figure J-B2. Finally, digital photographs with incorporated notes were developed to compliment the spread sheets and system map for further clarification. This collection of information was then categorized to get a clear picture of how the polder should be defined for risk assessment purposes. A summary of the reach and point definitions for NOE is provided in Figure J-B2 with a brief supporting narrative on each reach. Polder definition starts at the northwest corner of the polder where the floodwall along the IHNC intersects the floodwall along the Lakefront Airport (NOE1). This occurs at Sta. 4+02 B/L, which is equal to the DM stationing of 10+13 W/L. The end of the physical definition of the NOE polder occurs at the same point since it is self enclosed.

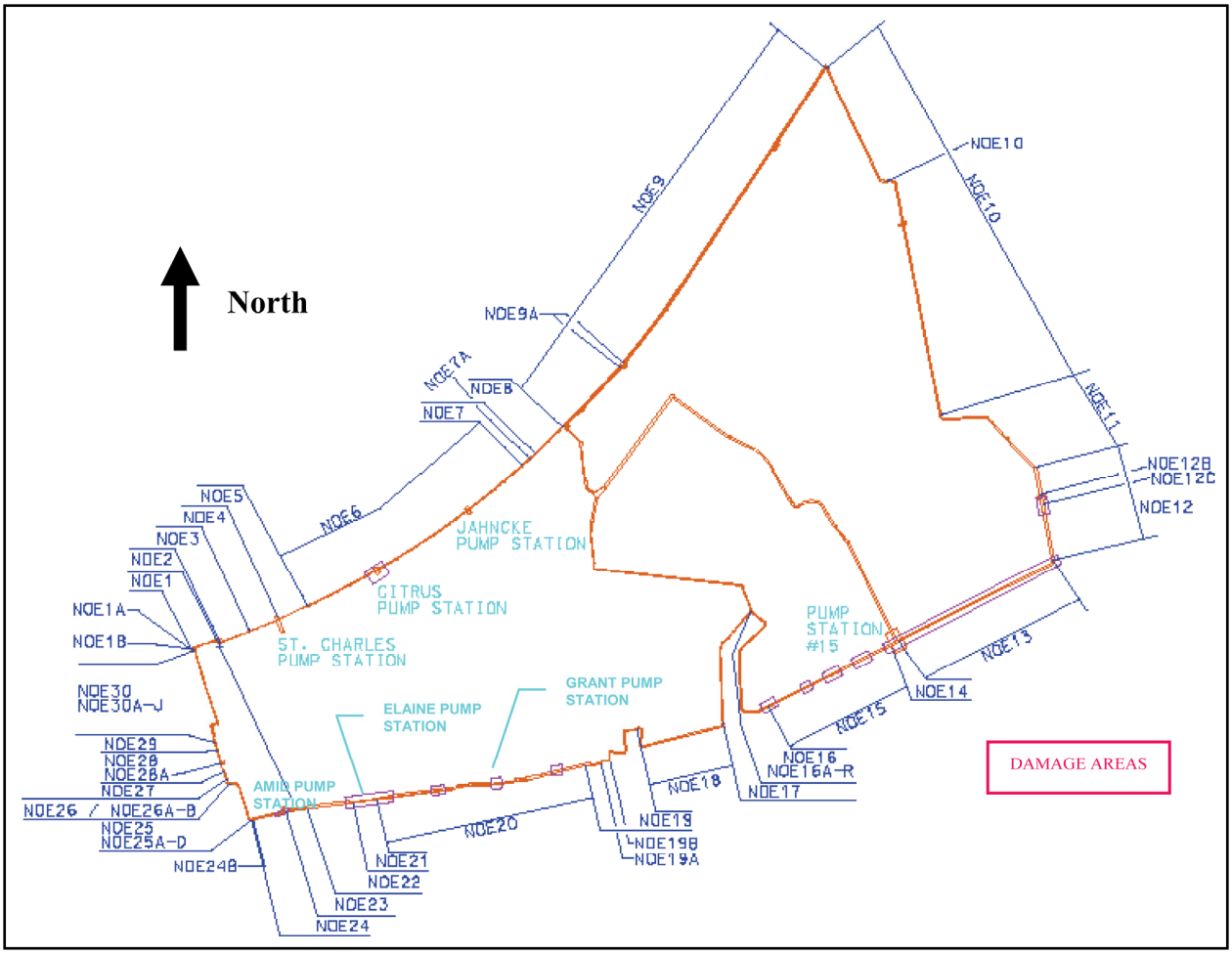

Figure J-B2. New Orleans East Polder – Reaches Defined

The details of each reach and key point is detailed in the spread sheet for the individual polders. The NOE is summarized by reach as follows:

Reach NOE1 (Lakefront Airport DM). This reach is defined by 2,326 linear feet of floodwall at the Lakefront Airport. It is located at the northwest end of the polder. There are two key points (NOE1a and NOE1b) within this reach, both closure gates, located near the end of this reach. The reach ends just after the second closure gate for Hayne Boulevard. There was significant scour from overtopping along this section of i-wall, as shown in Figure J-B3, but the wall performed well with no noticeable deformation.

Figure J-B3. Scour Behind Lakefront Airport FW from Overtopping

Reach NOE2 (Citrus Lakefront DM). This reach is defined by a short 97' transition levee between the end of the Lakefront Airport floodwall and the beginning of the Stars and Stripes Floodwall. There are no key points within this reach.

Reach NOE3 (Citrus Lakefront DM). This reach is defined by 2,325 linear feet of floodwall. There are two basic types of floodwall along this reach each consisting of about ½ the length of this reach. The first type is a short concrete capped i-wall with levee high on both sides and the second is a taller i-wall section where the protected side has a concrete sidewalk adjacent to a road.

Reach NOE4 (Citrus Lakefront DM). This reach is defined by 2,330 linear feet of the Stars and Stripes Levee. A small concrete i-wall for the discharge pipes at the St. Charles Pump Station is located near the end of this reach.

Reach NOE5 (Citrus Lakefront DM). This reach is defined by 2,270 linear feet of the Stars and Stripes floodwall. There are no key points within this reach.

Reach NOE6 (Citrus Lakefront DM). This reach is defined by a 19,112 linear feet segment of levee. It begins at the end of the Stars and Stripes floodwall and ends at the west side of the Lincoln Beach floodwall. There are two "key" points within this segment: two small floodwall sections embedded within the levee for the discharge pipes of the Citrus and Jahncke Pump Stations. There was some minor scouring and overtopping of this levee at various locations, as indicated in Figure J-B4, but no failures.

Figure J-B4. Minor Scour from Overtopping at Jahncke Pump Station

Reach NOE7 (Citrus Lakefront DM). This reach is defined by a 1,474 linear feet segment of floodwall near Lincoln Beach. There is one "key point" located in the flood wall, which is a closure gate, shown as NOE7a.

Reach NOE8 (Citrus Lakefront DM). This reach of levee, 2,724 linear feet, ends the Citrus Lakefront section at the intersection of Paris Road, the interior local levee, and the west side of the Lakefront Levee. There are no key points within this reach, although the levee height is considerably different as it proceeds to the Lakefront Levee section, as shown in Figure J-B5.

Figure J-B5. Begin Lakefront Levee at Citrus Lakefront and Paris Road (Lakefront Levee @ El. 19.0 +/- and Citrus Lakefront Levee @ 13.5+/-)

Reach NOE9 (Lakefront Levee DM). This reach covers 33,165 feet of levee along Lake Pontchatrain from Paris Road to South Point, which is the extreme northeast corner of the polder. There is 368' long i-wall around the Exxon/Mobil pipeline crossing that is the only "key point" within the reach, depicted at NOE9a in Figure J-B2.

Reach NOE10 (East Levee DM). This reach is defined by a 27,665 linear feet segment of levee from South Point to where Highway 90 crosses the levee. There are several "key points" within this stretch including 4 culverts through the levee (3 gravity structures and 1 USFWS pump station) and 1 gated closure at Highway 11. For clarity, these are not illustrated in Figure J-B2. Reference the spread sheet in the appendix for further details regarding their location and description.

Reach NOE11 (East Levee DM). This levee is 8,942' long and goes from Highway 11 and serves as a transition section where the design changes. There are no "key points" located within this reach.

Reach NOE12 (East Levee DM). The final reach of levee along the East section is 7,190' long and extends to the GIWW. There are 4 key points along the levee (3 culverts thru the levee and a gated closure at the railroad crossing). The railroad closure structure, shown as NOE12c in Figure J-B2, experienced severe damage during Katrina from overtopping. An aerial view of that damage is shown in Figure J-B6.

Figure J-B6. Aerial View of Damage at RR Closure Along East Levee (Point NOE12c on System Map)

Reach NOE13 (East Back Levee DM). This section of levee, measuring 22,257 linear feet, was heavily damaged during Katrina from overtopping. It begins at the east end where it ties into the East Levee and continues to the east end of the floodwall around the Orleans Parish Pump Station #15. There are no key points within this reach. Much of this levee was destroyed, as shown in Figure J-B7, and is in the process of being rebuilt.

Figure J-B7. Failure of Levee by Overtopping East of PS #15 (East Back Levee)

Reach NOE14 (East Back DM). This reach is defined by the floodwall around Pump Station #15. There are two types of walls within this reach, sheet pile walls at the edges and concrete i-walls around the discharge pipes. The total length of wall is 493 feet. Portions of the transition sheet pile sections were heavily damaged during Katrina from overtopping, as shown in Figure J-B8. There are no key points within this short reach.

Figure J-B8. Floodwall Failure Near Orleans Pump Station #15

Reach NOE15 (East Back DM). This 10,120 ft section of levee extends from the east end of the Orleans Parish #15 floodwall to the start of the floodwall on the east side of the Michoud Canal at the GIWW. There is one key point within this reach for a utility pipe crossing.

Reach NOE16 (East Back DM). This reach consists of the east floodwall around the Michoud Canal. It is approximately 10,757 feet long. It starts at the GIWW and continues along the Michoud Canal where it joins with the Citrus Back floodwall. There are 18 key points along this reach for gated closures at industry and road crossings. However, from site inspections, it appears as if 5 of these gates are placed in the permanently closed position. As shown in Figure J-B9, the transition sheet pile floodwall at the beginning of this reach failed during Katrina.

Reach NOE17 (Citrus Back DM). The beginning of the Citrus Back stretch starts with this reach at the northwest end of the Michoud Canal and ends at the southwest side of the Michoud Canal at the GIWW. This reach consists of 9,318 feet of floodwall with no key points within this reach.

Reach NOE18 (Citrus Back DM). This reach represents the 7,905' segment of levee between the Michoud Canal and Michoud Slip. There are no key points within this reach of levee.

Figure J-B9. Floodwall Failure at East End of Michoud Canal FW

Reach NOE19 (Citrus Back DM). The reach represents the 6,155 ft of floodwall around the Michoud Slip. There are 2 gates closures and 2 ramps within this reach.

Reach NOE20 (Citrus Back DM). This reach contains 15,940 ft of levee between the west end of the Michoud Slip and the east end of the combination floodwall for the bulk loading facility. There are three key points within this reach for culverts crossing the levee, including the discharge pipes for Grant Pump Station, as reference in Figure J-B2.

Reach NOE21 (Citrus Back DM). This reach is defined by the 1,820 ft combination floodwall built for the bulk loading facility and Elaine Pump Station, whose relative location is shown on the system map in Figure J-B2. This wall was heavily damaged during Katrina, as shown in Figure J-B10, and is currently being repaired.

Figure J-B10. Floodwall Failure at Bulk Loading Facility/Elaine PS

Reach NOE22 (Citrus Back DM). This reach is for the levee (3,453 ft long) between the floodwalls at the bulk loading facility/Elaine PS (east side) and Amid PS (west side). There are no key points within this reach.

Reach NOE23 (Citrus Back DM). This reach is the 1,587 ft section of floodwall located just east of the Amid Pump Station. This wall did suffer minor overtopping, but no major damage. There are no key points within this reach.

Reach NOE24 (Citrus Back DM). The final reach of this DM is 2,348 feet of levee extending from the end of the floodwall just east of the Amid Pump Station to its tie in with the Inner Harbor Navigation Canal (IHNC) east levee. There are two key points located within this reach including the discharge pipes over the levee at Amid PS and the railroad closure gate structure just east of the tie in with the IHNC levee. This structure was overtopped and sustained serious erosion problems, but no major structural damage, as indicated by the eroded areas in Figure J-B11.

Figure J-B11. Erosion Damage Around RR Closure (Citrus Back Levee)

Reach NOE25 (IHNC DM). This reach is 3,803 ft long and consists of levee. There are 4 closure gates within this reach each of which suffered erosion damage from overtopping during Katrina. Structural damage was minimal to these closure structures. The very end of this reach suffered a major washout area where the levee serves as a ramp just near the I-10 overpass. A photograph of this washout damage is shown in Figure J-B12.

Reach NOE26 (IHNC DM). This short reach of floodwall (537 ft) starts near the end of the washout area and extends just under the I-10 overpass. This section is considered a reach because it faces several different directions and contains two key points, both closure gates.

Figure J-B12. Major Washout Area from Overtopping Near I-10 Overpass (Citrus Back Levee)

Reach NOE27 (IHNC DM). This reach consists of a short transition levee (526 ft) between floodwalls. There are no key points within this short reach.

Reach NOE28 (IHNC DM). This section of floodwall (1,876 ft) starts between the I-10 and Highway 90 overpasses and ends where it serves as the foundation for the Dupuy Storage Facility (see Figure J-B12). There is one key point in this section which is the old Highway 90 overpass location. It does not appear as if remedial repairs were made this transition section when the overpass was relocated.

Reach NOE29 (IHNC DM). This short section of floodwall (643 ft) serves as the Dupuy Storage Building foundation, as shown in Figure J-B13. This section was deemed an individual reach because overtopping issues along this short reach may not be of major concern with the building.

Figure J-B13. Floodwall Serves as Building Foundation (Dupuy Storage Facility – IHNC East)

Reach NOE30 (IHNC DM). The last reach of the polder consists of 8,168 ft of floodwall. There are several key points within this reach including the Dwyer PS discharge pipes and several closure gates. Portions of this wall were overtopped as indicated by the erosion behind the floodwall adjacent to closure gate E-13 and shown in Figure J-B14. This erosion, which measures approximately 8' wide by 2.5' deep, did not cause major structural problems with the wall at this location.

Figure J-B14. Erosion Behind Floodwall Adjacent to Gate E-13 (IHNC East)

In summary, the NOE polder is divided into 30 reaches for the purposes of the risk analysis. There are a total of 14 floodwall reaches (49,749 linear feet) and 16 levee reaches (167,577 linear feet). Thus, the polder is roughly 23% floodwall and 77% levee for evaluation purposes. Approximately 6,700 feet of levee, primarily the East Back Levee section, was damaged or destroyed from overtopping during Katrina. An additional 24,600 feet of floodwall was damaged to some extent from overtopping. This was spread out across different sections of the polder. Some of the damage to the floodwalls will only require that landside fill be placed back where scouring took some of the resisting, passive wedge away. Other shorter sections of wall are being totally rebuilt as a result of the overtopping causing their failure.

NOE – Elevations Along the Defined Reaches

One of the critical inputs to completing the risk assessment for the hurricane protection system is a clear understanding of the elevations along each polder both pre-Katrina and as a result of any fixes from Task Force Guardian. There are different ways this can be addressed when conducting the risk assessment, but in order to get the best information, "average" lengths of elevations to the nearest ½ foot increment were developed. A variety of survey information was required to develop this information for NOE. Four different sources of data were required to obtain the best estimate of levee/floodwall elevations at the time of Katrina. A September 2005 LIDAR survey was used to establish elevations for most non-failed sections of levees. For the Citrus Back Levee, September 2000

Plan and Profile sheets were provided by TFG. For levee sections that had major failures (East Back Levee), October 2001 survey data was available and provided by TFG. Finally, LIDAR survey data is collected by aerial means and it did not pick up the top of floodwalls. In November 2005, a field survey was done using NAVD88 datum to determine top of floodwall elevations at the various locations along NOE.

The survey information for NOE was collected and categorized along each reach. The elevations vary considerably, but were developed where "average" ½ foot elevation changes occurred and then stations were matched to these locations. This information is provided in the NOE spread sheet. In summary, the weighted average of levee/floodwall height coupled with the range is provided in Table J-B1.

Table J-B1. Elevation Information by Reach for NOE Polder

Reach	DM	Weighted Average Elevation	Maximum Elevation in Reach	Minimum Elevation in Reach	Source
NOE1	Lakefront Airport	11.6	11.7	11.6	Nov05 Survey
NOE2	Citrus Lakefront	13.0	13.0	13.0	Sep05 LIDAR
NOE3	Citrus Lkfrt	need data	need data	need data	???
NOE4	Citrus Lakefront	13.2	13.5	11.5	Sep05 LIDAR
NOE5	Citrus Lakefront	14.3	14.6	14.1	Nov05 Survey
NOE6	Citrus Lakefront	13.0	13.5	12.0	Sep05 LIDAR
NOE7	Citrus Lakefront	12.5	12.7	12.2	Nov05 Survey
NOE8	Citrus Lakefront	12.9	13.0	12.5	Sep05 LIDAR
NOE9	Lakefront Levee	18.4	20.0	18.0	Sep05 LIDAR
NOE10	East Levee	15.1	15.5	12.5	Sep05 LIDAR
NOE11	East Levee	16.8	17.5	16.5	Sep05 LIDAR
NOE12	East Levee	17.8	19.0	13.5	Sep05 LIDAR
NOE13	East Back Levee	15.5	16.5	15.0	Oct01 Survey
NOE14	East Back Levee	19.9	22.2	17.5	Nov05 Survey
NOE15	East Back Levee	16.8	17.0	16.5	Oct01 Survey
NOE16	East Back Floodwall	17.9	18.0	17.5	Nov05 Survey
NOE17	Citrus Back Floodwall	20.7	21.0	20.5	Nov05 Survey
NOE18	Citrus Back Levee	17.4	17.5	17.0	Nov05 Survey
NOE19	Citrus Back Floodwall	17.2	17.1	17.8	Nov05 Survey
NOE20	Citrus Back Levee	14.6	15.0	14.0	Sep00 Plan & Profile
NOE21	Citrus Back Floodwall	need data	need data	need data	???
NOE22	Citrus Back Levee	14.0	14.0	14.0	Sep00 Plan & Profile
NOE23	Citrus Back Floodwall	14.5	15.1	14.4	Nov05 Survey
NOE24	Citrus Back Levee	13.6	14.0	13.0	Nov05 Survey
NOE25	IHNC East	12.0	12.5	11.5	Nov05 Survey
NOE26	IHNC East	12.5	12.5	12.5	Nov05 Survey

NOE27	IHNC East	12.5	12.5	12.5	Nov05 Survey
NOE28	IHNC East	13.2	13.5	12.0	Nov05 Survey
NOE29	IHNC East	13.5	13.5	13.5	Nov05 Survey
NOE30	IHNCE East	12.4	13.0	11.5	Nov05 Survey

Appendix C - Jefferson Polder

Appendix D - St. Charles Polder

Appendix E - Plaquemines Polder

Appendix F - St. Bernards Polder

Appendix G - Evaluation of Loss Exceedance Probabilities

In the case of using point estimates of probabilities, the results should be summarized as provided in Table J-G1, and the loss exceedance probabilities can be then computed. The events in Table J-G1 are assumed to be independent Bernoulli random variables with the following probability mass functions:

$$\mathrm{P}(E_i \text{ occurs}) = p_i \tag{J-G1}$$

$$P(E_\mathrm{i} \text{ does not occur}) = 1 - p_i \tag{J-G2}$$

If the events are indexed in reverse order of their losses (i.e., $L_i \geq L_{i+1}$), the mean (expected) exceedance probability for a given loss $EP(L_i)$, can be found as

$$\begin{aligned} EP(L_i) &= P(L>L_i) = 1\text{-}P(L\leq L_i) \\ &= 1-\prod_{j=1}^{i}(1-p_j) \end{aligned} \tag{J-G3}$$

The exceedance probability (*EP*) curve based on the data from Table J-G1 is shown in Figure J-G1.

If prediction capabilities are needed, a model can be that is simple and concave upward (i.e., similar to Figure J-G1). Such function should be positive and limited from the above by unity. These requirements are satisfied for the survivor function of Pareto distribution, which (for the random variable L) can be written as

$$P(L) = \left(1+\frac{L}{d}\right)^{-c} \tag{J-G4}$$

Table J-G1. Loss Exceedance Probabilities (Hypothetical Values).				
Event (E_i)	**Annual Probability of Occurrence (p_i)**	**Loss (L_i)**	**Exceedance Probability ($EP(L_i)$)**	**E(L) =(p_iL_i)**
$Event_1$	0.002	25,000,000	0.0020	50,000
$Event_2$	0.005	15,000,000	0.0070	75,000
$Event_3$	0.010	10,000,000	0.0169	100,000
$Event_4$	0.020	5,000,000	0.0366	100,000
$Event_5$	0.030	3,000,000	0.0655	90,000
$Event_6$	0.040	2,000,000	0.1029	80,000
$Event_7$	0.050	1,000,000	0.1477	50,000
$Event_8$	0.050	800,000	0.1903	40,000
$Event_9$	0.050	700,000	0.2308	35,000
$Event_{10}$	0.070	500,000	0.2847	35,000
$Event_{11}$	0.090	500,000	0.3490	45,000
$Event_{12}$	0.100	300,000	0.4141	30,000
$Event_{13}$	0.100	200,000	0.4727	20,000
$Event_{14}$	0.100	100,000	0.5255	10,000
$Event_{15}$	0.283	0	0.6597	0

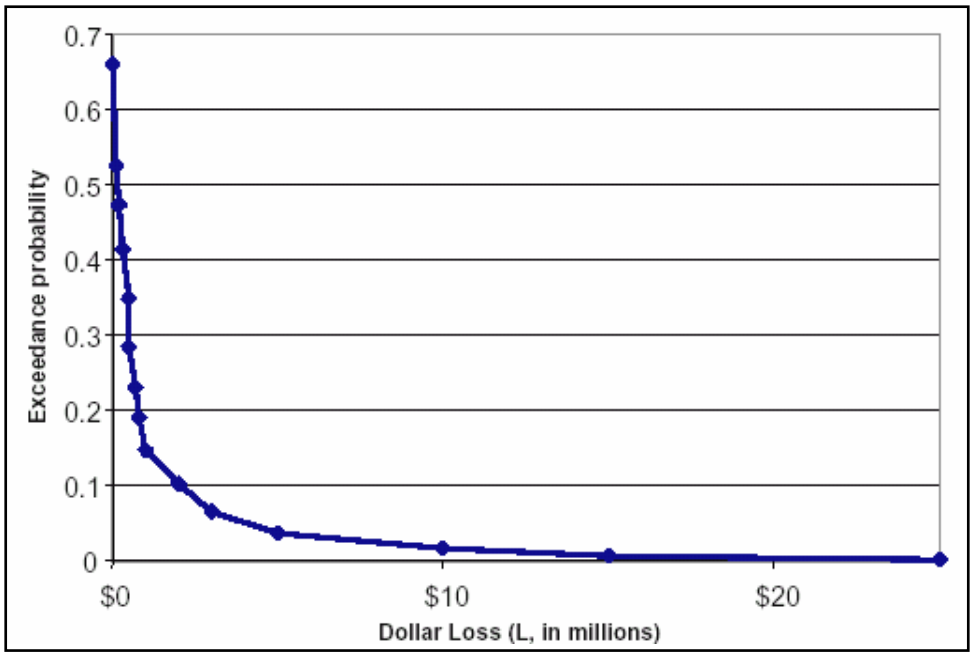

Figure J-G1. Mean Exceedance Probability Curve Based on Data from Table J-G1